TOWARDS UNIVERSAL QUANTUM COMPUTATION IN CONTINUOUS-VARIABLE SYSTEMS

Darran F. Milne

A Thesis Submitted for the Degree of PhD
at the
University of St. Andrews

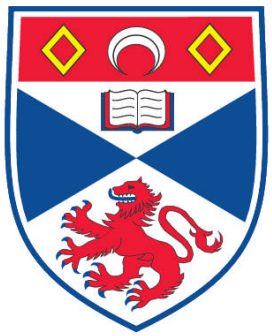

2012

Towards universal quantum computation in continuous-variable systems

Darran F. Milne

PhD Thesis

School of Physics and Astronomy

University of St Andrews

North Haugh

St Andrews

KY16 9SS

July 25, 2012

Abstract

In this thesis we explore the possibility of creating continuous-variable quantum systems that are capable of supporting universal quantum computation. We begin by examining the measurement-based model, which employs sequences of measurements on highly entangled resource states, known as a cluster states. We suggest a method for the construction of Gaussian cluster states based on ensembles of atoms and quantum non-demolition interactions. We then go on to expand our model to allow for the inclusion of light modes as part of the cluster. This yields a new class of states, the composite cluster states. This leads us to propose a new architecture for the measurement-based model that uses these composite clusters to increase resource efficiency and reduce computational errors.

The second part of this thesis concerns topological quantum computation. In states exhibiting topological degrees of freedom, quantum information can be stored as a non-local property of the physical system and manipulated by braiding quasiparticles known as anyons. Here we show how these ideas can be extended to continuous variables. We establish a continuous variable analogue of the Kitaev toric code, show that excitations correspond to continuous versions of Abelian anyons and investigate their behaviour under the condition of finite squeezing of the resource state.

Finally, we expand our continuous variable topological model to include non-abelian excitations by constructing superpositions of CV toric code anyons. We derive the fusion and braiding behaviour of these non-abelian excitations and find that they correspond to a CV analog of Ising anyons. Using these resources, we go on to suggest a computational scheme that encodes qubits within the fusion spaces of the CV Ising anyons and derive one- and two-qubit quantum gates operations that are implemented in a topological manner.

Declarations

1. Candidate's declarations:

I, Darran Milne, hereby certify that this thesis, which is approximately 30,000 words in length, has been written by me, that it is the record of work carried out by me and that it has not been submitted in any previous application for a higher degree.

I was admitted as a research student in October 2008 and as a candidate for the degree of Doctor of Philosophy in October 2008; the higher study for which this is a record was carried out in the University of St Andrews between 2008 and 2012.

Date: July 25, 2012

Signature of candidate

2. Supervisor's declaration:

I hereby certify that the candidate has fulfilled the conditions of the Resolution and Regulations appropriate for the degree of Doctor of Philosophy in the University of St Andrews and that the candidate is qualified to submit this thesis in application for that degree.

Date: July 25, 2012

Signature of supervisor

3. Permission for electronic publication: (to be signed by both candidate and supervisor)
In submitting this thesis to the University of St Andrews I understand that

I am giving permission for it to be made available for use in accordance with the regulations of the University Library for the time being in force, subject to any copyright vested in the work not being affected thereby. I also understand that the title and the abstract will be published, and that a copy of the work may be made and supplied to any bona fide library or research worker, that my thesis will be electronically accessible for personal or research use unless exempt by award of an embargo as requested below, and that the library has the right to migrate my thesis into new electronic forms as required to ensure continued access to the thesis. I have obtained any third-party copyright permissions that may be required in order to allow such access and migration.

The following is an agreed request by candidate and supervisor regarding the electronic publication of this thesis:

Access to printed copy and electronic publication of thesis through the University of St Andrews.

Date: July 25, 2012

Signature of candidate

Signature of supervisor

Contents

Foreword

I consider myself to have been extraordinarily lucky during the course of my Ph.D. I have had the opportunity to work with some truly remarkable people from across the globe and make at least a small contribution to an incredibly interesting and conceptually challenging field. Over the last three years, many people have influenced and contributed to my understanding of the physical world and how my work fits within it, none more so than my supervisor Dr. Natalia Korolkova whom I would like to thank, for her constant guidance and support. Our discussions (and the occasional chocolate) kept me inspired during the inevitable, difficult moments in a Ph.D. student's life.

I also had the good fortune of working in the theoretical quantum optics group at the Max Plank Institute for the Science of Light. I would like to express my gratitude to the group for their hospitality and the many interesting discussions. In particular I would like to thank Dr. Peter van Loock, our meetings increased my understanding of quantum theory immeasurably and kept me driven and enthusiastic during the course of my research.

Also thanks to all my friends and colleagues in the Physics department. Unfortunately there are far too many to recount here, but I owe a debt of gratitude to them all for the many insightful chats and essential cups of coffee.

I have found few things as satisfying as the quest for knowledge and the joy that new, mind expanding concepts can bring. However, such a path can be difficult, the hours can be unsociable and the mind constantly works on problems that can distract from people and relationships. So then, my final thanks go to Hannah. It is difficult to express how grateful I am for the patience and grace she has shown throughout my studies. I can only say that her love, compassion and understanding have been a vital source of inspiration countless times over the last few years.

Publications

The following is a list of publications that that I have produced during the course of my studies.

- D. F. Milne and N. V. Korolkova,
  Composite cluster state and alternative architectures for measurement-based quantum computation,
  Phys. Rev. A **85**, 032310, (2012)
- D. F. Milne, N. V. Korolkova and P. van Loock,
  Universal quantum computation with continuous-variable abelian anyons,
  Phys. Rev. A **85**, 052325, (2012).
- D. F. Milne, N. V. Korolkova,
  Electromagnetically induced invisibility cloaking,
  arXiv:1206.3944v1 [physics.optics] (2012).

Manuscripts in Preparation

- D. F. Milne, N. V. Korolkova, P. van Loock
  Topological quantum computation with non-Gaussian states
  June 2012

Conference Presentations

The following is a list of conferences, summer schools and presentations in which I have taken part.

1. QNLO Summer school, Hven, Sweden (2008).
2. 11^{th} International Conference on Squeezed States and Uncertainty Relations, Olomouc, Czech Republic, Poster Presentation (2009).
3. Summer School on Scalable Quantum Computing with Light and Atoms, Cargese, Corsica, Poster Presentation (2009).
4. 17^{th} Central European Workshop on Quantum Optics, St Andrews, United Kingdom, Poster Presentation (2010).
5. International Workshop on Continuous Variable Quantum Information Processing (CVQIP'10), Herrsching, Germany, Poster Presentation (2010).
6. International Conference Photon10 QEP-19, Southampton, United Kingdom, Poster Presentation (2010).
7. 11^{th} Canadian Summer School on Quantum Information and 8th Canadian Student Conference on Quantum Information, Jouvence, Qubec, Canada, Poster Presentation (2011).
8. Invited colloquia, Max Planck Institute for the Science of Light, Erlangen, Germany, Oral Presentation (2011).
9. Quantum Information Scotland (QUISCO), Scotland, Oral Presentation (2011).

Research visits

- DAAD funded collaboration with the Optical Quantum Information Theory Group, Max-Planck Institute for the Science of Light, Erlangen, Germany (2010)

- DAAD funded collaboration with the Optical Quantum Information Theory Group, Max-Planck Institute for the Science of Light, Erlangen, Germany (2011)
- Informatics department, University of Edinburgh, (2001)

Chapter 1

Introduction

Undoubtedly one the greatest innovations of the 20th century was the establishment of information theory and the subsequent development of the computer. This breakthrough has changed every facet of our day to day lives, everything from near instantaneous world wide communication to accurate simulation of complex phenomena. However, it is well known that computation in its present form is rapidly approaching a fundamental limit, known as Moore's law, which predicts that number of transistors on an integrated circuit will double every eighteen months. As new state of the art technologies are developed transistors are fast approaching a sufficiently small scale that quantum effects will interfere with their operation. However, ever the optimists, physicists, instead of seeing this as a major hurdle to progress, have seized on these potential issues and turned them to an advantage. This has led to the development of Quantum Computation (QC). Originally pioneered in the 1980s by Richard Feynmann [1] and David Deutsch [2] quantum computation has advanced rapidly along two main paths, which on casual inspection appear to have quite different objectives.

The first attempts to include quantum effects into computation by generalizing the Church Turing principle - the central idea in classical information science. This has led to the advent of a new field, *quantum information theory*, which as one of its primary aims, seeks to understand the effect of quantum mechanics on computation and the information processing capacity of quantum states [3]. As this field has advanced, it has led to many developments in our understanding of fundamental physics, generalizing concepts such as Shannon entropy and recently has led to the investigation of new classes of non-classical correlations [4, 5, 6]. The study of quantum information can be split further into two sub fields corresponding to systems that exhibit either discrete or continuous spectra. Discrete quantum information has been the basis for most of the fundamental advances in quantum computation as it provides a direct generalization of classical binary information theory to the quantum setting. However, discrete systems are not always

the most natural way to visualize quantum phenomena, particularly those which are continuously parameterized such as the position and momentum of a massive particle or the orthogonal components of macroscopic atomic spin [7]. These continuous variable (CV) systems are described by canonical conjugated coordinates x and p which are spanned by an infinite dimensional Hilbert spaces and thus contain a much richer mathematical structure than their discrete counterparts. The study of quantum information in these CV systems has recently emerged in parallel with the more traditional discrete systems though the two regimes are conceptually quite different. This has led to the development of protocols that make use of CV states to perform certain quantum tasks such as quantum teleportation [9, 10], quantum cryptography [11, 12] and importantly for this thesis, a CV version of quantum computation [13].

The second course in the study of quantum computation is based on the potential for simulating quantum mechanical systems for the purpose of studying fundamental physics. The simulation of quantum systems is generally computationally intractable for classical computers when considering any system with a large number of degrees of freedom. This has led to a branch of study that focuses on finding suitable physical systems that would support *universal quantum computation*. That is, we want to find or construct systems that will allow us to store a quantum state, apply arbitrary unitary operations and read out the result of our manipulations via a measurement. The traditional picture of a quantum computer is provided by the *quantum circuit model*. In this model input states are loaded into the physical system, processed by a sequence of quantum gates that enact the required unitary operation and finally the outcomes are measured and displayed when the computation is completed. There are many potential candidates that could support quantum computation, ranging from optical systems [14, 15, 16, 19] to NMR [17, 79] and in particular, condensed matter systems such as superconducting systems [20] or quantum dots [21]. While in principle each of these systems would be capable of supporting universal computation, it is yet unclear which will provide the best way forward for an experimental realization of a fully scalable quantum computer. This uncertainty has arisen due to the extremely high demands we must make on the candidate states. Not only do these states have to provide sufficient, stable resources to produce large-scale computers, they must also have the ability to protect the information stored within them from errors. The main cause of error in discrete variable computation is known as decoherence. Decoherence prevents us from observing quantum phenomena at large scales, however, since a quantum computer relies on such quantum phenomena for its operation, we must find methods to shield any quantum information stored within the systems from these effects. In principle, we could just totally isolate the quantum computer from its environment, however this can never be perfect and usually becomes harder as the computational system

increases in size and complexity. In the CV regime the main perpetrator of error comes from the lack of perfect resource states. It is usually assumed in CV protocols, that we can create perfect eigenstates of the position or momentum operators. Such states are idealized versions of real states and are highly unphysical since they require infinite squeezing of the canonical variables and hence infinite energy to create. Nevertheless, infinitely squeezed states are useful concepts in theory due to their simple mathematical representation. In realistic scenarios, CV states are actually represented as some quasi-probability distribution in phase-space. The most common CV states that feature in continuous-variable protocols are those that are represented by a Gaussian probability distributions. These are known as the *Gaussian states* and much effort has been expended in understanding their properties as they are relatively easy to realize experimentally. When we allow the use of such physical, Gaussian states in our continuous-variable theory of quantum computation, we find that our computational protocols are exposed to a new type of error not seen in the discrete case. The source of this is due to the lack of infinite squeezing which means the states are not localized in phase-space and any computational process is subject to some intrinsic imprecision that leads to errors that can propagate through the system, ruining the computation. Of course both the discrete and continuous regimes are subject to errors due to losses and detection limitations and any realistic quantum computer will have to take these into account as well. Advances in the study of such limitations have culminated in a new field known as *quantum error correction* (QEC). Initially, QEC took its inspiration from classical error correction models by adding redundancy into the storage of the quantum information. Such redundant codes tolerate errors up to some finite error rate which allows quantum computation to be performed fault-tolerantly [22, 23]. While QEC has advanced well beyond the simple redundancy codes for both discrete and CV systems [24, 25, 9] it remains an open problem to create physical states that have sufficient intrinsic protection against error to make use of them.

The main themes of this thesis are computational universality and fault tolerance. We seek to construct theoretical models for systems that will support universal quantum computation while protecting the information encoded within them. In particular, we investigate how such models can be generated in continuous variable systems. This leads us to examine alternatives to the circuit model such as *Measurement-Based Quantum Computation* (MBQC), where instead of processing states through a sequence of gates, unitary operations are carried out by successive measurements on a universal resource state, known as a *cluster state*. Cluster states are a class of multi-partite entangled graphs states that act as a computational substrate, upon which computational processes can be implemented. Such measurement-based schemes have been shown to be universal in both the discrete and CV regimes [26, 27, 28]. One of the main tasks in this field is

the design of protocols to generate cluster states in a manner that is practical and scalable. Even within just the CV regime there are many proposals for the generation of CV cluster states including linear optical constructions [29], methods involving optical parametric oscillators (OPO) [28, 31] and single quantum non-demolition schemes [32, 33]. These proposals are all based on optical resources but it is also possible to build cluster states from ensembles of polarized atoms [34, 35, 36] which can act as quantum memories, allowing short term information storage within the cluster states. However, as with circuit model constructions, cluster state computation is still inherently prone to issues associated with finite squeezing and we must look to other systems to provide a fundamental solution to the problem of errors correction and fault tolerance. For inspiration, we look to a recent development in discrete computational systems - *Topological Quantum Computation* (TQC) [140, 182]. TQC is a revolutionary idea that seeks to store quantum information in non-local degrees of freedom that have intrinsic protection from local errors. In the ideal case such systems would not require any further error correction and computational processes could be implemented with arbitrary precision.

Just like previous quantum computational proposals, one of the primary tasks here is to find suitable physical states with which to perform TQC protocols. It has long been known that certain condensed matter systems in two spatial dimensions such as the states at certain filling fractions in the Fractional Quantum Hall Effect (FQHE), exhibit topological degrees of freedom [186, 187]. These manifest themselves as quasiparticle excitations known as *anyons*. Anyons are exotic particles that do not obey Bose or Fermi statistics, but something in between. They can be divided into two main classes, abelian and non-abelian which can be distinguished by their fusion rules and braiding statistics. Simply put, braiding anyons evolves the multiparticle state by some unitary. In the case of abelian anyons this evolution just results in extra phase factors while braiding non-abelian anyons acts on the state by some higher dimensional unitary operator. This braiding behaviour has led to the suggestion that systems containing certain classes of non-abelian anyon can be used as a resource for quantum computation. Since the information is stored in these non-local degrees of freedom and quantum gates are enacted topologically via braiding, such systems are topologically protected from effects such as decoherence. However, accessing these states within a condensed matter setting has proved very difficult experimentally, which has led to proposals for the construction of artificial topological states. The first such artificial system that has been shown to exhibit anyonic excitations, is a spin lattice model proposed by Kitaev [140, 174], known as the *toric code*. The simplest version of the toric code only yields abelian statistics and is hence insufficient for universal quantum computation but it can serve as a topological quantum memory [38, 203]. However, in certain coupling regimes it is possible for the Kitaev models to

yield more useful non-abelian anyon types [205], some of which have been shown to provide universal gate sets through topological operations alone. A further recent development has been the generalization of these ideas to continuous variables [179]. In this model it has been shown that a CV analog of the toric code that supports abelian anyons can be generated. Like their discrete counterparts, these CV anyons produce phase rotations upon braiding which alone are insufficient for universal computation. However, as a proof of principle scheme, the CV toric code states have a significant advantage over the discrete versions as they are constructed from experimentally viable Gaussian resources and linear optics.

The outline of this thesis is as follows. We begin in Chapter 2 by introducing the continuous-variable formalism that we will be using throughout. This begins with a brief review of the quantization of the electromagnetic field as an example to aid the understanding of the key concepts that underpin continuous quantum systems. This leads us to a description of phase-space and quasi-probability distributions as a useful method to represent quantum states. With these general ideas in place, we specialize to the set of Gaussian states. The theory of Gaussian quantum states is very advanced and we state a few of the main results that we will use later in our work. In particular, we introduce the covariance matrix formalism which is a particularly convenient method to manipulate Gaussian states without having to resort to working with density matrices of infinite order. Our introduction to CV states concludes with some statements about CV entanglement. We give some relevant measures of bipartite entanglement that we will be using in later chapters.

In Chapter 3 we review the theory of quantum computation and universality. This begins with a discussion of quantum computation over qubits. This theory is well known so we keep it deliberately brief. The main result of this section is the construction of a set of universal quantum gates that we use to test to universality of our computational systems. We then explore the ideas behind continuous-variable computation. First, we give a definition of CV quantum computation before going on to identify suitable computational bases. Finally, we state the basic CV quantum gates and make some statements about universality in CV computation.

In Chapter 4 we present the first of the original results of this thesis. This begins with a discussion on cluster states, the resource states for Measurement-Based Quantum Computation (MBQC). We then specialize to continuous-variable cluster states and their use as computational resources. This leads us to examine specific physical systems where cluster states can be created, namely ensembles of neutral atoms. We go on to describe these ensembles and the interactions that we can enact between them. This brings us to the main results of this chapter. We derive protocols for the generation of small clusters state from atomic ensembles and show that this scheme can be generalized to construct cluster states of arbitrary size and shape.

We then go on to show how this method can be modified to include CV light modes as part of the the state to create *composite cluster states*. We investigate the entanglement properties of the composite cluster state and discuss how to expand to the multimode case. Our last section deals with an intrinsic problem of quantum computation over Gaussian cluster states, that of exponential decay of *localizable entanglement* leading to computational errors. We present an alternative architecture for MBQC based on our composite cluster states that seeks to lessen the effect of entanglement decay via improved resource efficiency.

In Chapter 5 we introduce our work on Topological Quantum Computation (TQC). This begins with a general introduction to the theory behind the emergence of anyons within topological systems. We then look at the requirements that an anyon model must satisfy to be considered complete before reviewing the main aspects of the discrete toric code model. We then turn to the key result of this chapter, the generalization of the toric code to the continuous-variable regime. We show that CV analogs of abelian anyons can be created, fused and braided to produce evolutions of the underlying state. We then investigate the properties of the CV Kitaev ground state under finite squeezing and the new anyon dynamics that emerge. Our next section deals with the question of universal CV quantum computation on these CV anyonic states. We derive protocols that make use of the topological properties of the state but find the topological gate operations are insufficient to form a universal set. We expand our gate set to included non-topological operations and show that a complete set of CV quantum gates can be performed on the CV anyons. Finally we discuss the fault tolerance of this topological model against finite squeezing and the effect on topological gate operations.

In Chapter 6 we expand on the CV topological model and suggest a scheme to include non-abelian excitations. We begin our analysis by reviewing the theory of non-abelian anyons, we define the relevant topological spaces and derive consistency conditions for general non-abelian models. We then show how the CV toric code can be enhanced to yield anyons with non-abelian statistics. We examine the braiding and fusion rules for these new excitations before making a simplification that allows us to identify our model as a CV version of the Ising anyon model. With this in mind we develop a computational model for qubits that only requires topological operations alone to enact a set of qubit quantum gates.

Finally, in Chapter 7 we gather our conclusions, present some open questions and give future direction for research.

Chapter 2

The continuous variable formalism

In this preliminary chapter we review the formalism that underlies the structure of states in the continuous-variable (CV) regime. Such states are the main theme of this thesis and so here we provide the relevant definitions and formulae that we shall come to rely on in later chapters. We begin by introducing a phase-space description and the corresponding quasi-probability distributions. We then restrict our interest to Gaussian states which allows us to introduce the symplectic formalism as an elegant method for calculating the effect of Gaussian maps on CV states. For further reading on these topics the interested reader is referred to [41, 42, 43, 44, 45, 46, 47].

In many ways continuous variables are a natural description of physical states. The canonical examples of continuous-variable systems are the quadratures of the electromagnetic (EM) field, however other well known examples rely on continuous parameters. These include the position and momentum of massive particles, the collective spin of an ensemble of polarized atoms and many others. This general description is possible because CV systems are described by two canonical degrees of freedom, $\hat{q}$ and $\hat{p}$, which correspond to observables. These observables must satisfy the canonical commutation relations.

$$[\hat{q}, \hat{p}] = i\mathbb{1}. \tag{2.1}$$

This commutation relation implies that the underlying Hilbert space cannot be finite dimensional. One can see this if we apply the trace on Eq.(2.1), then applying finite dimensional operator algebra the LHS gives $tr(\hat{q}\hat{p}) - tr(\hat{p}\hat{q}) = 0$ while the $RHS = i\dim(\mathcal{H})$. Where $\dim(\mathcal{H})$ is the dimension of the finite Hilbert space. This contradiction leads us to conclude that we cannot apply finite dimensional algebras to such systems. Also in the physical situations given above, there is no bound on the values that $\hat{q}$ and $\hat{p}$ can take. Then $\hat{q}$ and $\hat{p}$ possess a continuous spectra and act in an infinite dimensional Hilbert space.

These canonical operators only describe a single mode but we can extend the commutation relation to include multiple modes by ordering the operators in canonical pairs as $\hat{R}^T = (\hat{q}_1, \hat{p}_1, \hat{q}_1, \hat{p}_2, ..., \hat{q}_N, \hat{p}_N)$. Then we can restate the commutation relation as

$$[\hat{R}_i, \hat{R}_j] = i\mathbb{1}(\Omega_N)_{ij}, \tag{2.2}$$

where $i, j = 1, 2, ..., 2N$ and $\Omega_N = \bigoplus_{\mu=1}^{N} \Omega$ accounts for all modes. We call Ω the *symplectic matrix* which fulfills the conditions $\langle\eta|\Omega|\zeta\rangle = -\langle\zeta|\Omega|\eta\rangle$ $\forall\ \eta, \zeta \in \mathbb{R}^{2N}$ and $\langle\eta|\Omega|\zeta\rangle = 0 \Rightarrow \zeta = 0$. The symplectic matrix has the standard form

$$\Omega = \begin{pmatrix} 0 & 1 \\ -1 & 0 \end{pmatrix}. \tag{2.3}$$

The canonical commutation relations can also be expressed though the annihilation and creation operators $\hat{a}_\mu$ and $\hat{a}_\mu^\dagger$, which obey standard bosonic commutation relations

$$[\hat{a}_\mu, \hat{a}_\nu^\dagger] = \delta_{\mu\nu}, \quad [\hat{a}_\mu, \hat{a}_\nu] = [\hat{a}_\mu^\dagger, \hat{a}_\nu^\dagger] = 0, \tag{2.4}$$

$\mu, \nu = 1, 2, ..., N$. The commutation relations (2.2) are related to the bosonic commutation relations by a unitary transformation

$$U = \frac{1}{\sqrt{2}} \begin{pmatrix} \mathbb{1}_N & i\mathbb{1}_N \\ \mathbb{1}_N & -i\mathbb{1}_N \end{pmatrix}, \tag{2.5}$$

such that

$$\hat{O}_i = U_{ij}\hat{R}_j, \tag{2.6}$$

where $\hat{O}^T = (\hat{a}_1, \hat{a}_2, ..., \hat{a}_N, \hat{a}_1^\dagger, \hat{a}_2^\dagger, ..., \hat{a}_N^\dagger)$. This connection to the creation and annihilation operators is particularly convenient when working with examples such as the electromagnetic field. In the following we will use the EM field as our physical example to relate these abstract concepts to something concrete. We will begin our discussion by briefly reviewing the quantization of the EM field and show how this connects with the canonical commutation relations and bosonic commutation relations.

2.1 Quantization of the electromagnetic field

The canonical method for the quantization of electromagnetic fields is well known, here we just state the main steps of the method. For a more in depth analysis, the reader is referred to the standard texts in quantum optics [48, 49, 50, 51, 52, 53]. The classical picture of electromagnetism is defined through two fields, the electric field, $\mathbf{E}(\mathbf{r}, t)$ and the magnetic field $\mathbf{B}(\mathbf{r}, t)$. The first step in quantization is to replace these fields by their quantum equivalents. Then the fields become operators corresponding to observables

and are written $\hat{\mathbf{E}}(\mathbf{r},t)$ and $\hat{\mathbf{B}}(\mathbf{r},t)$. This is accomplished by imposing the *Coulomb gauge*, $\nabla.\mathbf{A}(\mathbf{r},t)=0$, and solving the vacuum wave equation,

$$\nabla^2\mathbf{A}(\mathbf{r},t)=\frac{1}{c^2}\frac{\partial^2\mathbf{A}(\mathbf{r},t)}{\partial t^2} \tag{2.7}$$

under periodic boundary conditions. We can write the general solution of Eq. (2.7) as a Fourier decomposition over plane waves,

$$\mathbf{A}(\mathbf{r},t)=\frac{1}{\sqrt{\epsilon_0 V}}\sum_{\mathbf{k}}\sum_{s=1}^{2}\mathbf{e}_{\mathbf{k}s}(a_{\mathbf{k}s}e^{i\mathbf{k}.\mathbf{r}-i\omega t}+a^*_{\mathbf{k}s}e^{-i\mathbf{k}.\mathbf{r}+i\omega t}). \tag{2.8}$$

Where $\mathbf{e}_{\mathbf{k}s}$ are the unit polarization vectors. Each mode is labeled by a wave-vector $\mathbf{k}$ and polarization s. The wave-vectors are discrete due to the periodic boundary conditions that we imposed. These boundary conditions imply the field is constrained to an imaginary cube of volume V.

The quantization proceeds by replacing the coefficients $a_{\mathbf{k}s}$ and $a^*_{\mathbf{k}s}$ with the bosonic creation and annihilation operators $\hat{a}_{\mathbf{k}s}$ and $\hat{a}^\dagger_{\mathbf{k}s}$, which we defined above (Eq.(2.4)). Then the quantized vacuum solution becomes

$$\hat{\mathbf{A}}(\mathbf{r},t)=\sqrt{\frac{\hbar}{2\epsilon_0 V}}\sum_{\mathbf{k},s}\mathbf{e}_{\mathbf{k}s}(\hat{a}_{\mathbf{k}s}e^{i\mathbf{k}.\mathbf{r}-i\omega t}+\hat{a}^\dagger_{\mathbf{k}s}e^{-i\mathbf{k}.\mathbf{r}+i\omega t}) \tag{2.9}$$

then the field observables are obtained via the vector potential by calculating $\nabla\times\hat{\mathbf{A}}$ and $\hat{E}=-\partial_t\hat{\mathbf{A}}$. We then obtain the Hamiltonian of the field, which turns out to be

$$\hat{H}=\frac{1}{2}\int d^3\mathbf{r}(\epsilon_0\hat{\mathbf{E}}^2+\mu_0^{-1}\hat{\mathbf{B}}^2)=\sum_{\mathbf{k}s}\hbar\omega_{\mathbf{k}}(\hat{a}^\dagger_{\mathbf{k}s}\hat{a}_{\mathbf{k}s}+1/2). \tag{2.10}$$

However, we note that the right hand side of Eq.(2.10) is a sum of quantum harmonic oscillator Hamiltonians. This observation allows us to interpret the quantized EM field as an infinite set of independent oscillators, which is a particularly convenient result as we can understand the properties of the EM field by studying the quantum mechanical formalism for these oscillators.

For each oscillatory mode we can find a corresponding Hilbert space [54]. Since each mode is labeled by a wavenumber $\mathbf{k}$ and polarization s they each have a state space $\mathcal{H}_{\mathbf{k}s}$. Then entire state space has the following structure:

$$\mathcal{H}=\bigotimes_{\mathbf{k}}\mathcal{H}_{\mathbf{k}1}\otimes\mathcal{H}_{\mathbf{k}2}, \tag{2.11}$$

for $s=\{1,2\}$.

The eigenstates of the Hamiltonian define the Hilbert space associated with each mode. These are known as the *Fock* or photon number states, defined as

$$\hat{n}|n\rangle=\hat{a}^\dagger\hat{a}|n\rangle=n|n\rangle. \tag{2.12}$$

The Fock states correspond to some energy of the oscillator labeled by the number n. Here, the field operators $\hat{\mathbf{E}}(\mathbf{r},t)$ and $\hat{\mathbf{B}}(\mathbf{r},t)$ are responsible for creating and annihilating their associated quanta. This follows from the action of the creation and annihilation operators on Fock states,

$$\hat{a}|n\rangle = \sqrt{n}|n-1\rangle, \quad \hat{a}^\dagger|n\rangle = \sqrt{n+1}|n+1\rangle, \tag{2.13}$$

the operators $\hat{a}$ and $\hat{a}^\dagger$ lower and raise the photon number by one respectively. Then the $|n\rangle$ states describe a field composed of n photons each with an energy of $E = \hbar\omega(n+1/2)$. We can represent the absence of photons, the *vacuum state* as $|0\rangle$ with the property $\hat{a}|0\rangle = 0$. Note however that even the vacuum has an energy contribution, $E_0 = \hbar\omega/2$, known as the *zero point energy*.

We can populate the vacuum to obtain excited states $|n\rangle$ by application of the creation operator

$$\frac{(\hat{a}^\dagger)^n}{\sqrt{n!}}|0\rangle = |n\rangle, \tag{2.14}$$

The Fock states form a complete set so that

$$\sum_{n=0}^{\infty} |n\rangle\langle n| = 1 \tag{2.15}$$

that is, they span the whole Hilbert space of the electromagnetic oscillator. Additionally, the Fock states are orthonormal

$$\langle n|n'\rangle = \delta_{nn'}, \tag{2.16}$$

because they are eigenstates of the Hermitian operator $\hat{n}$. The Fock states form a very convenient orthonormal Hilbert-space basis in quantum optics known as the *Fock basis*.

2.1.1 Quadrature states

As we will see in the next section, the most convenient representation of quantum states is through a quantum phase-space. This is intimately related to the canonical position and momentum observables of each field mode. These observables are known as the *quadratures* of the field and are defined through the creation and annihilation operators as

$$\hat{Q}_{\mathbf{k}s} = \sqrt{\frac{\hbar}{2\omega_{\mathbf{k}}}}(\hat{a}_{\mathbf{k}s}(t) + \hat{a}^\dagger_{\mathbf{k}s}(t)), \quad \hat{P}_{\mathbf{k}s} = i\sqrt{\frac{\hbar\omega_{\mathbf{k}}}{2}}(\hat{a}^\dagger_{\mathbf{k}s}(t) - \hat{a}_{\mathbf{k}s}(t)). \tag{2.17}$$

These operators satisfy the usual commutation relation

$$[\hat{Q}_{\mathbf{k}s}(t), \hat{P}_{\mathbf{k}'s}(t)] = i\hbar\delta_{\mathbf{k}\mathbf{k}'}\delta_{ss'}. \tag{2.18}$$

These operators can be interpreted as the Fourier components of the electromagnetic field observables rather than the position and momentum of the underlying excitations. This can be shown explicitly by considering a single field mode (with constant polarization),

$$\hat{E}(\mathbf{r},t) = iE_0(\hat{a}e^{i(\mathbf{k}.\mathbf{r}-\omega t)} + \hat{a}^\dagger e^{-i(\mathbf{k}.\mathbf{r}+\omega t)}). \tag{2.19}$$

Now defining the *dimensionless* quadratures as

$$\hat{q} = \sqrt{\frac{\omega}{\hbar}}\hat{Q}, \qquad \hat{p} = \frac{1}{\sqrt{\hbar\omega}}\hat{P}, \tag{2.20}$$

and substituting the relation $\hat{a} = 1/\sqrt{2}(\hat{q} + i\hat{p})$ we find

$$\hat{E}(\mathbf{r},t) = E_0\sqrt{2}(\hat{q}\sin(\mathbf{k}.\mathbf{r} - \omega t) - \hat{p}\cos(\mathbf{k}.\mathbf{r} - \omega t)). \tag{2.21}$$

Then in this optical example, $\hat{q}$ and $\hat{p}$ represent the in-phase and out of phase components of the electric field amplitude of the spatial-temporal mode. From the bosonic commutation relations it is easy to check that $\hat{q}$ and $\hat{p}$ are canonically conjugate observables, $[\hat{q},\hat{p}] = i\hbar$. Then these operators are of the same form as those general position and momentum operators in Eq.(2.1). In this case $\hat{q}$ and $\hat{p}$ can be regarded as the position and momentum of the EM oscillator. They do not have a real space representation but they do have a meaning in the phase-space spanned by the complex vibrational amplitude $\hat{a}$ [52].

The quadrature operators have eigenstates $|q\rangle$ and $|p\rangle$, these satisfy

$$\hat{q}|q\rangle = q|q\rangle, \quad \hat{p}|p\rangle = p|p\rangle. \tag{2.22}$$

The eigenstates are orthogonal, $\langle q|q'\rangle = \delta(q - q')$, $\langle p|p'\rangle = \delta(p - p')$ and complete

$$\int_{-\infty}^{\infty} |q\rangle\langle q|dq = \int_{-\infty}^{\infty} |p\rangle\langle p|dp = 1. \tag{2.23}$$

Furthermore, the position and momentum states are mutually related to each other via the Fourier transform

$$\begin{aligned} |q\rangle &= \frac{1}{\sqrt{2\pi}}\int_{-\infty}^{\infty} e^{-iqp}|p\rangle dp, \\ |p\rangle &= \frac{1}{\sqrt{2\pi}}\int_{-\infty}^{\infty} e^{iqp}|q\rangle dq, \end{aligned} \tag{2.24}$$

2.2 Phase-space

The phase-space formulation of quantum mechanics can often provide useful physical insights. It offers a variety of advantages since it only requires that

we deal with constant number equations instead of operators. This remarkable feature arises from the fact that we can map the infinite dimensional complex Hilbert space, which can be mathematically cumbersome to the relatively simple linear algebra structure of the finite-dimensional real phase space. Here we extend this map and show how to characterize states and operations.

2.2.1 Phase-space description

We can rigorously define phase space as follows. In the classical setting we may describe a system of N canonical degrees of freedom by a $2N$-dimensional real vector space $V \cong \mathbb{R}^{2N}$. Together with the symplectic form it defines a symplectic real vector space - the phase-space $\mathcal{P} \cong \mathbb{R}^{2N}$. The phase-space is naturally equipped with a complex structure and can be identified with a complex Hilbert space $\mathcal{H}_{\mathcal{P}} \cong \mathbb{C}^N$. The connection between the Hilbert space and the phase space is given by

$$\langle \eta | \zeta \rangle = \langle \Omega \eta | \zeta \rangle_\Omega + i \langle \eta | \zeta \rangle_\Omega. \tag{2.25}$$

where the LHS is the scalar product in $\mathcal{H}_{\mathcal{P}}$ and the subscript Ω is the symplectic scalar product in $\mathcal{P}$. Notice that $\eta = (q, p) \in \mathcal{P}$ while $\eta = q + ip \in \mathcal{H}_{\mathcal{P}}$ such that any orthonormal basis in $\mathcal{H}_{\mathcal{P}}$ leads to a canonical basis $\mathcal{P}$.

2.3 Probability distribution functions

Working within quantum phase-space can be conceptually challenging, but we can find an intuitive understanding of the evolution of quantum states by examining the phase-space probability distributions. The most widely used is the Wigner distribution function though it is not defined uniquely for a given quantum state. In fact, several distribution functions with different properties, can be defined e.g., the normal ordered P-function, anti-normal Q-function or the generalized anti-normal Husimi function could be more convenient descriptions depending on the problem being considered. Here we will not be interested in the details of all the probability distributions, we will give a brief summary of just the totally symmetric, Weyl ordered Wigner distribution which will be relevant for later discussions. Our analysis is kept very brief as we do not directly use probability distributions to solve any problems encountered in this thesis but they do provide nice visual representations of the physical processes.

It should be kept in mind that since the joint probability distributions at fixed position $\hat{q}$ and momentum $\hat{p}$ are not allowed by Heisenberg uncertainty, the quantum phase-space distribution functions should just be considered mathematical tools. Further, the joint probabilities can be negative and

so one deals with quasi-probability distributions. However, as long as they give a correct description of physical observables we regard their use as acceptable.

2.3.1 States and probability functions

We motivate the description of CV states by probability distributions by recalling that the density operator, $\hat{\rho}$, defines a quantum states if it satisfies

$$\mathrm{tr}[\hat{\rho}] = 1, \quad \hat{\rho} \geq 0, \text{ and } \hat{\rho}^\dagger = \hat{\rho}. \tag{2.26}$$

Such operators belong to a bounded linear operator Hilbert space and we say a state is pure if $\hat{\rho} = |\psi\rangle\langle\psi|$. In CV systems, the density operator formalism is rather inconvenient since the state $|\psi\rangle$ will form density matrices with infinite order.

Probability distributions such as the Wigner function give a complete description of CV states without having to keep track of infinite dimensional Hilbert spaces. Given a state $\hat{\rho}$ corresponding to a single mode, the Wigner function is defined as

$$\mathcal{W}_\rho(q,p) = \frac{1}{\pi}\int dx e^{-2ipx}\langle q+x|\hat{\rho}|q-x\rangle. \tag{2.27}$$

This transformation is called the Weyl-Fourier transform and tells us how to move between density operators and distribution functions. Sometimes it is easier to compute the characteristic function

$$\chi_\rho(\zeta,\eta) = \mathrm{tr}\{\hat{\rho}\hat{D}_{(\zeta,\eta)}\}. \tag{2.28}$$

Where $\hat{D}_{(\zeta,\eta)}$ is the Weyl operator[1] that acts as a displacement in phase space. The distributions (2.27) and (2.28) are equivalent in that they both describe the quantum state. They are related through the symplectic-Fourier transform

$$\mathcal{W}_\rho(q,p) = \frac{1}{(2\pi)^2}\int d\zeta \int d\eta\ \chi_\rho(\zeta,\eta)e^{-i\zeta p+i\eta q}, \tag{2.29}$$

$$\chi_\rho(\zeta,\eta) = \int dq \int dp\ \mathcal{W}_\rho(q,p)e^{i\zeta p-i\eta q} \tag{2.30}$$

The Weyl-Fourier transformation is invertible and it provides a way to recover the density operator from both distribution functions

$$\begin{aligned}\hat{\rho} &= \frac{1}{2\pi}\int dq\int dp\int d\zeta\int d\eta\ \mathcal{W}_\rho(q,p)e^{-i\zeta p+i\eta q}\ \hat{W}_{(\zeta,\eta)} \\ &= \frac{1}{2\pi}\int d\zeta\int d\eta\ \chi_\rho(\zeta,\eta)\hat{D}_{(\zeta,\eta)}.\end{aligned} \tag{2.31}$$

[1]The Weyl displacement operator is defined as $\hat{D}_\zeta = e^{i\zeta^T.\Omega.\hat{R}}$ for $\zeta^T = (\zeta_1,\zeta_2,...,\zeta_{2N}) \in \mathbb{R}^{2N}$

The Wigner function can be generalized for dynamical systems by including time as a phase-space coordinate. Let us give some properties that the time dependent Wigner function must satisfy in order to represent a quantum state:

- *Quasidistribution.* It is a real-valued quasi-distribution because it admits negative values.
- *T-symmetry* It has time symmetry

$$t \to -t \Leftrightarrow \mathcal{W}(q,p,t) \to \mathcal{W}(q,-p,-t) \tag{2.32}$$

- *X-symmetry.* It has spatial symmetry

$$q \to -q \Leftrightarrow \mathcal{W}(q,p,t) \to \mathcal{W}(-q,-p,t) \tag{2.33}$$

- *Translation invariant.*

$$q \to q-a \Leftrightarrow \mathcal{W}(q,p,t) \to \mathcal{W}(q+a,p,t) \tag{2.34}$$

- *T-evolution.* The equation of motion of each point in phase-space is classical in the absence of forces.

$$\frac{d\hat{\rho}}{dt} = i[\hat{\rho}, H] \Leftrightarrow \frac{\partial \mathcal{W}(q,p,t)}{\partial t} = -\frac{p}{m}\frac{\partial \mathcal{W}(q,p,t)}{\partial q} \tag{2.35}$$

- *Bounded.* The function is bounded

$$|\mathcal{W}(q,p)| \leq \frac{1}{\pi} \tag{2.36}$$

  For pure states this leads to

$$\begin{aligned} |\mathcal{W}(q,p)|^2 &= \frac{1}{\pi^2}\left|\int dx e^{-2ipx}\psi^*(q-x)\psi(q+x)\right|^2 \\ &\leq \frac{1}{\pi^2}\int dx \left|e^{ipx}\psi(q-x)\right|^2 \int dx \left|e^{-ipx}\psi(q+x)\right|^2 = \frac{1}{\pi^2} \end{aligned} \tag{2.37}$$

- *Normalized.* The function is normalized

$$\int dq \int dp\, \mathcal{W}(q,p) = 1, \tag{2.38}$$

- *Quantum marginal distributions.* It possesses well behaved marginal distributions

$$\bar{\mathcal{W}}(q) = \int dp\, \mathcal{W}(q,p) = \langle q|\hat{\rho}|q\rangle \geq 0, \tag{2.39}$$

$$\bar{\mathcal{W}}(p) = \int dq\, \mathcal{W}(q,p) = \langle p|\hat{\rho}|p\rangle \geq 0, \tag{2.40}$$

- *Orthonormal.* Orthonormality is preserved

$$\left| \int dq \psi^*(q)\phi(q) \right|^2 = 2\pi \int dq \int dp \; \mathcal{W}_\psi(q,p)\mathcal{W}_\phi(q,p). \tag{2.41}$$

  As a corollary of this we note that if the distributions are equal, $\psi = \phi$ we find $\int dq \int dp \mathcal{W}^2(q,p) = 1/2\pi$ for all pure states which excludes classical distributions such as $\mathcal{W}(q,p) = \delta(q-q_0)\delta(p-p_0)$. If the states are orthogonal, then $\int dq \int dp \mathcal{W}_\psi(q,p)\mathcal{W}_\phi(q,p) = 0$ which confirms that the Wigner function cannot be positive everywhere.

- *Completeness.* The set of functions $\mathcal{W}_{nm}(q,p)$ forms a complete orthonormal set. Let

$$\mathcal{W}_{nm}(q,p) = \frac{1}{\pi} \int dx \; e^{-2ipx} \psi_n^*(q-x)\psi_m(q+x), \tag{2.42}$$

  then as long as $\psi_n(q)$ form a complete set,

$$2 \int dq \int dp \; \mathcal{W}_{nm}^*(q,p)\mathcal{W}_{n'm'}(q,p) = \frac{1}{2\pi}\delta_{nn'}\delta_{mm'}, \tag{2.43}$$

There are several reasons to employ the Wigner function description of quantum states. The Wigner functions allow for a convenient visualization of some state $\hat{\rho}$ in terms of a distribution in phase-space with canonical coordinates (q,p). Then just by examining the Wigner function corresponding to a state we can easily read off the quadrature amplitudes with their quantum fluctuations, we can say whether a state is Gaussian or non-Gaussian and see if a state exhibits interference effects. Wigner functions also give an intuitive description of how classical a state may be. This arises due the fact that the Wigner function can give negative values for allowed quantum states. This negativity of the Wigner function gives us a way to quantify the non-classicality of a state. For example, highly non-classical states such as Fock states or Schrodinger cat states show Wigner functions with a high degree of negativity.

The Wigner function allows the calculation of expectation values by using the trace rule [52]:

$$\mathrm{Tr}(\hat{\rho}\hat{A}) = 2\pi \int_{-\infty}^{\infty} dqdp \; W_\rho(q,p)W_A(q,p), \tag{2.44}$$

This equation would also be the rule for predicting expectations in classical statistical physics, the Wigner function $W_\rho(q,p)$ plays the role of a classical phase-space density, whereas $W_A(q,p)$ appears as the physical quantity that is averaged with respect to $W_\rho(q,p)$.

The Wigner function can be extended to a field of N modes We can write the function for the N mode field state $\hat{\rho}$ as,

$$W(q_1, p_1, ..., q_N, p_N) = \frac{1}{(2\pi)^N} \int_{-\infty}^{\infty} ... \int_{-\infty}^{\infty} \prod_{j=1}^{N} dx_j e^{ip_j x_j} \times \langle q_1 - x_1, ..., q_N - x_N | \hat{\rho} | q_1 + x_1, ..., q_N + x_N \rangle \tag{2.45}$$

Later we will see how for Gaussian states we can write this N mode Wigner function in a compact and convenient form using covariance matrices. Now that we have established the phase-space description of quantum systems, we now examine specific examples of the various types of states and operations that will be relevant throughout this thesis.

2.4 Gaussian States: Properties and Operations

In this section, we will review the main definitions and results for Gaussian states which are a subset of the continuous-variable states. We will also introduce definitions and criteria for entanglement between Gaussian states that will be used to characterize scalability of computational models later in this thesis. We define the set of Gaussian states as those states with Gaussian characteristic functions and quasi-probability distributions on the multi-mode quantum phase space.

2.5 Covariance matrices and symplectic operations

Gaussian functions are mathematically completely defined by their first and second moments. Hence it follows that any Gaussian state $\hat{\rho}$ is characterized by the first and second moments of the quadrature field operators. We denote the first moments by

$$\bar{R} = (\langle \hat{R}_1 \rangle, \langle \hat{R}_2 \rangle, ..., \langle \hat{R}_N \rangle, \langle \hat{R}_n \rangle) \tag{2.46}$$

and the second moments by the covariance matrix (CM) σ of elements

$$\sigma_{ij} = \langle \hat{R}_i \hat{R}_j + \hat{R}_j \hat{R}_i \rangle - 2 \langle \hat{R}_i \rangle \langle \hat{R}_j \rangle \tag{2.47}$$

First moments can be arbitrarily adjusted by local unitary operations, which are merely displacements in phase space. These can be performed by applying single-mode displacement operators to the Gaussian function corresponding to each single mode. From the phase-space picture we developed above it is obvious that such operations leave the structure of the Gaussian state invariant and hence any information contained within states are unaffected by first-moment evolutions.

We can incorporate covariance matrices into the phase-space picture through the Wigner function, which can be written,

$$W(\mathbf{R}) = \frac{e^{-(\mathbf{R}-\mathbf{d})\sigma^{-1}(\mathbf{R}-\mathbf{d})^T}}{\pi^N \sqrt{\mathbf{Det}(\sigma)}} \tag{2.48}$$

where $\mathbf{R}$ is the real phase-space vector $(q_1, p_1, ..., q_N, p_N)$ and $\mathbf{d}$ is the displacement vector. This allows a complete description of an arbitrary Gaussian state with just a $2N \times 2N$ covariance matrix σ. Then the CM can be used to denote the second moments of the Gaussian state or the state itself. In the formalism of statistical mechanics, the CM elements are the two-point truncated correlation functions between the $2N$ canonical continuous variables. We note that the entries of the CM can be expressed as energies by multiplying them by the quantity $\hbar\omega_k$, where ω_k is the frequency of each mode k, in such a way that $Tr(\sigma)$ is related to the mean energy of the state, i.e. the average of the non-interacting Hamiltonian. This mean energy is generally unbounded in CV systems.

As the real CM contains the complete locally-invariant information on a Gaussian state, there are constraints that must be obeyed for σ to represent a CV Gaussian state. These constraints reflect the requirements of positive-semidefiniteness of the associated density matrix ρ. These conditions, together with the canonical commutation relations imply

$$\sigma + i\Omega \geq 0, \tag{2.49}$$

This is the only necessary and sufficient constraint that σ has to fulfill to be the CM corresponding to a physical Gaussian state [66, 67]. More generally, this is a necessary condition for the CM of any non-Gaussian CV state. Note however, that non-Gaussian states cannot be fully characterized by the covariance matrix alone since in principle they contain moments of any order.

It is often useful to decompose a given CM into its separate subsystems. For example, we can write the CM σ for an N-mode Gaussian state in terms of two by two submatrices as

$$\sigma_{1,...,N} = \begin{pmatrix} \sigma_1 & C_{1,2} & ... & C_{1,N} \\ C_{1,2}^T & ... & ... & ... \\ ... & ... & ... & C_{N-1,N} \\ C_{1,N}^T & ... & C_{N-1,N}^T & \sigma_N \end{pmatrix} \tag{2.50}$$

Each diagonal block σ_k is the local CM corresponding to the reduced state of mode k, for all $k = 1, ..., N$. The off-diagonal matrices $C_{i,j}$ encode the classical and quantum correlations between the subsystems i and j. The matrices $C_{i,j}$ are zero for product states.

The advantage of the CM formalism is the ease with which Gaussian states can be represented and operated upon. In the following we present

some examples of well known Gaussian states with their covariance matrix representation. We begin with single-mode states, these are characterized by (2×2) CMs. All the pure one-mode Gaussian states can be obtained from the vacuum by appropriate displacements, rotations and squeezing operations on the vacuum state. We list the states below

- (Vacuum state): This is characterized by the action of the annihilation operator, $\hat{a}|0\rangle = 0$. This has CM and displacement vector,

$$\sigma_0 = \begin{pmatrix} 1 & 0 \\ 0 & 1 \end{pmatrix}, \quad d_0 = \begin{pmatrix} 0 \\ 0 \end{pmatrix}. \tag{2.51}$$

  Vacuum states exhibit the lowest quantum fluctuations in both quadrature distributions. In this sense they are the minimum uncertainty states over both quadratures.

- (Pure coherent states): Coherent states are eigenstates of the annihilation operator, $\hat{a}|\alpha\rangle = \alpha|\alpha\rangle$. To discuss coherent states we introduce the displacement operator $\hat{D}(\alpha) = \exp(\alpha\hat{a}^\dagger - \alpha^*\hat{a})$ and $\alpha = 1/\sqrt{2}(q_0 + ip_0)$. This is a unitary operation and as its name suggests this $\hat{D}(\alpha)$ induces a displacement on the amplitude $\hat{a}$ by an amount α,

$$\hat{D}^\dagger(\alpha)\hat{a}\hat{D}(\alpha) = \hat{a} + \alpha. \tag{2.52}$$

  Coherent states can then be interpreted as displaced vacuums, $|\alpha\rangle = \hat{D}(\alpha)|0\rangle$, in the CM picture this takes the form

$$\sigma_{D(\alpha)} = \begin{pmatrix} 1 & 0 \\ 0 & 1 \end{pmatrix}, \\ d_{D(\alpha)} = \begin{pmatrix} q_0 \\ p_0 \end{pmatrix}. \tag{2.53}$$

- (Pure squeezed states): As we noted above, minimum uncertainty in both quadratures is achieved in the vacuum and coherent states. However it is possible to reduce the variance in one of the quadratures at the expense of the conjugate variable. We parameterize the deviation of the variances from their vacuum values by a real number r called the *squeezing parameter*,

$$\Delta^2 q = \frac{1}{2}e^{-2r}, \quad \Delta^2 p = \frac{1}{2}e^{2r}. \tag{2.54}$$

  This still satisfies the Heisenberg uncertainty relation since $\Delta q \Delta p = 1/2$ but we have the freedom to modify the variances by adjusting the value of r. Squeezing is achieved via a unitary operation known as the *squeezing operator*:

$$\hat{U}^{sq}(r) = \exp\left[\frac{r}{2}(\hat{a}^2 - \hat{a}^{\dagger 2})\right]. \tag{2.55}$$

Applying this to $|0\rangle$ we obtain the squeezed vacuum state, $|r\rangle = \hat{U}^{sq}(r)|0\rangle$, which has CM and displacement

$$\sigma_{U^{sq}(r)} = \hat{S}(r)\sigma_0\hat{S}^T(r) = \begin{pmatrix} e^{-2r} & 0 \\ 0 & e^{2r} \end{pmatrix},$$
$$d_{U^{sq}(r)} = S_{S(r)}d_0 + s_{S(r)} = \begin{pmatrix} 0 \\ 0 \end{pmatrix}. \tag{2.56}$$

We also consider multi-mode states, an important example of a two mode Gaussian state is the *two mode squeezed state*, $|\psi^{sq}\rangle_{i,j} = \hat{U}^{sq}_{i,j}(r)(|0\rangle_i \otimes |0\rangle_j)$, the two-mode squeezing operator is

$$\hat{U}^{sq}_{i,j}(r) = \exp\left[-\frac{r}{2}(\hat{a}_i^\dagger\hat{a}_j^\dagger - \hat{a}_i\hat{a}_j)\right] \tag{2.57}$$

In the limit of infinite squeezing this state approaches the ideal Einstein-Podolsky-Rosen (EPR) state [55], which is the simultaneous eigenstate of total momentum and relative position of the two subsystems, which then share perfect entanglement. We will be discussing the EPR state in more detail in a later section. A two-mode squeezed state with squeezing factor r can be described by the covariance matrix

$$\sigma^{sq}_{i,j}(r) = \begin{pmatrix} \cosh(2r) & 0 & \sinh(2r) & 0 \\ 0 & \cosh(2r) & 0 & -\sinh(2r) \\ \sinh(2r) & 0 & \cosh(2r) & 0 \\ 0 & -\sinh(2r) & 0 & \cosh(2r) \end{pmatrix}. \tag{2.58}$$

We note that the CM of N-mode coherent states, including the vacuum is just the $2N \times 2N$ identity matrix. Now that we have found covariance matrix representations of the relevant states we now turn to the question of how to effect unitary transformations on these states in the symplectic picture.

2.5.1 Symplectic operations - The continuous-variable toolbox

Transformations of a Gaussian state that preserve their Gaussian character are known as Gaussian operations. These are completely positive maps that can be implemented by application of Gaussian unitary operators with homodyne measurements. Homodyne and heterodyne detection are fundamental Gaussian operations, as they allow for measurement of the canonical coordinates. Here we will concentrate on the symplectic operations which are the set of canonical transformations S that preserve the canonical commutation relations. That is, if we transform our canonical operators $\hat{R}_S = S.\hat{R}$, then Eq.(2.2) is fulfilled. In an equivalent way, we can define symplectic

transformations as maps that preserve the symplectic scalar product and therefore

$$S^T.\Omega.S = \Omega. \tag{2.59}$$

The set of real $2N \times 2N$ matrices S satisfying the above condition form a group known as the symplectic group, $Sp(2N, \mathbb{R})$. To construct the affine symplectic group we just need to add the phase-space translations s that transform $\hat{R}_S = S.\hat{R} + s$ and whose group generators are $\hat{G}_i^{(0)} = \Omega_{ij}\hat{R}_j$. We find the remaining group generators of the representation of $Sp(2N, \mathbb{R})$ which physically correspond to the Hamiltonians that perform the symplectic transformations on the states. These generators are of the form $\hat{G}_{ij} = \frac{1}{2}\{\hat{R}_i, \hat{R}_j\}$, which corresponds to hermitian Hamiltonians of quadratic order in the canonical operators. When rewriting them in terms of creation/annihilation operators we can divide the generators into two groups. The passive generators (compact)

$$\hat{G}_{\mu\nu}^{(1)} = \frac{i}{2}(\hat{a}_\mu^\dagger \hat{a}_\nu - \hat{a}_\nu^\dagger \hat{a}_\mu), \quad \hat{G}_{\mu\nu}^{(2)} = \frac{i}{2}(\hat{a}_\mu^\dagger \hat{a}_\nu + \hat{a}_\nu^\dagger \hat{a}_\mu), \tag{2.60}$$

and active generators (non-compact)

$$\hat{G}_{\mu\nu}^{(3)} = \frac{i}{2}(\hat{a}_\mu^\dagger \hat{a}_\nu^\dagger - \hat{a}_\nu \hat{a}_\mu), \quad \hat{G}_{\mu\nu}^{(4)} = \frac{i}{2}(\hat{a}_\mu^\dagger \hat{a}_\nu^\dagger + \hat{a}_\nu \hat{a}_\mu). \tag{2.61}$$

The passive generators commute with all number operators $\hat{n}_\mu = \hat{a}_\mu^\dagger \hat{a}_\mu$, and so they preserve the total number. In our example of the electromagnetic field, the passive operations are those that preserve the total number of photons. Passive transformations can be implemented in the optical scenario by beam-splitters, phase-shifts and mirrors. In fact, these components can only ever implement Hamiltonians constructed from linear combinations of the compact generators. The non-compact generators correspond to higher order Hamiltonians, usually performed through interactions with non-linear media. Then to perform all the Gaussian unitaries $U_\lambda = e^{i\lambda.\hat{G}}$ we require physical systems that allow us to implement both compact and non-compact generators.

To act on the states in the CM picture we must find the symplectic matrix corresponding to the required operation and apply it in the manner of Eq.(2.59). This is a particularly convenient and compact method when considering states composed of multiple modes as we shall see below with the aid of some simple examples. We begin with the single-mode operations.

Single-mode operations

We can generate any single-mode Gaussian transformation from just three basic operations. The first is the phase-shift operator $\hat{U}_\theta = e^{i\theta\hat{a}^\dagger\hat{a}}$, this is a

passive operator with corresponding symplectic operation in phase-space is

$$S(\theta) = \begin{pmatrix} \cos\theta & \sin\theta \\ -\sin\theta & \cos\theta \end{pmatrix}. \tag{2.62}$$

The second is also passive and corresponds to phase-space translations described by the unitary $\hat{U}_\alpha = e^{\alpha\hat{a}^\dagger - \alpha^*\hat{a}}$. This has symplectic form

$$s_{D(\alpha)} = \begin{pmatrix} q_0 \\ p_0 \end{pmatrix}. \tag{2.63}$$

where $\alpha = \frac{1}{\sqrt{2}}(q_0 + ip_0)$ is the amplitude of the displacement.

Our remaining operation is the single-mode squeezer which belongs to the non-compact set of generators and hence is an active transformation. The squeezing operator, (2.55), has symplectic representation

$$S(r) = \begin{pmatrix} e^{-r} & 0 \\ 0 & e^{r} \end{pmatrix}. \tag{2.64}$$

The action of the squeezing operator is to reduce the variance of uncertainty in one canonical variable at the expense of increasing the uncertainty in another. For example, it squeezes position while stretches (anti-squeezes) the momentum by the same factor in such a way that the volume of the state in phase-space is kept constant. When the squeezing parameter r is positive we call it a q-squeezer. Analogously p-squeezers occur for negative r.

Mulitmode operations

Multimode systems are described on a tensorial Hilbert space structure. The total Hilbert space is given by the tensor product of the subsystems, $\mathcal{H} = \bigotimes_{k=1}^{N} \mathcal{H}_k$. The structure of the covariance matrices for mulitmode systems is represented as a direct sum, $\bigoplus$, of each party's associated CM. The clear advantage of this feature when working with Gaussian states is that we can fully describe a state by finite dimensional $N \times N$ matrices plus an $N \times 1$ vector instead of its corresponding infinite dimensional density matrix. Additionally, the dimensionality of phase-space increases at a slower rate as dimensions are summed instead of multiplied.

A simple example of a multi-mode operation is the basic two-mode, ideal, phase-free, beam-splitter, with action $\hat{U}_{BS} = e^{\theta(\hat{a}_i\hat{a}_j^\dagger - \hat{a}_i^\dagger\hat{a}_j)/2}$ on modes i and j. A beam-splitter with transmittivity τ corresponds to a rotation of $\theta = \arccos\sqrt{\tau}$ in phase space ($\theta = \pi/4$ is a balanced 50:50 beam-splitter) and has symplectic form

$$S_{BS_{i,j}}(\tau) = \begin{pmatrix} \sqrt{\tau} & 0 & \sqrt{1-\tau} & 0 \\ 0 & \sqrt{\tau} & 0 & \sqrt{1-\tau} \\ \sqrt{1-\tau} & 0 & -\sqrt{\tau} & 0 \\ 0 & \sqrt{1-\tau} & 0 & -\sqrt{\tau} \end{pmatrix} \tag{2.65}$$

We also have the two-mode squeezing operator,

$$U(r) = e^{r(\hat{a}_1^\dagger \hat{a}_2^\dagger - \hat{a}_1 \hat{a}_2)}, \tag{2.66}$$

which corresponds to the symplectic transformation

$$S_{TMSS_{i,j}}(r) = \begin{pmatrix} \cosh(2r) & 0 & \sinh(2r) & 0 \\ 0 & \cosh(2r) & 0 & -\sinh(2r) \\ \sinh(2r) & 0 & \cosh(2r) & 0 \\ 0 & -\sinh(2r) & 0 & \cosh(2r) \end{pmatrix} \tag{2.67}$$

where the matrix is understood to act on the modes i and j. Then the two mode squeezed state is obtained from the vacuum (represented by the 4×4 identity matrix) as $\sigma_{i,j}^{sq}(r) = S_{i,j}(r) 1 S_{i,j}^T(r)$.

A useful feature of Gaussian states is that their reduced states are again Gaussian. Say we have a bipartite Gaussian state $\hat{\rho}$ with covariance matrix σ composed of $N = N_A + N_B$ modes. Any bipartite Gaussian state can be written in a block structure as

$$\sigma = \begin{pmatrix} \sigma_A & \sigma_C \\ \sigma_C^T & \sigma_B \end{pmatrix}, \tag{2.68}$$

where $A = A^T (= \sigma_A)$ and $B = B^T (= \sigma_B)$ are block matrices of dimension N_A and N_B respectively, corresponding to the two subsystems, C correspond to correlations between A and B. Tracing out the N_B modes corresponds to the reduced state $\hat{\rho} = \mathrm{tr}_B \hat{\rho}$ with covariance matrix σ_A obtained by the upper left $N_A \times N_A$ block, similarly we can trace out A to find σ_B.

A typical operation that reduces a Gaussian state is Homodyne detection. Homodyning realizes a projective measurement of one quadrature operator, say $\hat{x}$, with associated POVM $|x\rangle\langle x|$. Later, we shall be using homodyne measurements to construct quantum states so here we explicitly show how to implement a homodyne measurement on a given CM σ.

We start with a Gaussian state γ of N-modes. As we saw above, this can be divided into $N_A \times N_B$ modes as

$$\sigma = \begin{pmatrix} \sigma_A & \sigma_C \\ \sigma_C^T & \sigma_B \end{pmatrix}, \tag{2.69}$$

with zero displacement vector. Then a homodyne measurement of $\hat{x}$ on subsystem B can be described by a Gaussian operator $\hat{\rho}_x$ with covariance matrix

$$\Gamma_x = \lim_{r \to \infty} \begin{pmatrix} \cosh r \mathbb{1}_{N_A} & \sinh r \theta_{N_A} & 0 \\ \sinh r \theta_{N_A} & \cosh r \mathbb{1}_{N_A} & 0 \\ 0 & 0 & \begin{pmatrix} 1/r & 0 \\ 0 & r \end{pmatrix} \mathbb{1}_{N_B} \end{pmatrix}. \tag{2.70}$$

and displacement vector

$$\Delta_x^T = (0, 0, ..., x, x, ...) \tag{2.71}$$

Then measuring the x-component of the last N_B modes corresponding to B, and obtaining the result $(x_1, x_2, ..., x_{N_B})$, system A will be left with covariance matrix

$$\sigma'_A = \sigma_A - \sigma_C^T (X\sigma_B X)^{-1} \sigma_C \tag{2.72}$$

and displacement

$$d'_A = \sigma_C^T (X\sigma_B X)^{-1} d'_B, \tag{2.73}$$

where $d'_B = (x_1, 0, x_2, 0, ..., x_{N_B}, 0)$, the inverse is the Moore-Penrose pseudo inverse and X is the diagonal projector with entries $\mathrm{diag}(1, 0, 1, 0, ...,)$.

Heterodyne measurement, whose POVM corresponds to $\frac{1}{\pi}|\alpha\rangle\langle\alpha|$, and in general all POVMs of the form $|\gamma, d\rangle\langle\gamma, d|$, can be achieved with homodyne measurement using ancillary systems and beam-splitters.

2.5.2 Symplectic Eigenvalues

Another symplectic transformation is that which realizes the decomposition of a Gaussian state into normal modes. The Williamson theorem [57] guarantees that the CM of an N-mode Gaussian state can always be written in the so-called Williamson normal, or diagonal form

$$\sigma = S^T \nu S \tag{2.74}$$

where $S \in Sp(2N, \mathbb{R})$ and ν is the CM

$$\nu = \bigoplus_{k=1}^{N} \begin{pmatrix} \nu_k & 0 \\ 0 & \nu_k \end{pmatrix} \tag{2.75}$$

corresponding to a tensor product state with a diagonal density matrix $\rho^{\otimes}$ given by

$$\rho^{\otimes} = \bigotimes_k \frac{2}{\nu_k + 1} \sum_{n=0}^{\infty} \left(\frac{\nu_k - 1}{\nu_k + 1}\right) |n\rangle_k \langle n|. \tag{2.76}$$

where $|n\rangle_k$ denotes the number state of order n in the Fock space. In the Williamson form, each mode with frequency ω_k is a Gaussian state in thermal equilibrium at a temperature T_k, characterized by an average number of thermal photons $\bar{n}_k$ which obeys Bose-Einstein statistics

$$\bar{n}_k = \frac{\nu_k - 1}{2} = \frac{1}{\exp\left(\frac{\hbar\omega_k}{k_B T_k}\right) - 1}. \tag{2.77}$$

The ν_k's form the *symplectic spectrum* of the CM σ, and are invariant under the action of global symplectic transformations on the matrix σ. The

symplectic eigenvalues can be computed as the orthogonal eigenvalues of the matrix $|i\Omega\sigma|$ [58] and are thus determined by N invariants of the characteristic polynomial of the CM [59] (whose invariance is a consequence of Det $S = 1$, $\forall S \in Sp(2N, \mathbb{R})$, which once computed in the Williamson diagonal form reads

$$\text{Det } \sigma = \prod_{k=1}^{N} \nu_k^2. \tag{2.78}$$

To summarize, in general, symplectic transformations in phase space are generated by exponentiation of matrices written as $J\Omega$, where J is antisymmetric. Note that the generators can be symmetric or antisymmetric. Operations such as $S_{BS_{i,j}}(\tau)$, generated by antisymmetric operators are orthogonal and, acting by congruence on the CM σ, preserve the value of $\mathbf{Tr}[\sigma]$. The $\mathbf{Tr}[\sigma]$ is interpreted as the contribution to the average Hamiltonian $H = \sum \hat{a}_k^\dagger \hat{a}_k$ from the second moments of the state. The operations that preserve $\mathbf{Tr}[\sigma]$ are said to be passive and they belong to a compact subgroup of $Sp(2N, \mathbb{R})$. On the other hand, operations such as $S_{TMSS_{i,j}}(r)$, generated by symmetric operations, are not orthogonal and do not preserve $\mathbf{Tr}[\sigma]$. They then belong to a non-compact subgroup of $Sp(2N, \mathbb{R})$. This mathematical difference between squeezers and phase-space rotations account for the difference between *active* (energy consuming) and passive (energy preserving) optical transformations [56].

2.6 Entanglement in Continuous-Variable systems

In the following we will give an introduction to the concept of entanglement in the context of CV systems and Gaussian states in particular. Entanglement is widely regarded as one of the fundamental aspects of quantum theory. Originating from the superposition principle and non-factorizability, this is a purely quantum effect. Further, entanglement is the key ingredient in the realization of quantum information protocols, which can perform processes that are impossible in a classical setting. Due to its importance in quantum information processes, many methods for identifying systems that contain entanglement and quantifying the degree of correlation between different parties have been proposed. Here we discuss the concept of continuous-variable entanglement. We go on to give a formal definition and give some simple criteria and measures for bipartite entanglement.

Though entanglement has been extensively studied in the discrete variable regime, the original formulation by Einstein, Podolsky and Rosen (EPR) was actually for two-particle states, correlated in their position and momenta. To illustrate the main concepts we review an example of a simple CV entangled state [41]. Consider the position wave function $\psi(x_1, x_2) = C\delta(x_1 - x_2 - u)$ with a vanishing normalization constant C. The correspond-

ing quantum state is then

$$\int dx_1 dx_2 \psi(x_1, x_2)|x_1, x_2\rangle \propto \int |x, x-u\rangle, \tag{2.79}$$

which implies that the position and momenta are perfectly correlated since $x_1 - x_2 = u$ and $p_1 + p_2 = 0$. Note that while this state cannot be physically realized, it remains a useful example as it can be thought of as the limiting case of a properly normalized state where the positions and momenta are correlated to some finite extent. An example of finitely correlated states are the two-mode squeezed vacuums [52],

$$\begin{aligned}\psi(x_1, x_2) &= \sqrt{\frac{2}{\pi}} \exp[-e^{-2r}(x_1 + x_2)^2/2 - e^{2r}(x_1 - x_2)^2/2], \\ \bar{\psi}(p_1, p_2) &= \sqrt{\frac{2}{\pi}} \exp[-e^{-2r}(p_1 - p_2)^2/2 - e^{2r}(p_1 - p_2)^2/2],\end{aligned} \tag{2.80}$$

which approaches $C\delta(x_1 - x_2)$ and $C\delta(p_1 + p_2)$ respectively in the limit of infinite squeezing, $r \to \infty$. We can write down the corresponding Wigner function [60, 61]:

$$W(R) = \frac{4}{\pi^2} \exp\{-e^{-2r}[(x_1+x_2)^2+(p_1-p_2)^2] - e^{2r}[(x_1-x_2)^2+(p_1+p_2)^2]\}, \tag{2.81}$$

where $R = (x_1, p_1, x_2, p_2)$. This Wigner function approaches $C\delta(x_1 - x_2)\delta(p_1 + p_2)$ in the limit of infinite squeezing, corresponding to the perfectly correlated and maximally entangled EPR state. We can calculate the marginal distributions for the two positions by integrating over the momenta or the distributions for the momenta by integrating over the positions. This yields,

$$\int dp_1 dp_2 W(R) = |\psi(x_1, x_2)|^2 = \frac{2}{\pi} \exp[-e^{-2r}(x_1 + x_2)^2 - e^{2r}(x_1 - x_2)^2], \tag{2.82}$$

$$\int dx_1 dx_2 W(R) = |\bar{\psi}(p_1, p_2)|^2 = \frac{2}{\pi} \exp[-e^{-2r}(p_1 - p_2)^2 - e^{2r}(p_1 + p_2)^2], \tag{2.83}$$

Though having well defined relative position and total momentum for large squeezing, the two modes of the two-mode squeezed vacuum state exhibit increasing uncertainties in their individual positions and momenta as the squeezing grows. In fact, tracing our either mode of the Wigner function we obtain a thermal state

$$\int dx_1 dp_1 W(R) = \frac{2}{\pi(1 + 2\bar{n})} \exp\left(-\frac{2(x_2^2 + p_2^2)}{1 + 2\bar{n}}\right), \tag{2.84}$$

with mean photon number $\bar{n} = \sinh^2 r$. We may also write the two-mode squeezed state in the Fock basis by applying the two-mode squeeze operator,

Eq.(2.66) to two vacuum modes,

$$\begin{aligned}\hat{U}_{ij}^{sq}(r)|00\rangle &= e^{r(\hat{a}_i^\dagger \hat{a}_j^\dagger - \hat{a}_i \hat{a}_j)}|00\rangle \\ &= e^{\tanh(r)\hat{a}_i^\dagger \hat{a}_j^\dagger} \left(\frac{1}{\cosh(r)}\right)^{\hat{a}_i^\dagger \hat{a}_j^\dagger + \hat{a}_i \hat{a}_j + 1} e^{-\tanh(r)\hat{a}_i \hat{a}_j}|00\rangle, \\ &= \sqrt{1-\lambda}\sum_{n=0}^{\infty} \lambda^{n/2}|n\rangle|n\rangle, \end{aligned} \tag{2.85}$$

where $\lambda = \tanh^2(r)$. The form of Eq.(2.85) shows us that the modes of the two-mode squeezed vacuum are correlated in photon number and phase. The two-mode squeezed vacuum is the quantum optical representative for bipartite continuous-variable entanglement. We now expand our discussion to more general states and define CV entanglement rigorously. Later we will be introducing entangled states composed of multiple modes but for now we limit our discussion to just two systems.

2.6.1 Bipartite entanglement

A general two-party quantum state is separable if its total density operator is a mixture (a convex sum) of product states [62],

$$\hat{\rho}_{12} = \sum_i \eta_i \hat{\rho}_{i,1} \otimes \hat{\rho}_{i,2}. \tag{2.86}$$

Otherwise, it is inseparable. A convenient method to test inseparability is given by the Peres criterion [63]. For a separable state such as in Eq.(2.86), transposition of either density matrix yields another allowed, non-negative density operator with unit trace,

$$\hat{\rho}'_{12} = \sum_i \eta_i \hat{\rho}_{i,1}^T \otimes \hat{\rho}_{i,2}, \tag{2.87}$$

since $\hat{\rho}_{i,1}^T = \hat{\rho}_{i,1}^*$ is a legitimate density matrix. This allows us to state a key result for general bipartite states:

NPPT Peres criterion: *Given a bipartite state $\hat{\rho}$, if it has non-positive partial transpose ($\hat{\rho}_{i,1}^T \not\geq 0 \Rightarrow \hat{\rho}_{i,2}^T \not\geq 0$), then $\hat{\rho}$ is entangled.*

Hence a single negative eigenvalue of the partially transposed density matrix is a sufficient condition for inseparability. In general, for states of arbitrary dimension we have an equivalent condition [64],

NPPT Horodecki criterion: *In $\mathbb{C}^2 \otimes \mathbb{C}^2$ and $\mathbb{C}^2 \otimes \mathbb{C}^3$ given a bipartite state $\hat{\rho}$, it is entangled iff it has non-positive partial transpose ($\hat{\rho}^{T_A} \not\geq 0 \Rightarrow$*

$\hat{\rho}^{T_B} \not\geq 0$*).*

The Horodecki criterion is only sufficient for inseparability. Similarly, for arbitrary mixed states, the occurrence of violations of inequalities imposed by local realism is also only a sufficient, but not necessary condition for inseparability [62].

For continuous-variable states, the Peres criterion still hold and the Horodecki criterion is true as long as the state is composed of $1 \times N$ modes. In particular for Gaussian states, time reversal is easy to implement on the CM level by performing the symplectic transformation

$$P = \begin{pmatrix} 1 & 0 \\ 0 & -1 \end{pmatrix}. \tag{2.88}$$

So we can rewrite the Horodecki criterion for Gaussian states [147].

NPPT Simon criterion: *For $1 \times N$ modes given a bipartite Gaussian state σ, it is entangled iff it has non-positive partial transpose ($P_A \sigma P_A^T + i\Omega \not\geq 0 \Rightarrow P_B \sigma P_B^T + i\Omega \not\geq 0$).*

We can also quantify the degree of entanglement present in a bipartite system. For this we define measures of entanglement. The simplest measure, defined for pure states is the *Entropy of Entanglement*:

$$E_S(\hat{\rho}) = S(\hat{\rho}_A) = -\mathrm{tr}(\hat{\rho}_A \log_2 \hat{\rho}_A), \tag{2.89}$$

where $S(\hat{\rho})$ is the von Neumann Entropy of a state $\hat{\rho}$ and $\hat{\rho}_A$ is the density matrix for subsystem A. For any CV state this reduces to

$$E_S(\hat{\rho}) = -\sum_{i=1}^{\infty} \lambda_i^2 \log_2 \lambda_i^2, \tag{2.90}$$

while for Gaussian states we can state this in terms of the symplectic eigenvalues ν_i,

$$E_S(\gamma) = -\sum_{i=1}^{N_A} \left[\frac{(\nu_i + 1)}{2} \log_2 \frac{(\nu_i + 1)}{2} - \frac{(\nu_i - 1)}{2} \log_2 \frac{(\nu_i - 1)}{2} \right], \tag{2.91}$$

The entropy of entanglement is a unique measure of entanglement for pure states. It depends only on the Schmidt coefficients and not on the choice of basis, therefore is invariant under local unitary operations.

More generally, for mixed states we define another measure known as *Logarithmic negativity* [68]:

$$E_N(\hat{\rho}) = \log_2 ||\hat{\rho}^{T_A}||_1 \tag{2.92}$$

where $||.||_1$ is the trace norm. For any CV state it can be written in terms of the negative elements of the partial transpose as

$$E_N(\hat{\rho}) = log_2 \left[1 + 2 \sum_{i=1}^{\infty} |\min(\tilde{\lambda}_i, 0)| \right]. \tag{2.93}$$

For Gaussian states, we can state this in terms of the symplectic eigenvalues of the partial transpose

$$E_N(\sigma) = -\sum_{i=1}^{N} \log_2[\min(\tilde{\nu}_i, 0)]. \tag{2.94}$$

The negativity $N(\hat{\rho})$ is a computable measure of entanglement for mixed states. It quantifies the violation of the NPPT criterion, i.e., how much the partial transposition of a density matrix fails to be positive. It is invariant under local unitaries and for Gaussian states reads

$$N(\sigma) = \frac{1}{2} \left[\prod_{i=1}^{N} \frac{1}{\min(\tilde{\nu}_i, 1)} - 1 \right]. \tag{2.95}$$

This concludes our review of the continuous-variable formalism. As we will discover in the following chapters, this description of physical states presented gives us an intuitive picture that allows us to perform calculations on states characterized by Gaussian probability distributions with relative ease. As we noted earlier, such states have many uses in the field of quantum information but here we are mainly interested in their use for quantum computation. However, it is not readily obvious how such states could define a computational basis or how we would design quantum gates operations to manipulate information stored within the states. This is the subject of our next chapter.

Chapter 3

The two sides of Quantum computation

A classical computer can be simply visualized as a series of logical gates that takes an input signal, applies some function, dependent on the type and order of the gates, and outputs some desired result. The outcomes of the logical process are then displayed by some means for the user to interpret. Similarly, the most intuitive way to understand quantum computation is to imagine a sequence of *quantum* logic gates, connected by some quantum wires that convey information between them. Once the sequence of gates have outputted the result, a measurement is performed which collapses the quantum state to give a classical outcome which could then be interpreted by our user. This is usually referred to as the *circuit model of quantum computation*. The circuit model, while conceptually simple has proven to be quite difficult to realize directly in practice. This has led to the development of many alternatives, [69, 26, 152] that while theoretically more complex, may provide an avenue to realize quantum computation in an experimental setting. Such innovative computational constructs have also greatly increased our understanding of the fundamental theory of quantum computation and more generally quantum information. We also note that despite how involved our computational schemes may become, they must alway be simulatable by the standard circuit model and vice versa in order to be considered a proper model for quantum computation. This useful property allows us to decompose any quantum computational model into a sequence of quantum logic gates. Such a representation is often useful when dealing with abstract computational encodings where the logical operations on the stored information can be extremely abstruse.

There currently exist two main paradigms within quantum computation. The first considered here is the traditional approach, where information is stored in discrete d-dimensional systems as objects known as *qudits*. The most commonly used version of the qudit is the two dimensional *qubit*. The

second approach is based on the continuous-variable states of the previous chapter where quantum information is stored within the canonical position and momenta of a given CV system. The finite-dimensional version is conceptually most like the familiar classical computation so we will begin our discussion there.

3.1 Quantum computation over qubits

In discrete-variable quantum computing, we usually store information in the form of a two-dimensional object known as a qubit. This state can be interpreted in the following way, say our system can acquire two values, $|0\rangle$ and $|1\rangle$, of course classically, the state of the system must assume one of these values at a given time. In quantum mechanics however, we are allowed to construct linear superpositions of state and so we define a qubit to be

$$|\psi\rangle = \alpha|0\rangle + \beta|1\rangle \tag{3.1}$$

where $|\alpha|^2 + |\beta|^2 = 1$. While the simplest realization of qubits could just be a two-level system in a quantum dot or some other discrete system, these states are extremely fragile since they can be collapsed by interaction with the environment in a process known as decoherence. Much theoretical and experimental work has been carried out to create systems containing stable qubits that are insensitive to decoherence and yet can be manipulated for quantum computational purposes. The literature on this subject is extensive, I refer the reader to [73, 74, 75, 76, 77, 78, 79] and references therein for further reading. We shall be seeing later that quantum information generally and qubits in particular can be stored in rather abstract spaces such as the topological spaces of certain states. In general the qubit model just requires a two-dimensional state space and some method to mediate transitions between the two states. Below we list the basic transformations that can be implemented on our qubit states. These transformations correspond to quantum logic gates, the logical operations go beyond the standard boolean logic of classical computation and allow for the creation of superposition and even entangled states.

For our discussion here we will describe our quantum gates in the circuit model. This is particularly convenient as it admits a simple pictorial description. An example is given in Fig.(3.1). The horizontal lines represent quantum wires that transfer qubits around the circuit, by convention, the progress is from left to right. Note that these denote progress through time, not space so quantum operations are not constrained to be spatially separated.

The actual processing of the qubits is performed by a sequence of quantum gates. We split the set of gates into two types; those that act on a

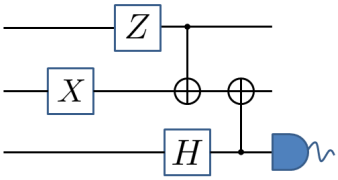

Figure 3.1:

single qubit and those that enact interaction between qubits, which we refer to as *controlled gates*. The quantum gates represent unitary operations transforming the state of one or two qubits.

Single-qubit gates

Here we list the single-qubit gates of interest to us in this thesis. We begin with the simple qubit rotations about the X, Y and Z axes. These are given by

$$X(\theta) = e^{-i\theta X/2}, \quad Y(\theta) = e^{-i\theta Y/2}, \quad Z(\theta) = e^{-i\theta Z/2} \tag{3.2}$$

where X, Y and Z are the Pauli matrices σ_x, σ_y and σ_z respectively and hence we refer to these as the Pauli gates. The most commonly used are the X and Z rotations.

$$X = \begin{pmatrix} 0 & 1 \\ 1 & 0 \end{pmatrix}, \quad Z = \begin{pmatrix} 1 & 0 \\ 0 & -1 \end{pmatrix}. \tag{3.3}$$

These have the following effect on the computational basis

$$X : |\psi\rangle = |0\rangle + |1\rangle \rightarrow |1\rangle + |0\rangle, \quad Z : \ |\psi\rangle = |0\rangle + |1\rangle \rightarrow |1\rangle - |0\rangle \tag{3.4}$$

Then the Pauli X corresponds to a bit flip and the Pauli Z is a phase rotation between the states. The Z gate can be generalized to yield arbitrary rotations with the $R(\theta)$ gate, with matrix representation

$$R(\theta) = \begin{pmatrix} 1 & 0 \\ 0 & e^{i\theta} \end{pmatrix} \tag{3.5}$$

The evolution on the computational basis is

$$R(\theta) : |\psi\rangle = |0\rangle + |1\rangle \rightarrow |0\rangle + e^{i\theta}|1\rangle, \tag{3.6}$$

then the $R(\theta)$ operation induces a phase change by some arbitrary angle θ. The $R(\theta)$ gate has two important special cases; the *phase gate*, S and the T gate

$$S = \begin{pmatrix} 1 & 0 \\ 0 & i \end{pmatrix}, \quad T = \begin{pmatrix} 1 & 0 \\ 0 & e^{i\pi/4} \end{pmatrix}. \tag{3.7}$$

Another common single-qubit gate we will make use of is the Hadamard gate H. This is represented as

$$H = \frac{1}{\sqrt{2}} \begin{pmatrix} 1 & 1 \\ 1 & -1 \end{pmatrix}, \tag{3.8}$$

This unitary represents a acts to change the computational basis. The Hadamard gate takes the input $|0\rangle$ and outputs $\frac{1}{\sqrt{2}}(|0\rangle + |1\rangle)$ and inputing $|1\rangle$ gives $\frac{1}{\sqrt{2}}(|0\rangle - |1\rangle)$.

Two-qubit gates

In general a controlled unitary operation is one of the form

$$C(U) = \begin{pmatrix} 1 & 0 & 0 & 0 \\ 0 & 1 & 0 & 0 \\ 0 & 0 & \sigma_{11} & \sigma_{12} \\ 0 & 0 & \sigma_{21} & \sigma_{22} \end{pmatrix} \tag{3.9}$$

where the lower right 2×2 matrix is one the Pauli matrices σ_x, σ_y or σ_z. Due to this we sometimes refer to these gates as 'controlled-X', 'controlled-Y' or 'controlled-Z'. Perhaps the most common two qubit gate is the controlled-X which is usually referred to as the controlled-NOT gate. The two qubits involved are labeled the control and target. The state of the target qubit is dependent on the state of the control. The representation is now a 4×4 matrix, the first and second rows correspond to the control qubit while third and fourth are the target.

$$C(X) \equiv CNOT = \begin{pmatrix} 1 & 0 & 0 & 0 \\ 0 & 1 & 0 & 0 \\ 0 & 0 & 0 & 1 \\ 0 & 0 & 1 & 0 \end{pmatrix} \tag{3.10}$$

In the computational basis the action of the CNOT gate is given by

$$CNOT : |x, y\rangle \rightarrow |x, y \oplus x\rangle, \tag{3.11}$$

where $\oplus$ is addition modulo 2. That is, if the control is set to 1 the target bit is flipped, otherwise it is unchanged.

The other two-qubit gate we will consider is the controlled-Z.

$$C(Z) = \begin{pmatrix} 1 & 0 & 0 & 0 \\ 0 & 1 & 0 & 0 \\ 0 & 0 & 1 & 0 \\ 0 & 0 & 0 & -1 \end{pmatrix} \tag{3.12}$$

This acts similarly to the CNOT but instead of performing control dependent bit flips on the target, it performs a π rotation on the target qubit. In the computational basis this is represented as

$$C(Z) : |x, y\rangle \rightarrow (-1)^{xy}|x, y\rangle \tag{3.13}$$

More generally we have the CPHASE gate:

$$C(Z) = \begin{pmatrix} 1 & 0 & 0 & 0 \\ 0 & 1 & 0 & 0 \\ 0 & 0 & 1 & 0 \\ 0 & 0 & 0 & e^{i\theta} \end{pmatrix} \tag{3.14}$$

Which performs general rotations on the target. In order to construct efficient computational systems, we want to find a minimal set of quantum gates that can perform any unitary evolution on a set of input qubits. Such sets of gate are known as *universal gate sets* which, if we have access to, allow for universal quantum computation.

3.1.1 Universality in the qubit model

Universal quantum computers represent the ideal in the field of quantum computation as such devices would be able to implement any desired quantum algorithm. The definition of a universal quantum computer may be stated as follows: A system that applies quantum gates, which correspond to local operations, that effects only a few variables at a time which, by repeated application of such local operations can effect any unitary transformation over a finite number of those variables to any desired degree of precision [70, 71].

A set of gates is said to be *universal* for quantum computation if any unitary operation may be approximated to arbitrary accuracy by a quantum circuit involving only those gates [22, 80]. There are many equivalent set of quantum gates that are universal. The standard universal set for qubits is

$$H,\ S,\ CNOT \text{ and } T \tag{3.15}$$

That is, the combination of the complete set of single qubit gates plus the CNOT is universal for quantum computation. It is important to note that this set is not unique and in fact is usually quite difficult to implement due to the T gate. There are however other two-qubit gates which can be used to form a universal set, most notably the $C(Z)$ gate. Then an equivalent universal set is

$$H,\ R(\theta), \text{ and } C(Z). \tag{3.16}$$

We can see this is equivalent since (3.16) can generate the standard set (3.15). This is easily demonstrated since the application of H to the target

qubit before and after the $C(Z)$ yields the CNOT gate [82]. This concludes our discussion on discrete-variable quantum computation. For further reading and proofs see [22, 23, 81]. Now we turn to the question of quantum computation over continuous-variables. We shall see that though the concept is quite different, we can draw some parallels in terms of gate operations with the qubit model.

3.2 Quantum computation over continuous-variables

The idea for extending quantum computation to the continuous variable regime was originally proposed by Lloyd and Braunstein [13], furthermore, they showed that universal QC over CV can be achieved with a finite number of quantum gates. In the CV approach, the continuous degrees of freedom can be used directly, as we will see in the computational scheme of Chapter 5. Alternatively we can encode finite-dimensional systems within the continuous modes as in the GKP proposal [87]. We will be using a variation on this idea in Chapter 6 to encode qubits into CV resources. We first consider the necessary and sufficient conditions for constructing a universal quantum computer using continuous variables.

3.2.1 Universality in the CV model

To define an arbitrary unitary transformation over even a single continuous variable requires an infinite number of parameters. Such a transformation cannot typically be approximated by any finite number of quantum operations. This would seem to imply that quantum computation over continuous variables is difficult or even impossible to define let alone achieve in a realistic physical setting. However, it is still possible to define a notion of universal computation over continuous variables for some subclasses of transformations, namely those that correspond to Hamiltonians that are polynomial functions of the operators over the continuous variables. With this in mind, we can define our notion of universality:

Definition 1. *A set of continuous quantum operations is termed universal for a particular set of transformations if one can by a finite number of applications of the operations approach arbitrarily closely to any transformation in the set.*

Let us now construct a set of Hamiltonians that allow for universal QC under this definition. Consider a single continuous variable corresponding to dimensionless operator $\hat{q}$, with conjugate variable $\hat{p}$ satisfying $[\hat{q}, \hat{p}] = i$. The simplest Hamiltonians that we must apply are just $\pm\hat{q}$ and $\pm\hat{p}$. The action of these in the Heisenberg picture gives a time evolution for an operator $\hat{A}$ given by

$$\hat{A}(t) = e^{iHt} A(0) e^{-iHt}, \tag{3.17}$$

Then performing the Hamiltonian $\hat{q}$ for a time t enacts the transformations $\hat{q} \to \hat{q}$, $\hat{p} \to \hat{p} + \frac{t}{2}$, similarly applying $\hat{p}$ gives $\hat{p} \to \hat{p}$, $\hat{q} \to \hat{q} + \frac{t}{2}$. The effect of these Hamiltonians is to shift the conjugate variables by a constant. These Hamiltonians are very limited, to find more interesting behaviour we require higher orders in $\hat{q}$ and $\hat{p}$. The lemma below gives us a method by which to find all the possible allowed Hamiltonians.

Lemma 3.2.1. *The only Hamiltonians it is possible to construct are those in the algebra generated from the original set by commutation.*

Let us apply this result to find a useful set of Hamiltonians. First, just performing displacement operations $\pm\hat{q}$ and $\pm\hat{p}$ for short periods of time allows for the construction of any Hamiltonian of the form $a\hat{q} + b\hat{p} + c$. However, this only yields linear transformations. For the purposes of universal computation this is clearly insufficient and we have to postulate higher order Hamiltonians. To that end, assume we can apply,

$$H_1 = \hat{q}^2 + \hat{p}^2. \tag{3.18}$$

Applying this Hamiltonian for time t makes the transformation

$$\begin{aligned} \hat{q} &\to \cos t\hat{q} - \sin t\hat{p}, \\ \hat{p} &\to \cos t\hat{p} + \sin t\hat{q} \end{aligned} \tag{3.19}$$

In our electromagnetic field example, such an operation corresponds to a phase shift. The commutation relations between H_1, $\hat{q}$ and $\hat{p}$ imply that the addition of H_1 allows Hamiltonians of the form $aH_1 + b\hat{q} + c\hat{p} + d$ to be generated.

We can also assume another type of quadratic Hamiltonian H_2 defined by

$$H_2 = \hat{q}\hat{p} + \hat{p}\hat{q}. \tag{3.20}$$

This has quite a different effect on the canonical variables. H_2 gives the transformations

$$\begin{aligned} \hat{q} &\to e^t\hat{q}, \\ \hat{p} &\to e^{-t}\hat{p}. \end{aligned} \tag{3.21}$$

We recognize this as the squeezing operation, stretching $\hat{q}$ while squeezing $\hat{p}$. We find the commutation relation between H_1 and H_2 is

$$[H_1, H_2] = 2i(\hat{q}^2 - \hat{p}^2) \tag{3.22}$$

which gives us a further form of quadratic operation. In fact, the algebra generated from $\hat{q}$, $\hat{p}$, H_1 and H_2 by commutation, allows the construction of any Hamiltonian that is quadratic in $\hat{q}$ and $\hat{p}$ though importantly, none of higher order.

To find higher order Hamiltonians, we require non-linear effects. One example is the *Kerr* Hamiltonian

$$H_K = (\hat{q}^2 + \hat{p}^2)^2. \tag{3.23}$$

In our optical scenario, this would correspond to a $\chi^{(3)}$ non-linear process. This Hamiltonian has the useful property that commuting it with a polynomial in $\hat{q}$ and $\hat{p}$ increases its order. One can see this by evaluating the commutators,

$$\begin{aligned}
[H_K, \hat{q}] &= -2i(\hat{q}^2\hat{p} + \hat{p}^3) + \text{lower order terms}, \\
[H_K, \hat{p}] &= -2i(\hat{q}\hat{p}^2 + \hat{q}^3) + \text{lower order terms}, \\
[\hat{q}, [H_K, H_2]] &= -8\hat{p}^3 + \text{lower order terms}, \\
[\hat{p}, [H_K, H_2]] &= 8\hat{q}^3 + \text{lower order terms},
\end{aligned} \tag{3.24}$$

we can see that the algebra that we generate with the addition of H_2 includes all third order polynomials in $\hat{q}$ and $\hat{p}$. With these operations, we can prove the following:

Theorem 3.2.2. *The algebra generated from commutation of the Hamiltonians $\hat{q}$, $\hat{p}$, H_1, H_2 is sufficient to construct Hamiltonians of arbitrary order in $\hat{q}$ and $\hat{p}$.*

Proof. Suppose we can construct a polynomial of order M consisting of any specific term

$$\hat{q}^{M-n}\hat{p}^n, \tag{3.25}$$

for $M \geq n$. Since we may create any quadratic Hermitian Hamiltonian and since

$$\begin{aligned}
[\hat{q}^2, \hat{q}^{M-n}\hat{p}^n] &= i\frac{n}{2}\hat{q}^{(M-n+1)}\hat{p}^{n-1} + \text{lower order terms}, \\
[\hat{p}^2, \hat{q}^{M-n}\hat{p}^n] &= -i\frac{M+n}{2}\hat{q}^{(M-n-1)}\hat{p}^{n+1} + \text{lower order terms}
\end{aligned} \tag{3.26}$$

then we see that we can create all polynomials of order M. □

A useful extension to this that we will be using extensively later it that by commutation of $\hat{q}^3$ and $\hat{p}^3$ with monomials of order M we can construct any monomial of order $M+1$. Since any polynomial of order $M+1$ can be constructed from monomials of order $M+1$ and lower by applying linear operations and a single non-linear operation a finite number of times one can construct polynomials of arbitrary order in $\hat{q}$ and $\hat{p}$ to any desired degree of accuracy. Then the use of the Kerr Hamiltonian was not essential, we can use any Hamiltonian that is higher than quadratic order. In particular, commutation of $\hat{q}$, $\hat{p}$, H_1, H_2 and a Hamiltonian of order three (or higher)

allows for the construction of arbitrary Hermitian polynomials of any order in $\hat{q}$ and $\hat{p}$.

To summarize, we have seen that simple linear operations, together with a single non-linear operation, allow one to construct a arbitrary polynomial Hamiltonian transformations on a single quantum variable. We will be using this result to form the universal set of gates for CV computation, but first we have to consider the case where we allow different modes to interact.

Suppose we have multiple variables, $\{\hat{q}_i, \hat{p}_i\}$, on which, the operations described above can be performed. Now we allow the variables to interact. Let us assume we can apply the interaction Hamiltonian $\pm B_{ij}$ defined by

$$B_{ij} = (\hat{p}_i \hat{q}_j - \hat{q}_i \hat{p}_j). \tag{3.27}$$

By restating this Hamiltonian in terms of creation/annihilation operators we recognize this as the beam-splitter interaction. A more complicated interaction can be enacted by simply performing appropriate single mode operations on modes i and j. The Hamiltonian affects the following transformation

$$\begin{aligned} \hat{A}_i &\to \cos t\hat{A}_i + \sin t\hat{A}_j, \\ \hat{A}_j &\to \cos t\hat{A}_j - \sin t\hat{A}_i \end{aligned} \tag{3.28}$$

where $\hat{A}_i = \{\hat{q}_i, \hat{p}_i\}$ and $\hat{A}_j = \{\hat{q}_j, \hat{p}_j\}$. By repeatedly taking commutators of B_{ij} with polynomials in $\hat{q}_i$ and $\hat{p}_j$, for different i, then it is possible to build up arbitrary Hermitian polynomials in $\{\hat{q}_i, \hat{p}_i\}$.

Then we can conclude that simple linear operations on continuous variables, together with any nonlinear operation and some interaction between different variables suffice to enact arbitrary Hamiltonians to a given degree of accuracy. This concludes our discussion on the requirements for a universal CV quantum computer. Now we can look at the specific encodings and gate operations that perform these Hamiltonians.

3.3 Encoding information in CV systems

The basic unit of quantum information in continuous variables is known as a *qumode*, which correspond physically to the quadrature states of the CV system. Then this is a system described by an infinite-dimensional Hilbert space spanned by a continuum of orthogonal states labeled $|s\rangle_q$, where $s \in \mathbb{R}$. We define the conjugate basis states over the conjugate canonical variable$|s\rangle_p$. Then both bases satisfy the standard orthogonality conditions associated with the quadrature states,

$${}_q\langle r|s\rangle_q = \delta(r-s), \quad {}_p\langle r|s\rangle_p = \delta(r-s), \tag{3.29}$$

and the bases are related by a Fourier transform:

$$|s\rangle_p = F|s\rangle_q = \frac{1}{2\pi}\int_{-\infty}^{\infty} dr e^{irs}|r\rangle_q,$$
$$|s\rangle_q = F^\dagger|s\rangle_p = \frac{1}{2\pi}\int_{-\infty}^{\infty} dr e^{-irs}|r\rangle_p \tag{3.30}$$

These relations define the first of our CV operators, the unitary operator F. From the definition of our quadrature states, Eq.2.22, applying $\hat{p}$ generates positive position translations while, $-\hat{q}$ is the generator for positive momentum translations. We can write an arbitrary position and momentum eigenstates as

$$|s\rangle_q = X(s)|0\rangle_q, \quad |s\rangle_p = Z(s)|0\rangle_p, \tag{3.31}$$

where the translation operators are given by $X(s) = e^{-is\hat{p}}$ and $Z(s) = e^{is\hat{x}}$ producing displacements in the computational and conjugate spaces respectively. These operators generate the Heisenberg-Weyl (HW) group of phase space displacements. An arbitrary pure quantum state $|\phi\rangle$ of a CV system may be decomposed as a superposition of either $|s\rangle_q$ or $|s\rangle_p$.

A qumode is a minimum uncertainty state if the product of the quadrature deviations $\Delta\hat{q}$ and $\Delta\hat{p}$ satisfies

$$\Delta\hat{q}\Delta\hat{p} = \frac{1}{2} \tag{3.32}$$

The ground state $|0\rangle$ is defined by $\hat{a}|0\rangle = 0$ is of particular interest. It represents a Gaussian superposition centered about 0 in either the computational or conjugate basis,

$$|0\rangle = \frac{1}{\pi^{1/4}}\int ds\ e^{-s^2/2}|s\rangle_q = \frac{1}{\pi^{1/4}}\int ds\ e^{-s^2/2}|s\rangle_p. \tag{3.33}$$

The vacuum state is a specific example of the Gaussian states that we described in the previous Chapter 2. The vacuum state is often used in computational protocols as the initial state of the physical resources.

3.4 Continuous variable quantum gates

Having derived the necessary set of Hamiltonians for our CV computer, we state the corresponding CV quantum gates. As with the qubit case, we only require a finite set of theses gates to implement universal operations. These gates may be thought of as a CV analog of the Pauli gates which perform bit-flips, phase-flips or a combinations of these. The CV equivalent of the Pauli operators are the Heisenberg-Weyl operators

$$X(s) = e^{-is\hat{p}}, \quad Z(t) = e^{it\hat{q}}, \tag{3.34}$$

for $s, t \in \mathbb{R}$. These operators are non-commutative and obey

$$X(s)Z(t) = e^{-ist}Z(t)X(s) \tag{3.35}$$

On the computational basis these act as

$$X(t)|s\rangle = |s+t\rangle, \quad Z(t)|s\rangle = e^{ist}|s\rangle. \tag{3.36}$$

The Fourier transform F is the CV analogue of the Hadamard transformation. It is defined as

$$F = e^{i\pi(\hat{q}^2+\hat{p}^2)/2} \tag{3.37}$$

its action on the Pauli operators is

$$\begin{aligned} F : X(s) &\to Z(s) \\ Z(t) &\to X(t)^{-1}. \end{aligned} \tag{3.38}$$

The phase-gate $P(\eta)$ is the squeezing operation defined by

$$P(\eta) = e^{i\eta\hat{q}^2} \tag{3.39}$$

with action on the Pauli operators

$$\begin{aligned} P(\eta) : X(s) &\to e^{i\eta\hat{q}^2}X(s)Z(\eta s), \\ Z(s) &\to Z(s), \end{aligned} \tag{3.40}$$

which is the analogue of the discrete variable phase gate. Finally, we require multi-mode operation. We choose the SUM gate which is the CV analogue of the CNOT. This provides the basis interaction between CV modes i and j and is defined by

$$\mathrm{SUM}_{ij} = e^{-i\hat{q}_i \otimes \hat{p}_j}. \tag{3.41}$$

The action of this two-mode gate on the Pauli operators is given by

$$\begin{aligned} \mathrm{SUM}_{ij} : & X_i(s) \otimes \mathbf{1}_j \to X_i(s) \otimes X_j(s), \\ & Z_i(t) \otimes \mathbf{1}_j \to Z_i(t) \otimes \mathbf{1}_j, \\ & \mathbf{1}_i \otimes X_j(s) \to \mathbf{1}_i \otimes X_j(s), \\ & \mathbf{1}_i \otimes Z_j(t) \to Z_i(t)^{-1} \otimes Z_j(t) \end{aligned} \tag{3.42}$$

This gate describes a quantum non-demolition interaction since there is no back-action on the control state due to the target.

These CV operations are sufficient to simulate all possible quadratic Hermitian Hamiltonians as we saw from our proof above. However, by the Gottesman-Knill theorem for CV computation [106] these on there own do not provide any speedup over classical computation. In order to gain an advantage over classical simulation one must include a gate described by a

Hamiltonian of higher than quadratic order. Transformations generated by these Hamiltonians do not preserve linear structure of the generators and are much harder to deal with mathematically. In particular, higher order operations are not Gaussian maps and so when dealing with such operators is it no longer sufficient to apply our symplectic description of states as the function may acquire higher order moments.

3.5 Summary of CV computational operations

Here we have derived a set of quantum gates that are universal for CV quantum computation. Further, from the CV Gottesman-Knill theorem, it is possible to show that a universal gate set provides a speed up over classical computation. The set of CV gates that we use later in this thesis to test the universality of certain computational systems is

$$X(s),\ Z(t),\ P(\eta),\ F,\ \text{SUM and}\ V(\gamma), \tag{3.43}$$

where $V(\gamma) = e^{i\gamma\hat{q}^3}$ is known as the cubic phase gate. This is the nonlinear element that allows us to generate higher order Hamiltonians. In terms of the Gaussian transformations from the previous chapter, we note that all but the $V(\gamma)$ gate are Gaussian operations and are fully represented by modification of the second moments of the Gaussian states. However the cubic gate, which is required for universality cannot be decomposed into Gaussian transformations, this is a non-Gaussian element and cannot be represented by just transforming first and second moments of the Gaussian states. Such gates have proved difficult to enact in practice, however there have been various proposals put forward [83, 84].

Chapter 4

Continuous-variable cluster states

In this chapter we present the first of our alternatives to the standard circuit model of quantum computation, known as the *Measurement-Based model of Quantum Computation* (MBQC). Within this quantum computational paradigm all basic dynamical operations are performed by making measurements on a specially prepared multi-partite entangled state. Remarkably, the measurement-based scheme can simulate arbitrary quantum dynamics, including unitary dynamics. Here we focus on a class of measurement-based models proposed by Raussendorf and Briegel [89], the so-called *cluster state* model or *one-way quantum computer*. The cluster state model has a remarkably rich structure which differs substantially from the conventional unitary model of quantum computing. The differences have led to new insights into computational complexity [90], and to dramatic simplifications in experimental proposals for quantum computation [103, 92].

In the following we give a brief overview of the formalism of the measurement-based model. We begin by defining the special classes of entangled states that form the substrate for the one-way model. We extend out treatment to include finitely squeezed or Gaussian states and show how these Gaussian states can be modified through unitary operations and measurements. This leads us to the main subject of this Chapter, the generation of Gaussian cluster states from optical and atomic components. To accomplish this we derive certain interactions that allow atomic and light modes to couple together. Having established a set of interactions, we give explicit protocols for the generation of several types of atomic/light cluster. We go on to examine a fundamental barrier to the MBQC model over continuous-variables and suggest an alternative architecture for cluster state computing based on the resources that we have developed.

4.1 Cluster States

The measurement-based model relies on the creation of cluster states, which act as a universal substrate with quantum information encoded virtually within them. Though originally based on qubits, the cluster model has been generalized to higher dimensional discrete-variable systems (qudits) [93] as well as to continuous-variables [94]. The term cluster state, refers to a family of quantum states defined by mathematical graphs. That is, for some graph G on n vertices we can define an associated n-mode cluster state Then each vertex of the graph corresponds to a quantum system, and then applying a graph dependent preparation procedure to the quantum modes we generate entanglement between the modes. The correlations due to entanglement are represented by the edges of the graph, see Fig. (4.1). For a general introduction to the mathematical formalism of graphs see [95].

The original cluster state construction, based on qubits is defined on an undirected, unweighted graph $G = (V, E)$, having no self loops are constructed as follows. For each vertex of G, we initialize a qubit in the state $|+\rangle = (|0\rangle + |1\rangle)/\sqrt{2}$. For every edge in G linking two vertices, we apply a $C(Z)$ gate to the two corresponding qubits. Any unitary operation can be implemented on a tailor-made graph state using an appropriate sequence of single-qubit measurements.

However, dealing with the state function directly is rather cumbersome due to the large number of modes involved. Then rather than dealing with the states directly we turn to the stabilizer formalism [96]. Stabilizers provide an efficient way to represent any graph state. We say a state $|\phi\rangle$ is stabilized by an operator K if it is an eigenstate of K with unit eigenvalue, that is $K|\phi\rangle = |\phi\rangle$. It turns out that the set of stabilizers form an Abelian group under operator multiplication and if such a set exists for a given state, then we call that state a stabilizer state. The generators of the stabilizer group can then be used to uniquely define the state they stabilize. The stabilizers for qubit graph states are well known [89]. Given that $|\phi\rangle$ is an n-qubit graph state with associated graph $G = (V, E)$, it is stabilized by

$$K_i = X_i \prod_{j \in N(i)} Z_j \tag{4.1}$$

where $N(i)$ denotes the set of indices that define the set of vertices that neighbor v_i, i.e., $N(i) = \{j | (v_j, v_i) \in E\}$. The operators X and Z are the usual Pauli operators for qubits.

4.1.1 Continuous-Variable Graph States

In analogy to the qubit clusters, continuous-variable graph states can be used as resources for universal CV quantum computation [94]. In order to describe these states we introduce the nullifier formalism which is a variation

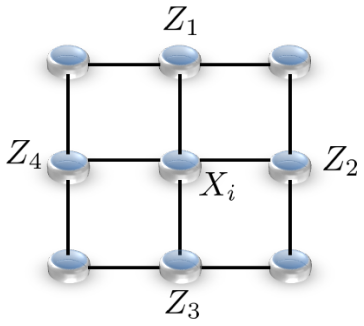

Figure 4.1: A representation of a nine-qubit cluster state. The qubits (blue circles) are entangled (black lines) to form a large multi-partite resources state. The cluster state is defined by its stabilizer operators. Node i is stabilized by $K_i = X_i Z_1 Z_2 Z_3 Z_4$.

on the CV stabilizers [29, 97]. These allow us to see how to compute how CV graph states transform under quadrature measurements.

To generalize to CV graph states we effectively replace elements of qubit cluster-state computation with their CV analogues: $|+\rangle$ becomes $|0\rangle_p$. The measurements that we make on the CV cluster are of $\hat{p}$ and $\hat{x}$ [1]. We can also perform the $C_Z = e^{i\hat{x}_i\hat{x}_j}$ gate, which entangles nodes i and j in analogy with the $C(Z)$ gate. As before each CV graph can be described by a graph $G = (V, E)$, where the set of vertices V corresponds to the individual qumodes, and the edge set E determines which qumodes interact via the C_Z operation. At the moment we consider only unweighted graphs (or equivalently, graphs where the edges weights are all $+1$).

4.1.2 Continuous-variable stabilizers and nullifiers

We can carry our analogy further by defining the stabilizer formalism for CV systems. This can be used to specify any CV graph state completely [100]. A zero-momentum eigenstate $|0\rangle_p$ is stabilized by $X(s)$ for all s, since it is a $+1$-eigenstate of those operators. This holds even though $X(s)$, being non-Hermitian, is not an observable. Mathematically, if K stabilizes $|\phi\rangle$, then $UKU^\dagger$ stabilizes $U|\phi\rangle$. This observation, together with the relation

$$e^{i\hat{x}_1\hat{x}_2}\hat{p}_1 e^{-i\hat{x}_1\hat{x}_2} = \hat{p}_1 - \hat{x}_2, \tag{4.2}$$

[1] For the remainder of this thesis we make the switch $\hat{q} \to \hat{x}$ for our position operator. This is to remain consistent with publications and make a separation between introductory material and new work.

which gives us the effect of applying a C_Z gate on some mode of the graph. Applying this to the next connected mode yields,

$$e^{i\hat{x}_1\hat{x}_3}e^{i\hat{x}_1\hat{x}_2}\hat{p}_1e^{-i\hat{x}_1\hat{x}_2}e^{-i\hat{x}_1\hat{x}_3} = \hat{p}_1 - \hat{x}_2 - \hat{x}_3. \tag{4.3}$$

Continuing in this manner we see how to write the stabilizers for an arbitrary CV graph state $|\phi\rangle$ on n qumodes with graph G:

$$K_i(s) = X_i(s) \prod_{j\in N(i)} Z_j(s), \quad i = 1, ..., n \tag{4.4}$$

for all $s \in \mathbb{R}$ and $N(i)$ is as above.

This group of CV stabilizers is described by its Lie algebra, the space of operators H such that $H|\phi\rangle = 0$. We refer to any element of this algebra as a *nullifier* of $|\phi\rangle$ and the entire algebra as the *nullifier space* of $|\phi\rangle$. The nullifier space of an n-qumode graph state $|\phi\rangle$ with graph $G = (V, E)$ is an n-dimensional vector space spanned by the following Hermitian operators:

$$H_i = \hat{p}_i - \sum_{j\in N(i)} \hat{x}_j, \quad i = 1, ..., n. \tag{4.5}$$

That is, any linear superposition $H = \sum_i c_i H_i$ satisfies $H|\phi\rangle = 0$. Note that $[H_i, H_j] = 0$ for all (i, j). This definition of the nullifiers relies on the creation of zero-momentum eigenstates, i.e., infinite squeezing of the initial resource states is required. Later, we will expand this definition to include non-ideal clusters that are created from Gaussian states.

We can compactly state the nullifiers of a cluster state in terms of the adjacency matrix, A, of the underlying graph [99].

$$(\hat{\mathbf{p}} - A\hat{\mathbf{x}})|\phi\rangle. \tag{4.6}$$

Where $\hat{\mathbf{p}}$ and $\hat{\mathbf{x}}$ are vectors of the momenta and positions of all the qumodes of the graphs. The entries of the adjacency matrix correspond to interactions between between modes. For unweighted graphs all the entries are either 0, which indicates no entanglement between modes, or 1 which corresponds to a edge between a pair of qumodes.

4.2 Quantum computation on CV graph states

Here we will show how the CV graph states we defined above can be used to perform measurement-based CV quantum computation. It is known that for any given CV unitary U, and any given input $|\phi\rangle$, there exists an appropriate graph state such that by entangling the graph state locally with $|\phi\rangle$ and applying an appropriated sequence of single-mode measurements $U|\phi\rangle$ is computed [29].

To implement any unitary operation on k qumodes, we apply the following algorithm. First, introduce a graph G. We designate k vertices of G as input vertices, and another set as output. Call these sets V_{in} and V_{out}. Note that the input/output sets may overlap. Then the following algorithm computes $U|\phi\rangle$:

- The qumodes corresponding to the vertices in V_{in} encode the input state $|\phi\rangle$, while the qumodes corresponding to the other vertices are each initialized in the state $|0\rangle_p$.
- For each edge $(v_j, v_k) \in E$, apply $C_Z = e^{i\hat{x}_j\hat{x}_k}$ between vertices j and k. Since all C_Z operations commute, their order does not matter.
- Measure each vertex v_i for all $v_i \notin V_{out}$ in a basis of the form $M_i = e^{-if_i(\hat{x})}\hat{p}e^{if_i(\hat{x})}$, where $f_i(\hat{x})$ is in general, a polynomial of $\hat{x}$. The exact form of each f_i is dictated by the unitary we wish to implement and the result of measurements on prior modes. Without loss of generality, we can label the vertices such that they are measured in numerical order.
- The remaining unmeasured qumodes encode $U|\phi\rangle$, modulo known single-mode rotations and translations.

This algorithm may be implemented by using an appropriate graph state as a resource. This algorithm is universal, that is, given an appropriate graph G and the ability to designate $V_{in}, V_{out} \subseteq V$, such that the algorithm implements U.

4.2.1 Quantum gates

We consider how each of the CV quantum gates may be implemented via measurements on CV cluster states. Note that $s \in \mathbb{R}$ throughout our analysis.

Gaussian operations

Quadrature displacements: These are implemented by measuring $\hat{p}_{s\hat{x}} = p + s$ which is equivalent to measuring $\hat{p}$ and adding on some s that we want to displace it by. There is no dependence on previous measurements since $\hat{p}_{s(\hat{x}+m)}$ is also equal to $\hat{p} + s$ and so no adaption is required.
Shears: Shears, given by $e^{is\hat{x}^2}$ correspond to measurements in the basis $\hat{p}_{s\hat{x}^2/2} = \hat{p} + s\hat{x}$. In this case adaptation for previous measurements is required. The new measurement basis is of the form $\hat{p}_{s(\hat{x}+m)^2/2} = \hat{p} + s\hat{x} + ms$, which differs from the original basis only by a measurement-dependent constant. This can be accounted for trivially by measuring in the original basis and adding ms to the result.
Fourier transform: The Fourier transform F is obtained for free simply

through the Gaussian correction applied with each measurement (see Appendix).
Controlled phase gate: The controlled phase is almost trivially performed since any two vertex graph is connected by a C_Z operation so we just label the nodes as both input and output and no measurement is required.

Non-Gaussian Operations

As we showed in the previous chapter, the only non-Gaussian operation we require for universality is the cubic phase gate. Any higher order unitary may be implemented by the cubic phase in combination with the Gaussian gates.
Cubic phase: The cubic phase gate, $e^{is\hat{x}^3}$, may be performed on the cluster by measuring in the basis $\hat{p}_{s\hat{x}^3/3} = \hat{p} + s\hat{x}^2$. This gate has the effect of changing the physical basis to $\hat{p}_{s(\hat{x}+m)^3/3} = \hat{p} + s\hat{x}^2 + \frac{2}{3}ms\hat{x} + \frac{1}{3}m^2s$ due to the presence of the non-commuting m dependent term $2ms\hat{x}/3$. This difference requires physically changing the basis of measurement. A general CV computation will require adaptive measurements for the non-Gaussian part of the computation. As to what these measurements correspond to depends greatly on the physical context.

4.3 Gaussian CV cluster states

Until now we have only considered cluster states with perfect correlations. That is, we have assumed the presence of momentum eigenstates to construct our states which are highly unphysical, requiring infinite squeezing and hence infinite energy to produce. However, all is not lost. The graph representation of a Gaussian pure state defined above yields a natural way to extend the graph representation of ideal CV cluster state to their finitely squeezed Gaussian approximants.

Here we examine the construction of CV clusters in detail with an aim to relaxing the infinite squeezing condition. To accomplish this we have to find a set of stabilizers and nullifiers for finite squeezed Gaussian clusters [99].

4.3.1 Stabilizers for Gaussian pure states

To find the stabilizer operators for the finitely squeezed canonical CV cluster states we must first find the stabilizer of the vacuum state $|0\rangle$ of a qumode $\hat{a}_k$. Then from this we may find the stabilizer for the momentum squeezed vacuum and then construct the cluster state stabilizer by entangling the momentum eigenstates with a set of C_Z gates.

Then for the operators $\hat{x}$ and $\hat{p}$, where $\hat{a} = \frac{1}{\sqrt{2}}(\hat{x} + i\hat{p})$, we have the vacuum stabilizer,

$$|0\rangle = \exp(\alpha \hat{a}_k)|0\rangle = \exp\left[\frac{\alpha}{\sqrt{2}}(\hat{x}_k + i\hat{p}_k)\right]|0\rangle. \tag{4.7}$$

We can find the stabilizer for a single-mode squeezed state by applying the squeezing operator, $\hat{S}(r_k) = \exp[\frac{i}{2} r_k(\hat{x}_k\hat{p}_k + \hat{p}_k\hat{x}_k)]$, with a squeezing parameter $r_k > 0$, to the vacuum state. The stabilizer equation can be written as

$$\begin{aligned}\hat{S}(r_k)|0\rangle &= \hat{S}(r_k)\exp\left[\frac{\alpha}{\sqrt{2}}(\hat{x}_k + i\hat{p}_k)\right]\hat{S}^\dagger(r_k)\hat{S}(r_k)|0\rangle \\ &= \exp\left[\frac{\alpha}{\sqrt{2}}(e^{+2r_k}\hat{x}_k + ie^{-2r_k}\hat{p}_k)\right]\hat{S}(r_k)|0\rangle \end{aligned}\tag{4.8}$$

We can also find the momentum squeezed state, $\hat{S}(-r_k)$,

$$\begin{aligned}\hat{S}(-r_k)|0\rangle &= \hat{S}(-r_k)\exp\left[\frac{\alpha}{\sqrt{2}}(\hat{x}_k + i\hat{p}_k)\right]\hat{S}^\dagger(-r_k)\hat{S}(-r_k)|0\rangle \\ &= \exp\left[\frac{\alpha}{\sqrt{2}}(e^{-2r_k}\hat{x}_k + ie^{+2r_k}\hat{p}_k)\right]\hat{S}(-r_k)|0\rangle \end{aligned}\tag{4.9}$$

Note that the exponential terms can be rewritten as phase-space displacements, $X(s) = e^{-is\hat{p}}$ and $Z(s) = e^{is\hat{x}}$.

$$\hat{S}(-r_k)|0\rangle = \exp\left(-\frac{1}{4}\alpha^2\right) X_k\left(-\frac{\alpha}{\sqrt{2}}e^{+2r_k}\right) Z_k\left(-i\frac{\alpha}{\sqrt{2}}e^{-2r_k}\right), \tag{4.10}$$

Now define $\alpha = -\sqrt{2}e^{-2r_k}s$ such that the momentum squeezed stabilizer becomes

$$\exp\left(\frac{1}{2}e^{-2r_k}s^2\right) X_k(s)Z_k(ie^{-2r_k}s). \tag{4.11}$$

Of course in the limit of infinite $\hat{p}$-squeezing ($r_k \to \infty$), this approaches $X_k(s)$. This stabilizes the infinite squeezed eigenstate $|0\rangle_{p_k}$, with $X_k(s)|0\rangle_{p_k} = |0\rangle_{p_k}$, for all $s \in \mathbb{R}$ as expected.

Now we can construct a CV cluster state in the usual way, that is, applying C_Z gates between pairs of modes, indicated by C_Z^{kl} between nodes k and l. The N stabilizers of the initial N momentum-squeezed modes, Eq.(4.11), with $k = 1, 2, ..., N$, are then transformed for each interaction with neighbour l as

$$\begin{aligned}&\exp\left(\frac{1}{2}e^{-2r_k}s^2\right) C_Z^{kl}X_k(s)C_Z^{kl\dagger}C_Z^{kl}Z_k(ie^{-2r_k}s)C_Z^{kl\dagger} \\ &\quad = \exp\left(\frac{1}{2}e^{-2r_k}s^2\right) X_k(s)Z_l(s)Z_k(ie^{-2r_k}s). \end{aligned}\tag{4.12}$$

Eventually, collecting all these interactions, we obtain the N new stabilizers

$$\exp\left(-\frac{1}{2}e^{-2r_k}s^2\right) X_k(s)Z_k(ie^{-2r_k}s) \prod_{l\in N(k)} Z_l(s), \tag{4.13}$$

where $N(k)$ is the set of neighbours of k. In the limit of infinite squeezing, we get back the well known, ideal CV cluster state stabilizers for unweighted graphs. However, this time, the stabilizers represent an approximate cluster state. The nullifiers are found by taking the log of the stabilizers:

$$\begin{aligned}
&\exp\left(-\frac{1}{2}e^{-2r_k}s^2\right) X_k(s)Z_k(ie^{-2r_k}s) \prod_{l\in N(k)} Z_l(s) \\
&\quad= \exp\left(-\frac{1}{2}e^{-2r_k}s^2\right) \exp[-is(\hat{p}_k - ie^{-2r_k}\hat{x}_k)] \exp\left(\frac{1}{2}e^{-2r_k}s^2\right) \prod_{l\in N(k)} \exp(is\hat{x}_l) \\
&\quad= \exp\left[-is\left(\hat{p} - ie^{-2r_k}\hat{x}_k - \sum_l \hat{x}_l\right)\right],
\end{aligned} \tag{4.14}$$

for all $k = 1, 2, ..., N$ and for all $s \in \mathbb{R}$. The nullifiers are therefore

$$\hat{p}_k - ie^{-2r_k}\hat{x}_k - \sum_{l\in N(k)} \hat{x}_l, \quad \forall k. \tag{4.15}$$

The corresponds to the complex nullifier

$$(\hat{p} - Z\hat{x})|\psi_Z\rangle = 0 \tag{4.16}$$

with complex adjacency matrix Z having imaginary diagonal entries ie^{-2r_k} and the remaining entries begin either 0 or 1 depending of the particular CV cluster state with unweighted edges. These diagonal elements correspond to complex weighted self-loops at each vertex of the graph. This result now allows us to deal with Gaussian cluster states in much the same way as their ideal counterparts, except now we have to keep track of the imaginary part corresponding to the self-loop.

4.3.2 Transformation Rules

In this section we will derive the rules for updating a graph after a quadrature measurement is made which will be of key importance in Chapters 5 and 6 to create ground states with topological properties. We will be making use of the ideal and the Gaussian clusters so we must be clear how to perform transformations for both cases.

The first thing when considering quadrature measurements is to define the nullifier that corresponds to the measurement outcome. This is the new nullifier that the post-measurement state must satisfy due to the projection

onto the measurement basis. Next we choose an appropriate invertible matrix M such that the entries in the new (ideal) nullifier vector $M\hat{p} - MV\hat{x}$ are such that only one of them fails to commute with the nullifier corresponding to the new measurement. This new nullifier vector also uniquely defines the pre-measurement state (since M is invertible), but because only one of the entries fails to commute with the measurement nullifier, all the remaining ones will also be nullifiers for the post-measurement state as well. The one that fails to commute is therefore discarded and replaced by the measurement nullifier to form the post-measurement nullifier vector [29].

All this still holds for complex nullifiers. For x-measurements on a mode j with outcome s_j means that the new state has $x_j - s_j$ as one of the nullifiers. However, since we are neglecting displacements, the post-measurement state will instead have x_j as the measurement nullifier. The usual nullifier for a Gaussian graph Z is $p - Zx$, from which we can see that all nullifiers commute with x_j except the j^{th} one.

The measurement of $\hat{x}$ on an ideal CV cluster state corresponds to deletion of the measured node from the cluster, along with all of its links, see Fig.(4.2(a)). The effect is the same on Gaussian graphs and can be seen in the nullifier formalism in that all references to p_j are gone, and linear combinations of the post-measurement nullifiers can be used to delete all references to x_j, as well. As an action on the adjacency matrix Z, this corresponds to deleting its j^{th} row and column.

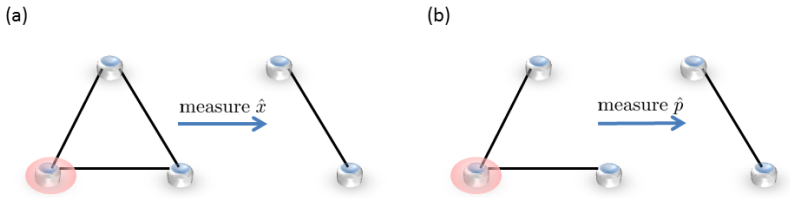

Figure 4.2: (a) A projective measurement of $\hat{x}$ on some node of the cluster state (Red) removes that node and all connections to it. (b) A projective measurement of $\hat{p}$ on some node of the cluster state removes that node but leaves the entanglement between the new nearest neighbours intact.

Measuring in p deletes the corresponding node but preserves the links between neighbouring nodes, up to local phase shifts (Fig.(4.2(b))). Due to the phase shifts, the resulting state is often impossible to represent as an ideal CV cluster state graph, but we can do it easily for approximate CV cluster states as a two step process: (1) perform an inverse Fourier

transform on the node to be measured. (2) Perform a x-measurement as described above, thereby deleting it and its links from the graph. This is not equivalent in total to a simple disconnection, however, because the phase shift generates additional connections in the neighbourhood of the measured node before the node is disconnected. This is the mechanism by which the links after a p-measurement are preserved even when the node is deleted.

4.4 Construction of continuous variable cluster states

In the following we present the main results of this chapter. We will show first how to generate Gaussian cluster states composed of ensembles of atoms, where each ensemble represents a qumode of the state. We then investigate how to include light modes to our atomic clusters to form *composite clusters*. These composite states lead us to consider an alternative architecture for MBQC that can reduce experimental overheads and errors due to entanglement loss.

There are many known protocols for the construction of Gaussian clusters. These mainly focus on optical clusters, where each qumode is a light pulse that is described by some continuous parameter. Such schemes include, the linear optical construction [27], the single optical parametric oscillator (OPO) method [31] and single quantum non-demolition (QND)-gate schemes [32, 33]. These are experimentally advantageous as they are deterministic, unlike the discrete variable counterparts which rely on nondeterministic interactions and postselection, [103, 104, 105]. However, as with any CV system, these protocols suffer the usual problems such as the lack of infinitely squeezed resources leading to finite squeezing errors.

Here our analysis will follow the canonical generation method discussed above. In this method the cluster states are created from single-mode squeezers and controlled-Z (C_Z) gates [94]. The controlled-Z is an example of a QND interaction and, for optical modes, can be implemented using beamsplitters and inline or offline squeezers [106, 107, 108]. This method, while experimentally challenging is achievable with current technology [109].

CV cluster states can be built, not only from optical modes but also from ensembles of polarized atoms where each ensemble is a different CV mode [110, 111, 35, 36]. The ensembles are entangled by performing interactions with off-resonant linearly polarized light, which, on the classical level, performs a Faraday rotation. The rotated light then serves as a carrier to encode information in each of the ensembles and homodyne measurements are performed to complete the protocol and project the state of the ensembles into the desired entangled state. We will begin by deriving this interaction and noting its behaviour on both a classical and quantum level. First though, we have to examine the physical systems involved in our interaction.

4.5 Quantum variables for Atoms and Light

In this section we introduce the quantum variables for light and atoms and describe an off-resonant dipole atom-light interaction which is applicable to such transitions as the $6S_{1/2}$ ground state to the excited $6P_{3/2}$ state in cesium. We use collective spin operators for atoms and Stokes operators for light as a convenient way to describe the interaction. The interaction has been investigated semi-classically in [138] and the quantum mechanical interaction Hamiltonian was derived for spin 1/2 systems in [130]. The interaction Hamiltonian for the realistic $F = 4$ system taking the complete level structure into account was derived in [114]. Here we will briefly review the interaction from both a classical and quantum perspective. We will then present the general effective Hamiltonian which describes the dynamics of the ground state spin and the polarization of the light. From this we derive the equations of motion for the light and atomic operators. We will find that the spin component along the direction of light propagation is mapped to the light without being perturbed by the interaction. This is known as a Quantum-Non-Demolition (QND) measurement, we increase our knowledge of a particular spin component, which amounts to squeezing the probability distribution of that variable. Finally, we rescale the atomic and light variables to obtain a common mathematical framework for the description of the systems. These canonical variables will be relied upon throughout the following discussion regarding the construction of cluster states.

4.5.1 Atomic Spin Operators

For the atomic quantum variables we are concerned with the total angular momentum $\mathbf{F}$. It is normal to restrict to one hyperfine level, which for cesium is $F = 4$ [2]. We denote by $\hat{j}_{k,i}$ the total angular momentum for a single atom and $\mathbf{J}$ denotes the collective angular momentum for the entire ensemble. This is defined by

$$\mathbf{J} = \sum_{i=1}^{N_{at}} \hat{j}_{k,i}, \quad k = x, y, z. \tag{4.17}$$

Where N_{at} is the number of atoms in the choses hyperfine level. In a typical experiment [113], the number of atoms is of the order 10^{12}. This implies that the eigenvalues of this operator are sufficiently close together close compared with the length of the spin vector that we can regard the $\hat{J}_y$ and $\hat{J}_x$ components of spin as continuous-variable operators. We assume the atoms are all polarized along the x-axis, which defines our axis of quantization. Then, fluctuations in the $\hat{J}_x$ component of collective spin are kept extremely

[2] This is for experimental convenience since the hyperfine splitting is large compared to the resolution of typical laser systems

small relative to the strong coherent excitation and we can just treat $\hat{J}_x$ as a classical quantity, $\hat{J}_x \approx \langle \hat{J}_x \rangle \equiv \hbar J_x = \hbar N_{atom} F$. This state is known as a Coherent Spin State (CSS). The orthogonal components of spin are unaffected by the x-polarization and quantum fluctuations around their mean value remain relatively large. Via the commutation relation the Heisenberg uncertainty relation sets a lower bound for the quantum fluctuations

$$[\hat{J}_y, \hat{J}_z] = iJ_x \tag{4.18}$$

which in turn leads to

$$\mathrm{Var}(\hat{J}_z).\mathrm{Var}(\hat{J}_y) \geq \frac{J_x^2}{4} \tag{4.19}$$

Here $\mathrm{Var}(\hat{J}_k) = \langle \hat{J}_k^2 \rangle - \langle \hat{J}_k \rangle^2$ is the width of the probability distribution for the operator $\hat{J}_k$. It has been shown that $\hat{J}_z$ and $\hat{J}_y$ have a Gaussian distribution with zero mean [115].

4.5.2 Polarization states of light

Since light pulses will be both meditating interactions between atomic ensembles and will be included in clusters states are qumodes, we require a description that puts the light modes on the same footing as the atomic modes. Upon interaction with the atomic ensembles, it turns out that the polarization of the light is the relevant quantum variable. The polarization state is well described by the Stokes operators. Consider a pulse of light, or collection of photons, traveling along the z-direction then the Stokes operators read,

$$\begin{aligned}
\hat{S}_x &= \frac{1}{2}(\hat{n}_{ph}(x) - \hat{n}_{ph}(y)) = \frac{1}{2}(\hat{a}_x^\dagger \hat{a}_x - \hat{a}_y^\dagger \hat{a}_y), \\
\hat{S}_y &= \frac{1}{2}(\hat{n}_{ph}(+45) - \hat{n}_{ph}(-45)) = \frac{1}{2}(\hat{a}_x^\dagger \hat{a}_y + \hat{a}_y^\dagger \hat{a}_x), \\
\hat{S}_z &= \frac{1}{2}(\hat{n}_{ph}(\sigma_+) - \hat{n}_{ph}(\sigma_-)) = \frac{i}{2}(\hat{a}_x^\dagger \hat{a}_y - \hat{a}_y^\dagger \hat{a}_x),
\end{aligned} \tag{4.20}$$

where $\hat{n}_{ph}$ is the number of photons with x-polarization, and so on. This form of the Stokes operators are dimensionless; they just count photons. As with the atomic modes defined above, we assume a strong polarization in along the x-direction. The polarization along y is much weaker. Then the x-mode operators $\hat{a}_x$ and $\hat{a}_x^\dagger$ can be regarded as classical quantities.

The Stokes operators satisfy angular momentum commutation relations,

$$[\hat{S}_y, \hat{S}_z] = iS_x \tag{4.21}$$

which leads to the uncertainty relation

$$\mathrm{Var}(\hat{S}_y)\mathrm{Var}(\hat{S}_z) \geq \frac{S_x^2}{4} \tag{4.22}$$

Similarly to the atomic ensembles, the polarization in the y and z directions are Gaussian distributed. This observation justifies our use of the symplectic formalism used later to calculate the effects on interactions between the polarized light and atomic ensembles.

4.5.3 Interaction: Semi-classical picture

We now turn to the question of how the interaction between the atomic ensembles and light modes affects the spin and polarization properties. The full multi-level interaction Hamiltonian has been derived in [130]. For a conceptual understanding of the interaction it is only necessary to consider the semi-classical case. Then we treat the light as a classical off-resonant field propagating through a polarizable medium with a strong incident magnetic field. This field is assumed sufficiently strong to exceed the spin orbit interaction, this ensures that we work in Paschen-Back regime. The light experiences a phase shift because of the index of refraction of the dispersive medium. Light linearly polarized along the x-axis can be linearly decomposed as

$$\hat{a}_+ = \frac{1}{\sqrt{2}}(\hat{a}_x + i\hat{a}_y), \quad \hat{a}_- = \frac{1}{\sqrt{2}}(\hat{a}_x - i\hat{a}_y). \tag{4.23}$$

With the z-axis as quantization axis this light will drive $\Delta m = 1$ and $\Delta m = -1$ transitions respectively. For a dispersive interaction with a two level

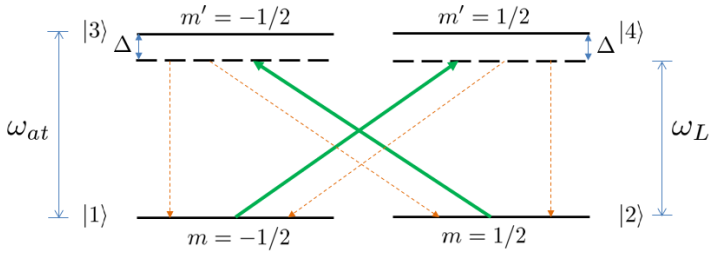

Figure 4.3: Two level Faraday interaction. Green lines denote transitions between hyperfine levels $m = \pm 1/2$ and $m' = \pm 1/2$, orange dotted lines correspond to emission. We have detuning Δ, atomic transition frequency ω_{at} and light frequency ω_L.

system. Fig. (4.3). This means that the σ_+ component will acquire a phase shift $\delta_+ = \delta_0 N_-$ proportional to the population in $m = -1/2$, N_- and correspondingly the σ_- component acquires a phase $\delta_- = \delta_0 N_+$. Then a rearrangement of Eq.(4.23) gives the effect of this phase shift on the linear

polarization

$$a_x = \frac{1}{\sqrt{2}}(a_- - a_+) = e^{i\delta_0(N_+ + N_-)/2}\cos(\delta_0(N_- - N_+))$$
$$a_y = \frac{i}{\sqrt{2}}(a_- + a_+) = e^{i\delta_0(N_+ + N_-)/2}\sin(\delta_0(N_- - N_+)) \quad (4.24)$$

where we took $a_x = 1$, $a_y = 0$, $a_+ = -1/\sqrt{2}$ and $a_- = 1/\sqrt{2}$. Then passing the light through a dispersive medium acts in the light by rotating its polarization by an angle proportional to the population difference in the two ground state levels. We note that apart from a factor of $1/2$ this is just $\hat{J}_z$. This effect is known as a Faraday rotation. However, there is no effect on the value of $\hat{J}_z$ as the spin is not rotated by the light. Then sending linearly polarized light through our atomic sample and subsequently measuring the polarization rotation implements a measurement of $\hat{J}_z$ without altering its value. This process can then be considered a QND measurement of the atomic spin and has been used in experiments to produce entanglement between atomic samples [113].

4.5.4 Interaction: Quantum Picture

Under the semi-classical picture we don't gain much intuition as to the effect on the interacting light field. In order to find the back-action effects on the light, we must apply the full quantum treatment. We consider a propagating beam of light coupled off-resonantly to a transition in the atomic sample (e.g. $6S_{1/2,F=4} \rightarrow 6P_{3/2,F'=3,4,5}$ transitions in cesium). Neglecting absorption effects and adiabatically eliminating the optically excited states, an effective Hamiltonian describing the light interacting with only the ground state degrees of freedom is obtained [114, 116, 117].

$$H_{int}^{eff} = \frac{-\hbar c\gamma}{8A\Delta}\frac{\lambda^2}{2\pi}\int_0^L (a_0.\hat{\phi}(z,t) + a_1.\hat{S}_z(z,t)\hat{j}_z(z,t) + a_2[\hat{\phi}(z,t)\hat{j}_z^2(z,t) - \hat{S}_-(z,t)\hat{j}_+^2(z,t) - \hat{S}_+(z,t)\hat{j}_-^2(z,t)])\rho A dz. \quad (4.25)$$

we have assumed a one-dimensional theory for the light which is sufficient for a beam cross section A that is much larger that the squared wavelength λ^2. The spin operators $\hat{j}_z(z,t)$ are dimensionless and refer to single atoms at position z and time t. The integration runs over the entire sample of length L with atomic density ρ. The factor γ is the natural FWHM line width of the optical transition and Δ is the detuning [115].

The operators $\hat{\phi}(z,t)$ are the photon flux per unit length, $\hat{S}_+ = \hat{S}_x + i\hat{S}_y = -\hat{a}_+^\dagger\hat{a}_-$ and $\hat{S}_- = \hat{S}_x - i\hat{S}_y = -\hat{a}_-^\dagger\hat{a}_+$ are the raising and lowering operators converting σ_+ photons into σ_- photons and vice versa. Similarly, $\hat{j}_\pm = \hat{j}_x \pm \hat{j}_y$ are the raising and lowering operators for the spin. The parameters a_0, a_1

and a_2 are given by

$$
\begin{aligned}
a_0 &= \frac{1}{4}\left(\frac{1}{1-\Delta_{35}/\Delta} + \frac{7}{1-\Delta_{45}/\Delta} + 8\right) \to 4, \\
a_1 &= \frac{1}{120}\left(-\frac{35}{1-\Delta_{35}/\Delta} - \frac{21}{1-\Delta_{45}/\Delta} + 176\right) \to 1, \\
a_2 &= \frac{1}{240}\left(\frac{5}{1-\Delta_{35}/\Delta} - \frac{21}{1-\Delta_{45}/\Delta} + 16\right) \to 0,
\end{aligned} \tag{4.26}
$$

where the limits are the behaviour for very large values of detuning. Now let us examine each of the terms of the Hamiltonian, the first, containing a_0 is a Stark shift to all the atoms independent of the internal state but proportional to the photon density $\hat{\phi}(z,t)$. The a_1 term rotates the Stokes vector $\mathbf{S}$ and the spin vector $\mathbf{J}$ around the z-axis, which is the Faraday rotation mentioned above. The a_2 term contains higher order couplings between the light and atoms, however, since a_2 tends to zero for sufficiently large detunings we can usually neglect this term entirely.

Each of these terms conserve the z-projection of the total angular momentum of light and atoms, e.g. $\hat{S}_-\hat{j}_+^2$ term can change a σ_+ photon in to a σ_- photon, which changes the angular momentum of the light along z by $-2\hbar$. The atoms in turn receive $2\hbar$ due to the spin raising operator $\hat{j}_+^2$. The total angular momentum along the z-axis must remain invariant since the physical system is axially symmetric around the direction of light propagation which we choose to be the z-axis.

The a_1 term is of most relevance to us. This term represents the QND interaction which as we saw above is the basis interaction for the creation of cluster states. From now on we neglect the higher order terms by assuming a large detuning and note the a_0 term just produces global phase shifts which can be ignored. Under this simplification we may derive the dynamics due to the interaction.

4.6 Atom/Light Coupling

From the Hamiltonian (4.25) we can derive the equations of motion for the light/atom interaction. For this we apply the Heisenberg equation

$$
\frac{\partial \hat{j}_i}{\partial t} = -\frac{i}{\hbar}[\hat{j}_i, H] \tag{4.27}
$$

and the Maxwell-Bloch equations

$$
\left(\frac{\partial}{\partial t} + c\frac{\partial}{\partial z}\right)\hat{S}_i(z,t) = -\frac{i}{\hbar}[\hat{S}_i(z,t), H] \tag{4.28}
$$

However, we can neglect the the $\partial/\partial t$ term by ignoring dynamics on the time scale L/c. So the speed of light across the atomic sample is effectively

infinite which amounts to ignoring retardation effects in the interaction. Then taking only the a_1 term from the Hamiltonian, we find

$$\begin{aligned}
\frac{\partial \hat{j}_x(z,t)}{\partial t} &= \frac{c\gamma}{8A\Delta}\frac{\lambda^2}{2\pi}a_1\hat{S}_z(z,t)\hat{j}_y(z,t),\\
\frac{\partial \hat{j}_y(z,t)}{\partial t} &= -\frac{c\gamma}{8A\Delta}\frac{\lambda^2}{2\pi}a_1\hat{S}_z(z,t)\hat{j}_x(z,t),\\
\frac{\partial \hat{j}_z(z,t)}{\partial t} &= 0,
\end{aligned} \tag{4.29}$$

and

$$\begin{aligned}
\frac{\partial \hat{S}_x(z,t)}{\partial z} &= \frac{\gamma\rho}{8\Delta}\frac{\lambda^2}{2\pi}a_1\hat{S}_y(z,t)\hat{j}_z(z,t),\\
\frac{\partial \hat{S}_y(z,t)}{\partial z} &= -\frac{\gamma\rho}{8\Delta}\frac{\lambda^2}{2\pi}a_1\hat{S}_x(z,t)\hat{j}_z(z,t),\\
\frac{\partial \hat{S}_z(z,t)}{\partial z} &= 0.
\end{aligned} \tag{4.30}$$

From Eq.(4.29) and Eq.(4.30) we conclude that the effect of this interaction is to rotate the spin around the z-axis by an amount proportional to $\hat{S}_z$, while the Stokes vectors rotate about z by an amount proportional to $\hat{j}_z$.

We can assume that in practice the rotations are small and so has little effect on the x-direction of spin or polarization. Then we can ignore the first lines of (4.29) and (4.30). Further, given the QND structure of the remaining equations, we can sum over the individual atomic spins and obtain the equations for the collective spin variables which in continuous notation is given by $\hat{J}_i(t) = \int_0^L \hat{j}_i(z,t)\rho A dz$. For the light operators we just take the input and output parts only by defining $\hat{S}_i^{in}(t) = c\hat{S}_i(z=0,t)$ and $S_i^{out}(t) = c\hat{S}_i(z=L,t)$. The factor c changes the normalization to units of photons per unit time instead of per unit length. Then integrating Eqs. (4.29,4.30) gives us

$$\begin{aligned}
\hat{S}'_y(t) &= \hat{S}_y(t) + aS_x\hat{J}_z(t),\\
\hat{S}'_z(t) &= \hat{S}_z(t),\\
\hat{J}'_y(t) &= \hat{J}_y(t) + aJ_x\hat{S}_z(t),\\
\hat{J}'_z(t) &= \hat{J}_z(t),
\end{aligned} \tag{4.31}$$

where

$$a = -\frac{\gamma}{8A\Delta}\frac{\lambda^2}{2\pi}a_1. \tag{4.32}$$

The apostrophe denoted the state of the atomic spin and light polarization after the interaction. This form is now very convenient from the point of view of a QND interaction since for large interaction strengths the $aS_x\hat{J}_z(t)$ is much larger than $\hat{S}_y(t)$ and hence a measurement on $\hat{S}'_y$ amounts to a QND measurement of the atomic spin $\hat{J}_z$.

4.6.1 Canonical Operators

We have seen in the preceding sections that the light and atoms share a very similar mathematical structure since they both obey angular momentum commutation relations. This is convenient for our purposes as it allows us to treat the spin and polarization in a similar manner. We have also prepared the two systems such that one of the quantum variables is reduced to a classical number so that both systems are described by two continuous-variables. To bring both systems to canonical operator form we apply the Holstein-Primakoff approximation [139] to rescale the two remaining quantum variables of each system with the classical third component. Physically, this approximation assumes the the disc of uncertainty associated to the spin system is sufficiently small compared to the length of the spin vector. Then the space in the vicinity of the uncertainty disc is essentially flat and we can transform form a three dimensional theory to a two dimensional one. For the atomic spin variables rescaling these orthogonal components fulfills the canonical commutation relations, $[\hat{J}_y/\sqrt{\hbar J_x}, \hat{J}_z/\sqrt{\hbar J_x}] = i\hbar$. In this canonical form, we can identify these variables as the "position" and "momentum" of the system defined in the following way

$$\hat{x}_A = \frac{\hat{J}_y}{\sqrt{\hbar J_x}}, \quad \hat{p}_A = \frac{\hat{J}_z}{\sqrt{\hbar J_x}}, \tag{4.33}$$

Similar to the atomic case, the approximation $\hat{S}_x \approx \langle \hat{S}_x \rangle \equiv N_{ph}\hbar/2$. The orthogonal components $\hat{S}_y$ and $\hat{S}_z$ are rescaled to fulfill the commutation relation $[\hat{S}_y/\sqrt{\hbar S_x}, \hat{S}_z/\sqrt{\hbar S_x}] = i\hbar$. Once again we make a connection with the canonical position and momenta,

$$\hat{x}_L = \frac{\hat{S}_y}{\sqrt{\hbar S_x}}, \quad \hat{p}_L = \frac{\hat{S}_z}{\sqrt{\hbar S_x}}. \tag{4.34}$$

From now on we will now only refer to the canonical operators $\hat{x}$ and $\hat{p}$ instead of collective spins and polarizations. In the canonical notation our equations of motion for the atom/light interaction (4.31) become

$$\begin{aligned} \hat{x}_L^{out} &= \hat{x}_L^{in} - \kappa \hat{p}_A^{in} \\ \hat{p}_L^{out} &= \hat{p}_L^{in} \\ \hat{x}_A^{out} &= \hat{x}_A^{in} - \kappa \hat{p}_L^{in} \\ \hat{p}_A^{out} &= \hat{p}_A^{in} \end{aligned} \tag{4.35}$$

The parameter describing the strength of the light/atom interaction is given by $\kappa = a\sqrt{J_x S_x T}$. In the next section we expand this set of equations to include the possibility of off axis interactions.

4.6.2 Interaction: Angular Dependence

Let us assume that a light beam propagates in the YZ plane and passes through a single ensemble at an angle α with respect to the z-direction. Then the atom-light interaction can be approximated by the effective QND Hamiltonian [114],

$$H_{eff}(\alpha) = \frac{\kappa}{T}\hat{p}_L(\hat{p}_A \cos\alpha + \hat{x}_A \sin\alpha), \tag{4.36}$$

where κ is the coupling constant. Again, applying the Heisenberg equation for the atoms and the Maxwell-Bloch equation (neglecting retardation) for the light. The variables characterizing the composite system transform according to the following rules:

$$\begin{aligned}
\hat{x}_A^{out} &= \hat{x}_A^{in} - \kappa\hat{p}_L^{in}\cos\alpha, \\
\hat{p}_A^{out} &= \hat{p}_A^{in} + \kappa\hat{p}_L^{in}\sin\alpha, \\
\hat{x}_L^{out} &= \hat{x}_L^{in} - \kappa(\hat{p}_A^{in}\cos\alpha + \hat{x}_A^{in}\sin\alpha), \\
\hat{p}_L^{out} &= \hat{p}_L^{in}.
\end{aligned} \tag{4.37}$$

These are straightforwardly generalized to the case in which a single light beam propagates through many atomic ensembles, impinging on the i^{th} sample at an angle α_i. This set of equations are the basis for the schemes that we discuss in the remainder of this chapter. Note that with the angular dependence included, we have greater control over the specific interaction that can be performed just be choosing the angle at which the light impinges on the atomic sample relative to the polarization axis (x-axis).

4.7 Generation of atomic cluster states

In this section we will use our atomic ensembles with the interactions described above to design protocols for the generation of atomic cluster states. In these states each atomic ensemble, described by the orthogonal spin operators $\hat{J}_z$ and $\hat{J}_y$, serve as qumodes which correspond to the vertices of the underlying graph. We recall that the canonical method for constructing cluster states is to entangle zero-momentum eigenmodes via the C_Z operation. Conveniently, the C_Z is an example of a QND interaction, which is optically implemented with a beam-splitter. Here however it is possible to realize such entangling operations with the Faraday effect described in the previous section. Our method can be thought of as an extension to the work of [113, 114, 115], where it was shown that macroscopic spin states of two atomic ensembles can be entangled via the Faraday interaction.

In the following, we regard the light pulses as information carriers. Under interaction with an ensemble their rotated polarization retains the collective spin information of the ensemble. This spin information can then

be deposited on another ensemble by a further QND interaction. Since the ensembles share information their spins become correlated and the states are entangled. Recall however, that for cluster states, the correlations must satisfy a set of constraints known as the nullifier conditions. We proceed by calculating the effects on the state nullifiers, this allows us to read off instantly when a given evolution yields a cluster state.

4.7.1 Atomic cluster: Nullifier Formalism

Recall the cluster state nullifier conditions,

$$\hat{p}_k - \sum_{j \in N(k)} \hat{x}_j \to 0, \quad i = 1, ..., n, \tag{4.38}$$

this set relates the position and momentum combinations of adjacent modes, $N(k)$, for each mode k. We can construct an n-mode cluster state by arranging a sequence of interaction such that the nullifier set, Eq.(4.38), is satisfied.

Let us first establish some notation. We denote by $\hat{x}_{A_k}$ and $\hat{p}_{A_k}$ the canonical position and momentum of the k^{th} atomic ensemble respectively. The interacting light pulses are denoted by $\hat{x}_{i,j}$ and $\hat{p}_{i,j}$, where these are the quadratures for the j^{th} interacting light mode. We will be using two special cases of the interaction Hamiltonian (4.36). The first, $H_1 = \kappa \hat{p}_i \hat{x}_A$, corresponds to an angle of $\alpha = \pi/2$, and so the light impinges on the atomic ensemble at 90 degrees to the polarization axis. This Hamiltonian has the following effect on the position and momentum quadrature of the light and atoms.

$$\begin{aligned}
\hat{x}_A^{out} &= \hat{x}_A^{in} \\
\hat{p}_A^{out} &= \hat{p}_A^{in} - \kappa \hat{p}_L^{in} \\
\hat{x}_i^{out} &= \hat{x}_i^{in} + \kappa \hat{x}_A^{in} \\
\hat{p}_i^{out} &= \hat{p}_i^{in}
\end{aligned} \tag{4.39}$$

The second Hamiltonian $H_2 = \kappa \hat{x}_A \hat{x}_i$, generated by performing a Fourier transform on the light to make the change, $\hat{p}_i \to \hat{x}_i$. The evolutions associated with this Hamiltonian are

$$\begin{aligned}
\hat{x}_A^{out} &= \hat{x}_A^{in} \\
\hat{p}_A^{out} &= \hat{p}_A^{in} - \kappa \hat{x}_i \\
\hat{x}_i^{out} &= \hat{x}_i^{in} \\
\hat{p}_i^{out} &= \hat{p}_i^{in} - \kappa \hat{x}_A
\end{aligned} \tag{4.40}$$

The task is now to construct the appropriate nullifier combinations in each of the atomic ensembles through the use of these interactions. Once completed the outgoing light pulses can be measured. Assuming the pulses

have interacted using the correct Hamiltonian and in the particular order required the light pulses will contain the atomic spin information from the ensembles. Measuring the light is therefore a QND measurement of the spin quadrature combinations of the ensembles. This reduces the variance in these quadratures (ideally to zero) and the cluster state is generated.

In general the procedure for an n-mode cluster state is as follows:

- First assume we have some ensemble $A_k \in n$. We want to entangle this with neighbours $A_{j_1}, A_{j_2}, ..., A_{j_p} \in N(k)$.
- We must choose the configuration of the cluster state. i.e. Linear, square, etc. This give us the form for the nullifier conditions.
- An interaction pulse i_k is sent through ensemble j_1. This interacts via H_1 and the polarization is rotated proportional to $\hat{x}_{A_{j_1}}$.
- The pulse i_k then interacts with j_2 via H_1. This rotates the polarization of the interaction pulse again, so the total change is proportional to $\hat{x}_{A_{j_1}} + \hat{x}_{A_{j_2}}$.
- The pulse continues to through all the atomic mode, $N(k)$, so the total effect on the interaction pulse is a rotation proportional to $\hat{x}_{A_{j_1}} + \hat{x}_{A_{j_2}} + \hat{x}_{A_{j_3}} + ... + \hat{x}_{A_{j_p}} = \sum_p \hat{x}_{A_{j_p}}$. Then this pulse contains spin information from all the adjacent modes.
- This information is encoded onto ensemble A_k by interacting it with i_k mediated by H_2. Then the atomic spin information is deposited onto ensemble A_k. This has the effect of rotating the collective spin of A_k proportional to the polarization of the interaction pulse i.e. $\hat{p}_{A_k} \rightarrow \hat{p}_{A_k} - \sum_p \hat{x}_{A_{j_p}}$.
- Repeat these steps for all $A \in n$ to encode the quadrature combinations onto all the ensembles that compose the cluster state.
- The protocol is completed by performing a homodyne measurement on the outgoing interaction light pulse. This corresponds to a QND measurement of the required spin quadrature combinations. This minimizes the variance of the nullifier and the state is entangled.

We note that this procedure is not perfect, every interaction between a light pulse and atomic ensemble has an associated back-action that performs an extra spin rotation. We will discuss this further next when we consider an examples of this procedure.

4.7.2 Example: Four-node linear cluster

Here we consider the four-node linear cluster or *quantum wire*, Fig.(4.4). These are used in computational processes to move information around the

cluster and under appropriate measurements can implement single mode unitaries on the state. We will use our general procedure outlined above to generate a four-node linear atomic cluster state. That is, we entangle four atomic ensembles $A_1, ..., A_4$, each one corresponding to a vertex of the associated graph. Then we find the required nullifier correlations, from the general nullifier condition, (4.38).

$$\begin{aligned} &\hat{p}_{A_1} - \hat{x}_{A_2} \to 0, \quad \hat{p}_{A_2} - \hat{x}_{A_1} - \hat{x}_{A_3} \to 0, \\ &\hat{p}_{A_3} - \hat{x}_{A_2} - \hat{x}_{A_4} \to 0, \quad \hat{p}_{A_4} - \hat{x}_{A_3} \to 0. \end{aligned} \tag{4.41}$$

Figure 4.4: A four-node linear cluster state, composed of four atomic ensembles $A_1, ..., A_4$

Then we proceed as follows. (a) Our first step is to assemble the required quadrature combinations on ensemble 1. A light pulse i_1 is passed through ensemble 2, interacting via H_1. Note that since we use multiple interactions, we denote by apostrophes the outcomes of single interactions. When a particular mode has completed its part in the sequence it is labeled *out*. The quantum variables following the first interaction are

$$\begin{aligned} \hat{p}'_{i_1} &= \hat{p}^{in}_{i_1}, \\ \hat{x}'_{i_1} &= \hat{x}_{i_1} + \kappa \hat{x}_{A_2}, \\ \hat{p}'_{A_2} &= \hat{p}^{in}_{A_2} - \kappa \hat{p}_{i_1}, \\ \hat{x}'_{A_2} &= \hat{x}_{A_2}. \end{aligned} \tag{4.42}$$

We note that the light mode has picked up atomic spin information on its $\hat{x}$-quadrature. This spin information is then encoded onto ensemble 2 via the H_2 interaction:

$$\begin{aligned} \hat{p}^{out}_{i_1} &= \hat{p}^{in}_{i_1} - \kappa \hat{x}_{A_1}, \\ \hat{x}^{out}_{i_1} &= \hat{x}_{i_1} + \kappa \hat{x}^{in}_{A_2}, \\ \hat{p}'_{A_1} &= [\hat{p}^{in}_{A_1} - \kappa^2 \hat{x}^{in}_{A_2}] - \kappa \hat{x}_{i_1}, \\ \hat{x}'_{A_1} &= \hat{x}^{in}_{A_1}. \end{aligned} \tag{4.43}$$

(b) For ensemble 2, interaction i_2 is passed through first ensemble 3 then ensemble 1 interacting via H_1. This yields

$$\begin{aligned}
\hat{p}'_{i_2} &= \hat{p}_{i_2}, \\
\hat{x}''_{i_2} &= \hat{x}_{i_2} + \kappa(\hat{x}^{in}_{A_3} + \hat{x}^{in}_{A_1}), \\
\hat{p}'_{A_3} &= \hat{p}^{in}_{A_3} - \kappa\hat{p}_{i_2}, \\
\hat{x}'_{A_3} &= \hat{x}^{in}_{A_3}, \\
\hat{p}'_{A_1} &= [\hat{p}^{in}_{A_1} - \kappa^2\hat{x}_{A_2}] - \kappa(\hat{x}_{i_1} + \hat{x}_{i_2}), \\
\hat{x}'_{A_1} &= \hat{x}^{in}_{A_1}.
\end{aligned} \tag{4.44}$$

Then coupling i_2 to ensemble 2 yields

$$\begin{aligned}
\hat{p}^{out}_{i_2} &= \hat{p}_{i_2} - \kappa\hat{x}^{in}_{A_2}, \\
\hat{x}^{out}_{i_2} &= \hat{x}_{i_2} + \kappa(\hat{x}^{in}_{A_3} + \hat{x}^{in}_{A_1}), \\
\hat{p}^{out}_{A_2} &= [\hat{p}^{in}_{A_2} - \kappa^2(\hat{x}^{in}_{A_3} + \hat{x}^{in}_{A_1})] - \kappa(\hat{p}_{i_1} + \hat{x}_{i_2}), \\
\hat{x}^{out}_{A_2} &= \hat{x}^{in}_{A_2}.
\end{aligned} \tag{4.45}$$

Giving us the correct condition on atomic mode 2. (c) Ensemble 3 requires information from ensembles 2 and 4 which we obtain through interaction pulse i_3:

$$\begin{aligned}
\hat{p}'_{i_3} &= \hat{p}_{i_3}, \\
\hat{x}''_{i_3} &= \hat{x}_{i_3} + \kappa(\hat{x}^{in}_{A_2} + \hat{x}^{in}_{A_4}), \\
\hat{p}'_{A_4} &= \hat{p}^{in}_{A_4} - \kappa\hat{p}_{i_3}, \quad \hat{x}'_{A_4} = \hat{x}^{in}_{A_4}, \\
\hat{p}'_{A_2} &= [\hat{p}^{in}_{A_2} - \kappa^2(\hat{x}_{A_3} + \hat{x}_{A_1}] - \kappa(\hat{p}_{i_1} + \hat{x}_{i_2} + \hat{p}_{i_3}), \\
\hat{x}'_{A_2} &= \hat{x}^{in}_{A_2}.
\end{aligned} \tag{4.46}$$

Then encoding onto ensemble 3, (H_2), we find

$$\begin{aligned}
\hat{p}^{out}_{i_3} &= \hat{p}_{i_3} - \kappa\hat{x}^{in}_{A_3}, \\
\hat{x}^{out}_{i_3} &= \hat{x}_{i_3} + \kappa(\hat{x}^{in}_{A_2} + \hat{x}^{in}_{A_4}), \\
\hat{p}^{out}_{A_3} &= [\hat{p}^{in}_{A_3} - \kappa^2(\hat{x}^{in}_{A_4} + \hat{x}^{in}_{A_2})] - \kappa(\hat{p}_{i_2} + \hat{x}_{i_3}), \\
\hat{x}^{out}_{A_3} &= \hat{x}^{in}_{A_3}.
\end{aligned} \tag{4.47}$$

(d) Finally, to encode onto ensemble 4, we use interaction pulse i_4. We collect spin information from ensemble 3:

$$\begin{aligned}
\hat{p}'_{i_4} &= \hat{p}_{i_4}, \\
\hat{x}'_{i_4} &= \hat{x}_{i_4} + \kappa\hat{x}^{in}_{A_3}, \\
\hat{p}'_{A_3} &= [\hat{p}^{in}_{A_3} - \kappa^2(\hat{x}^{in}_{A_4} + \hat{x}^{in}_{A_2})] - \kappa(\hat{p}_{i_2} + \hat{x}_{i_3} + \hat{p}_{i_4}), \\
\hat{x}'_{A_3} &= \hat{x}^{in}_{A_3}
\end{aligned} \tag{4.48}$$

Then interacting with ensemble 4 via H_2,

$$\begin{aligned}
\hat{p}_{i_4}^{out} &= \hat{p}_{i_4}, \\
\hat{x}_{i_4}^{out} &= \hat{x}_{i_4} + \kappa \hat{x}_{A_3}^{in}, \\
\hat{p}_{A_4}^{out} &= [\hat{p}_{A_4} - \kappa^2 \hat{x}_{A_3}^{in}] - \kappa(\hat{p}_{i_3} + \hat{x}_{i_4}) \\
\hat{x}_{A_4}^{out} &= \hat{x}_{A_4}^{in}.
\end{aligned} \tag{4.49}$$

In summary, the quadrature combinations that are assembled on the atomic modes are of the form

$$\begin{aligned}
\hat{p}_{A_1}^{out} &= [\hat{p}_{A_1}^{in} - \kappa^2 \hat{x}_{A_2}^{in}] - N_1, \\
\hat{p}_{A_2}^{out} &= [\hat{p}_{A_2}^{in} - \kappa^2 (\hat{x}_{A_1}^{in} + \hat{x}_{A_3}^{in})] - N_2, \\
\hat{p}_{A_3}^{out} &= [\hat{p}_{A_3}^{in} - \kappa^2 (\hat{x}_{A_2}^{in} + \hat{x}_{A_4}^{in})] - N_3, \\
\hat{p}_{A_4}^{out} &= [\hat{p}_{A_4}^{in} - \kappa^2 \hat{x}_{A_3}^{in}] - N_4.
\end{aligned} \tag{4.50}$$

Where $N_1, ..., N_4$ are the back-action terms from the QND interactions. We see that this procedure has given the correct quadrature combinations, up to the back-action terms. Then measuring the outgoing light modes completes the protocol and the linear cluster is generated.

4.7.3 Example: Four-node square cluster

Square cluster states form the basis for two-mode quantum gates. The four-node square cluster is the smallest unit of a large array that can be used to perform multi-mode operations. We find that the nullifiers for a four-mode square cluster can be written as:

$$\begin{aligned}
&\hat{p}_{A_1} - \hat{x}_{A_2} - \hat{x}_{A_3} \to 0, \quad \hat{p}_{A_2} - \hat{x}_{A_1} - \hat{x}_{A_4} \to 0, \\
&\hat{p}_{A_3} - \hat{x}_{A_1} - \hat{x}_{A_4} \to 0, \quad \hat{p}_{A_4} - \hat{x}_{A_2} - \hat{x}_{A_3} \to 0.
\end{aligned} \tag{4.51}$$

To entangle the ensembles we use light pulses labeled, $i_1, ..., i_4$. We make use of our QND Hamiltonians H_1 and H_2 to mediate the interaction between the ensembles and light pulses. The protocol to generate atomic cluster states is depicted in Fig.(4.5). (a) Spin information is picked up from A_2 and A_3 by pulse i_1 via the interaction H_1. This pulse encodes the information onto A_1 through the interaction H_2. (b) Spin information is picked up from A_1 and A_4 by pulse i_2 via the interaction H_1. This pulse encodes the information onto A_2 through the interaction H_2. (c) Spin information is picked up from A_1 and A_4 by pulse i_3 via the interaction H_1. This pulse encodes the information onto A_3 through the interaction H_2. (d) Spin information is picked up from A_2 and A_3 by pulse i_4 via the interaction H_1. This pulse encodes the information onto A_4 through the interaction H_2. When this

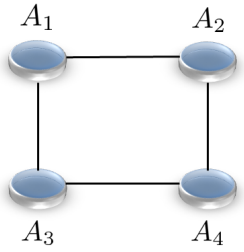

Figure 4.5: A four-node square cluster state, composed of four atomic ensembles $A_1, ..., A_4$

procedure is completed, the ensembles have quadrature combinations:

$$\begin{aligned}
\hat{p}^{out}_{A_1} &= \hat{p}_{A_1} - \kappa^2 \hat{x}_{A_2} - \kappa^2 \hat{x}_{A_3} - \kappa N_1, \quad \hat{x}^{out}_{A_1} = \hat{x}_{A_1}, \\
\hat{p}^{out}_{A_2} &= \hat{p}_{A_2} - \kappa^2 \hat{x}_{A_4} - \kappa^2 \hat{x}_{A_1} - \kappa N_2, \quad \hat{x}^{out}_{A_2} = \hat{x}_{A_2}, \\
\hat{p}^{out}_{A_3} &= \hat{p}_{A_3} - \kappa^2 \hat{x}_{A_4} - \kappa^2 \hat{x}_{A_1} - \kappa N_3, \quad \hat{x}^{out}_{A_3} = \hat{x}_{A_3}, \\
\hat{p}^{out}_{A_4} &= \hat{p}_{A_4} - \kappa^2 \hat{x}_{A_2} - \kappa^2 \hat{x}_{A_3} - \kappa N_4, \quad \hat{x}^{out}_{A_4} = \hat{x}_{A_4},
\end{aligned} \tag{4.52}$$

where $N_1 = \hat{x}_{i_1} + \hat{p}_{i_2} + \hat{p}_{i_3}$, $N_2 = \hat{x}_{i_2} + \hat{p}_{i_1} + \hat{p}_{i_4}$, $N_3 = \hat{x}_{i_3} + \hat{p}_{i_1} + \hat{p}_{i_4}$ and $N_4 = \hat{x}_{i_4} + \hat{p}_{i_2} + \hat{p}_{i_3}$ are the back-action terms due to the QND interactions with the interaction pulses. Then for $\kappa = 1$ the remaining terms are exactly the nullifier relations, (4.73), for the four-mode square cluster state. To complete the protocol, homodyne measurements are made on the outgoing interaction pulses which project the ensembles into the required state.

While the examples we have given here are only four-modes, it is simple to add an arbitrary number of nodes by performing the protocol again on any mode in the state. This is a convenient observation, since we can add more resources to our state at any time. However we see that the number of noise terms increase with every node added. These noise terms disturb the correlations between ensembles by introducing extra fluctuations in the spin variables. In a sufficiently big cluster this added uncertainty in the spins can destroy the entanglement and render the state useless for quantum computational purposes. In large clusters, we can minimize these fluctuations through careful control of the interaction strength κ and ensuring that the polarization magnitudes of the interaction pulses themselves are relatively small compared to the spin magnitudes. We can draw an analogy with the optical generation of cluster states. There, the back-action terms that destroy entanglement are due to the lack of infinite squeezing. Here, while the atomic ensembles are not directly squeezed, it is the lack of squeezing

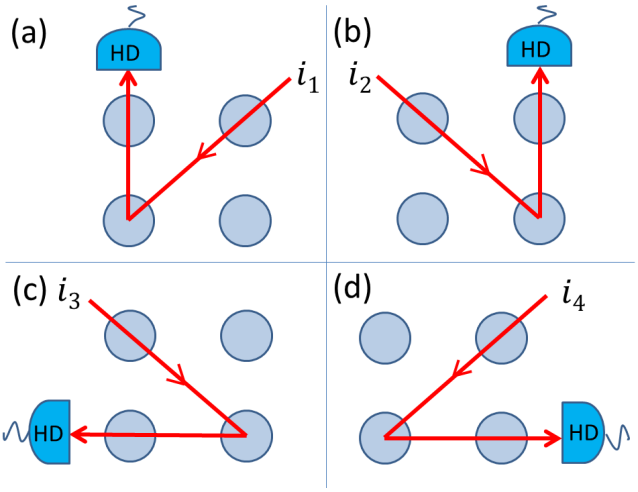

Figure 4.6: Atomic cluster state generation protocol (HD - Homodyne detection): (a) Light pulse i_1 interacts with ensembles A_2 and A_3, picks up atomic spin information which is encoded onto A_1. (b) Light pulse i_2 interacts with ensembles A_1 and A_4, picks up atomic spin information which is encoded onto A_2. (c) Light pulse i_3 interacts with ensembles A_1 and A_4, picks up atomic spin information which is encoded onto A_3. (d) Light pulse i_4 interacts with ensembles A_2 and A_3, picks up atomic spin information which is encoded onto A_4. The interaction pulses are homodyne measured once these steps have been completed to form the cluster state.

available for the interaction pulses that contributes to the noise. It seems that even in these atomic systems we cannot get away from this fundamental problem. In the following sections we show that while we cannot beat the fundamental limits due to finite squeezing in general, we may design more efficient states that are less prone to error build up than in the standard MBQC method.

4.8 Composite cluster states

In the preceding sections we have shown how to make arbitrary atomic cluster states using our QND measurements. Here we generalize this idea and ask the question: Is it possible to include a light mode as one of the nodes of a cluster state? Then light would not just mediate the interactions, it could be used as a computational resource along side the atomic ensembles. Such a state, which we term a *composite cluster state*, since it is composed of both atomic and optical elements, is simple to generate using linear optics and the ordinary QND interaction studied above.

We begin with the simplest case; the two mode composite cluster composed from one atomic ensemble and one optical mode to demonstrate the principle. Then the general cluster state nullifiers reduce to just two conditions on the quantum variables,

$$\hat{p}_A - \hat{x}_L \to 0, \quad \hat{p}_L - \hat{x}_A \to 0 \tag{4.53}$$

where the subscript A refers to the atomic ensemble and L is the light mode. Unlike standard two-mode entangled states, the two-mode cluster state mixes the position and momentum quadratures of different nodes. As above, we make use of light modes i_k to carry information to each node forming the cluster. However, to include a light mode as part of the cluster we require a method of transferring polarization information from light to light. This can be accomplished using a beam-splitter interaction which we discuss now.

4.8.1 Beam-splitters as QND interactions

It was shown in, [106], that beam-splitters and single mode squeezers can be used for approximate QND interactions between light modes under certain conditions.

This is based on the *Bloch Messiah* reduction theorem. The idea that an arbitrarily complicated combination of interactions, such as linear multi-port inferometers, squeezers, down converters etc, that are all described by a quadratic Hamiltonian, may be decomposed into two linear multi-port unitary transformations and single-mode squeezers.

As a first step, we note that any optical system that is modeled by linear Bogoliubov transforms can be decomposed into linear and non-linear

components. Linear optical components have Bogoliubov transformations given by

$$\hat{b}_j = \sum_k U_{jk}\hat{a}_k, \tag{4.54}$$

where U is an arbitrary unitary matrix and there is no mixing of the mode annihilation and creation operators. Any such unitary can be constructed from linear optical components. In contrast, non-linear optical components, such as squeezers, down converters etc, produce linear mixing of the creation and annihilation operators. There is a decomposition theorem that splits up any operation into linear and non-linear parts.

Theorem 4.8.1. *(Bloch-Messiah Reduction)*
For a general linear unitary Bogoliubov transformation (LUBO) of the form

$$\hat{b}_j = \sum_k (A_{jk}\hat{a}_k + B_{jk}\hat{a}_k^\dagger) + \beta_j \tag{4.55}$$

where $\hat{a}_j$, $\hat{b}_j$ are bosonic annihilation operators, the matrices A and B may be decomposed into a pair of unitary matrices U and V and a pair of non-negative diagonal matrices A_D and B_D satisfying

$$A_D^2 = B_D^2 + \boldsymbol{1} \tag{4.56}$$

with $\boldsymbol{1}$ being the identity matrix, by

$$A = UA_DV^\dagger, \quad B = UB_DV^T. \tag{4.57}$$

We apply the Bloch-Messiah reduction to QND coupling between a pair of optical quadrature-phase amplitudes. The Bogoliubov transformations corresponding to the QND interaction can be written as

$$\begin{aligned} \hat{b}_1 &= \hat{a}_1 - \frac{1}{2}\hat{a}_2 + \frac{1}{2}\hat{a}_2^\dagger \\ \hat{b}_2 &= \frac{1}{2}\hat{a}_1 + \hat{a}_2 + \frac{1}{2}\hat{a}_1^\dagger \end{aligned} \tag{4.58}$$

According to the Block Messiah theorem, we can find matrices A and B that affect these Bogoliubov transforms. These can be decomposed to,

$$A = \begin{pmatrix} \sin\theta & -i\cos\theta \\ \cos\theta & i\sin\theta \end{pmatrix} \begin{pmatrix} \frac{\sqrt{5}}{2} & 0 \\ 0 & \frac{\sqrt{5}}{2} \end{pmatrix} \begin{pmatrix} \cos\theta & -i\sin\theta \\ \sin\theta & i\cos\theta \end{pmatrix}^\dagger \tag{4.59}$$

$$B = \begin{pmatrix} \sin\theta & -i\cos\theta \\ \cos\theta & i\sin\theta \end{pmatrix} \begin{pmatrix} \frac{1}{2} & 0 \\ 0 & \frac{1}{2} \end{pmatrix} \begin{pmatrix} \cos\theta & -i\sin\theta \\ \sin\theta & i\cos\theta \end{pmatrix}^T \tag{4.60}$$

where $\theta = \frac{1}{2}\sin^{-1}(2/\sqrt{5})$. These matrices describe a pair of squeezers with squeezing parameters of $r = ln[(1+\sqrt{5})/2]$ (corresponding to $\approx 4.18dB$)

and a pair of unequal unbalanced beam-splitters with energy transmission coefficients of 27.65% and 72.36%. This can be improved by noting that the singular value eigenvalues in (4.59) and (4.60) are degenerate and so the decomposition is not unique. Then a simpler contruction, using 50:50 beamsplitters is given by

$$U = \begin{pmatrix} ie^{i\theta} & ie^{-i\theta} \\ -e^{i\theta} & e^{-i\theta} \end{pmatrix}, \quad V = \begin{pmatrix} -e^{-i\theta} & e^{i\theta} \\ -ie^{-i\theta} & -ie^{i\theta} \end{pmatrix} \tag{4.61}$$

with θ as above. Hence we can achieve a coupling between light mode corresponding to the QND interaction Hamiltonian $H_{BS} = \kappa\hat{x}_i\hat{x}_j$ using a beam-splitter, followed by two single-mode squeezers followed by another beam-splitter. This was further simplified in [27] where it was shown that the same coupling can be engineered with just one pair of squeezers and one beam-splitter acting on vacuum modes. We use this result in the following protocols to allow light modes to be added to our atomic cluster states.

4.8.2 Two-node composite cluster state protocol: Nullifier formalism

Using the interaction pulses we can assemble the quadrature combinations (4.53) in the following way. We pass our first interaction pulse, i_1 though the atomic ensemble (see Fig.4.7(a)). By careful choice of the angle at which the light impinges on the atomic sample we can couple the light and the atoms via the QND Hamiltonian $H = \kappa\hat{x}_A\hat{p}_{i_1}$. The interaction pulse picks up an atomic quadrature term in its position variable, $\hat{x}'_{i_1} = \hat{x}^{in}_{i_1} + \kappa\hat{x}^{in}_A$. Then the interaction pulse is combined with the cluster light mode, L, on a beam-splitter with effective interaction, $H = \hat{x}_L\hat{x}_{i_1}$. This modifies the quadratures of the light mode by rotating $\hat{p}_L$ to $\hat{p}'_L = [\hat{p}^{in}_L - \kappa\hat{x}^{in}_A] - \hat{x}^{in}_{i_1}$. Our second interaction pulse i_2 is first passed through the beam-splitter with light mode L (Fig.4.7(b)). The quadrature action on i_2 is a rotation of $\hat{p}_{i_2}$, $\hat{p}'_{i_2} = \hat{p}^{in}_{i_2} - \hat{x}_L$ with the associated back-action on the light mode. Interaction of the pulse with the atomic ensemble via $H = \kappa\hat{x}_A\hat{p}_{i_2}$ results in the output $\hat{p}^{out}_A = [\hat{p}^{in}_A - \kappa\hat{x}_L] - \kappa(\hat{p}_{i_2} - \hat{x}_{i_1})$. Note that the momenta of the light and atomic modes now have the correct form as given by (4.53) for the quadrature combinations for a two mode cluster state plus the expected noise terms. To complete the protocol, the outgoing interaction pulses undergo homodyne measurements which project the composite system into a cluster state.

4.8.3 Two-node composite cluster state protocol: Symplectic description

In this simple two-mode case we can gain insight into the entanglement properties of the system by constructing the covariance matrix of the final

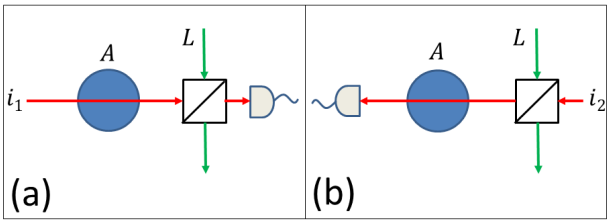

Figure 4.7: Schematic description of the creation of a two mode composite cluster state. Light modes can be combined with atomic ensembles to form the cluster states by enacting a QND interaction with squeezers and beam-splitters. (a) The first interaction encodes atomic quadratures onto the light mode L. (b) The second interaction encodes light quadratures onto the atomic ensemble A. These interactions are required to fulfill the nullifier condition of Eq. (4.53). Reprinted figure with permission from D. F. Milne and N. V. Korolkova,Phys. Rev. A **85**, 032310. Copyright (2012) by the American Physical Society.

quantum state. We have already established that the collective spin of the atomic ensembles and the polarization of the light have probability distribution that are Gaussian in nature. This allows us to fully describe the initial states with covariance matrices. Also, since QND interactions are bi-linear couplings between Stokes operators and collective spin they preserve the Gaussian character of the initial states. Then we can represent QND interactions as symplectic operations on the initial CM. Furthermore, the beam-splitter interactions that we use to include light modes in the cluster also yield a description in terms of Gaussian operations.

In general, to perform QND and beam-splitter interactions, we choose a covariance matrix of the form,

$$\sigma = \begin{pmatrix} A & C \\ C^T & B \end{pmatrix} \tag{4.62}$$

where the sub-matrix A corresponds to those modes that are nodes of the cluster, B are the light modes responsible for mediating the interactions between the nodes within the cluster states and C is the correlations between them. In this construction it is easy to read off the states of the individual modes as well as the interactions at each stage of the protocol.

Our QND interaction are represented by symplectic matrices, S. Recall, these act on the covariance matrix as

$$\sigma_{out} = S^T \sigma_{in} S. \tag{4.63}$$

We also require the ability to perform homodyne measurements of the $\hat{x}_L$ quadrature of the outgoing interaction pulses. We discussed in Chapter 2

how this can be performed in the CM formalism. We state the formula again here for convenience,

$$A' = A - C(XBX)^{-1}C^T, \tag{4.64}$$

assuming an initial displacement of zero. The measurement yields an outcome z_L which displaces the state by,

$$d_A = C(XBX)^{-1}(z_L, 0), \tag{4.65}$$

We assume the initial state of the composite system is given by the covariance matrix for the atoms, light and interaction pulses, $\sigma_{in} = \mathbb{1}_2^A \oplus \mathbb{1}_2^L \oplus \mathbb{1}_2^{i_1} \oplus \mathbb{1}_2^{i_2}$, where the 2×2 identity matrices stand for single modes.

As described in our protocol above, we begin by passing i_1 through the atomic ensemble and then combine it with the cluster light mode via a beam-splitter. The symplectic matrix for this operation is given by

$$S_{int_1} = \begin{pmatrix} 1 & 0 & 0 & 0 & \kappa & 0 & 0 & 0 \\ 0 & 1 & 0 & 0 & 0 & 0 & 0 & 0 \\ 0 & \kappa & 1 & 0 & 0 & -1 & 0 & 0 \\ 0 & 0 & 0 & 1 & 0 & 0 & 0 & 0 \\ 0 & 0 & 0 & -1 & 1 & 0 & 0 & 0 \\ 0 & \kappa & 0 & 0 & 0 & 1 & 0 & 0 \\ 0 & 0 & 0 & 0 & 0 & 0 & 1 & 0 \\ 0 & 0 & 0 & 0 & 0 & 0 & 0 & 1 \end{pmatrix}. \tag{4.66}$$

The second round of interactions with i_2, is given by the symplectic matrix

$$S_{int_2} = \begin{pmatrix} 1 & 0 & 0 & -\kappa & 0 & 0 & 0 & 0 \\ 0 & 1 & 0 & 0 & 0 & 0 & 1 & 0 \\ 0 & 0 & 1 & 0 & 0 & 0 & 0 & -1 \\ 0 & 0 & 0 & 1 & 0 & 0 & 0 & 0 \\ 0 & 0 & 0 & 0 & 1 & 0 & 0 & 0 \\ 0 & 0 & 0 & -1 & 0 & 1 & 0 & 0 \\ 0 & \kappa & 0 & 0 & 0 & 0 & 1 & 0 \\ 0 & 0 & 0 & 0 & 0 & 0 & 0 & 1 \end{pmatrix}. \tag{4.67}$$

Then the resulting state is described by the transformation $\sigma_{out} = S_{int_2}^T S_{int_1}^T \sigma_{in} S_{int_1} S_{int_2}$ which gives

$$\sigma_{out} = \begin{pmatrix} 3\kappa^2+1 & 0 & 0 & -\kappa & 2\kappa & 0 & 2\kappa & 0 \\ 0 & 1 & \kappa & 0 & 0 & -\kappa & 0 & -\kappa \\ 0 & \kappa & \kappa^2+3 & 0 & 0 & -(\kappa^2+1) & 0 & -(\kappa^2+1) \\ -\kappa & 0 & 0 & 1 & -1 & 0 & -1 & 0 \\ 2\kappa & 0 & 0 & -1 & 2 & 0 & 1 & 0 \\ 0 & -\kappa & -(\kappa^2+1) & 0 & 0 & \kappa^2+1 & 0 & \kappa^2 \\ 2\kappa & 0 & 0 & -1 & 1 & 0 & 2 & 0 \\ 0 & -\kappa & -(\kappa^2+1) & 0 & 0 & \kappa^2 & 0 & \kappa^2+1 \end{pmatrix}. \tag{4.68}$$

However, entanglement between the light mode and atomic ensemble is not produced until the interaction pulses are measured. We perform a homodyne measurement on the outgoing pulses i_1 and i_2 in the x-basis with results z_1 and z_2 to project into the final state described by the CM

$$\sigma_{fin} = \sigma^A - \sigma^C(X\sigma^B X)^{-1}\sigma^{C^T} \tag{4.69}$$

where σ^A is the upper left 4×4 matrix corresponding to the atomic and light modes, σ^B is the lower right 4 matrix representing the interaction pulses and σ^C and σ^{C^T} are the off diagonal matrices with entries corresponding to the correlations between the light mode, the atomic ensemble and the interaction pulses. The final covariance matrix for the two-mode composite state is given by

$$\sigma_{fin} = \begin{pmatrix} 1+\frac{\kappa^2}{3} & -\frac{2}{3}\kappa(1+\kappa^2) & -\frac{8\kappa^2}{3} & -\kappa-\frac{2}{3}\kappa(1+\kappa^2) \\ -\frac{2}{3}\kappa(1+\kappa^2) & 1+\frac{2}{3}\kappa(1+\kappa^2)^2 & \kappa-\frac{2}{3}\kappa(1+\kappa^2) & \frac{2}{3}\kappa(1+\kappa^2)^2 \\ -\frac{8\kappa^2}{3} & \kappa-\frac{2}{3}\kappa(1+\kappa^2) & 3-\frac{5\kappa^2}{3} & -\frac{2}{3}\kappa(1+\kappa^2) \\ -\kappa-\frac{2}{3}\kappa(1+\kappa^2) & \frac{2}{3}\kappa(1+\kappa^2)^2 & -\frac{2}{3}\kappa(1+\kappa^2) & 1+\frac{2}{3}(1+\kappa^2)^2 \end{pmatrix} \tag{4.70}$$

The final state is independent of the measurement outcomes, but they are present in the displacement vector.

4.9 Verification of Entanglement

On completion of the protocol, an analysis of the correlations induced between the atomic ensemble and light can be performed. Through the CM formalism we have complete access to all the information we need to verify entanglement. Since the full CM is available we can apply separability tests to the state. In this case we apply the positive partial transpose (PPT) test [121, 123, 124] which we introduced in chapter 2. Recall,, in phase space, any N mode Gaussian state can be transformed by symplectic operations in its Williamson diagonal form ν [125], such that $\sigma = S^T\nu S$, with $\nu = \text{diag}\{\nu_1, \nu_1, ..., \nu_n, \nu_N\}$. The set $\{\nu_i\}$ of all positive-defined eigenvalues of $|i\Omega\sigma|$ constitutes the symplectic spectrum of σ, the elements of which are the symplectic eigenvalues which must fulfill the conditions $\nu_i > 1$ to ensure the positivity of the density matrix associated with σ. The symplectic eigenvalues, ν_i, are determined by N symplectic invariants associated with the characteristic polynomial of the matrix $|i\Omega\sigma|$. In order to say something about entanglement, we recall that the CM's PPT is a necessary and sufficient condition for separability of all Gaussian states [126, 127]. If $\{\nu_i\}$ is the symplectic spectrum of the partially transposed CM $\tilde{\sigma}$, then a $(1+N)$-mode Gaussian state with CM σ is separable if and only if $\tilde{\nu}_i \geq 1\ \forall i$. If the partially time reversed CM does not fulfill the positivity condition, the corresponding state is entangled. We compute symplectic eigenvalues for the partially transposed CM $\tilde{\sigma}_{fin}$ as follows.

We partially transpose the matrix σ_{fin}. That is we apply the transformation $\tilde{\sigma}_{fin} = A^T \sigma_{fin} A$, where the matrix A is

$$A = \begin{pmatrix} 1 & 0 & 0 & 0 \\ 0 & 1 & 0 & 0 \\ 0 & 0 & 1 & 0 \\ 0 & 0 & 0 & -1 \end{pmatrix}. \tag{4.71}$$

This produces the time reversal (momentum sign change) that we require on the second mode. Then we find $|i\Omega\tilde{\sigma}_{fin}|$. This give us the matrix

$$\begin{pmatrix} -\frac{2}{3}i\kappa(1+\kappa^2) & i(1+\frac{2}{3}(1+\kappa^2)^2) & i(\kappa-\frac{2}{3}(1+\kappa^2)) & -i\frac{2}{3}(1+\kappa^2)^2 \\ -i(1+\frac{\kappa^2}{3}) & \frac{2}{3}i\kappa(1+\kappa^2) & \frac{8i\kappa^2}{3} & -i(\kappa+\frac{2}{3}(1+\kappa^2)) \\ i(\kappa+\frac{2}{3}\kappa(1+\kappa^2)) & -\frac{2}{3}i(1+\kappa^2)^2 & \frac{2}{3}i\kappa(1+\kappa^2) & i(1+\frac{2}{3}(1+\kappa^2)^2) \\ \frac{8i\kappa^2}{3} & i(\frac{2}{3}\kappa(1+\kappa^2)-\kappa) & i(\frac{5\kappa^2}{3}-3 & -\frac{2}{3}i\kappa(1+\kappa^2) \end{pmatrix}. \tag{4.72}$$

We can now compute the eigenvalues of this matrix. We find that for a realistic interaction strength $\kappa = 0.8$ the smallest eigenvalue of $|i\Omega\tilde{\sigma}_{fin}|$ is $\tilde{\nu} = 0.63$. Since this is less than one, the positivity condition is violated and the state must be entangled, confirming our nullifier analysis above.

4.10 Multi-mode composite cluster states

Here we extend our analysis to the multi-partite case. In general, composite clusters can be composed of m atomic modes with n light modes. We shall call these (m, n)-composite cluster states. Here we give the protocol for a $(4, 1)$ cluster, which will become the basic unit for the computational scheme in the next section.

Our protocol for the $(4, 1)$-composite cluster proceeds as follows. We construct a four-mode square cluster state from atomic ensembles labeled A_i (Fig.4.5), where $i = 1, ..., 4$ [110]. We include a light mode to form the composite state by entangling it with one of the atomic modes in the cluster. The $(4, 1)$-composite cluster, has nullifier relations

$$\begin{aligned} \hat{p}_{A_1} - \hat{x}_{A_2} - \hat{x}_{A_3} \to 0, \quad \hat{p}_{A_2} - \hat{x}_{A_1} - \hat{x}_{A_4} \to 0, \\ \hat{p}_{A_3} - \hat{x}_{A_1} - \hat{x}_{A_4} \to 0, \quad \hat{p}_{A_4} - \hat{x}_{A_2} - \hat{x}_{A_3} - \hat{x}_L \to 0 \\ \hat{p}_L - \hat{x}_{A_4} \to 0. \end{aligned} \tag{4.73}$$

We entangle a light mode L with ensemble A_4 (Fig.4.8). Following the four-mode atomic cluster protocol, the light mode is coupled to the existing atomic cluster with interaction pulses i_5 and i_6. The nullifiers of the atomic modes A_1, A_2 and A_3 are unaffected but the quadrature combinations for A_4 are now

$$\hat{p}^{out}_{A_4} = \hat{p}_{A_4} - \kappa^2 \hat{x}_{A_2} - \kappa^2 \hat{x}_{A_3} - \kappa^2 \hat{x}_L - \kappa N'_4, \tag{4.74}$$

where $N_4' = \hat{x}_{i_4} + \hat{p}_{i_2} + \hat{p}_{i_3} + \hat{p}_{i_5} + \hat{p}_{i_6}$ is the new back-action term. The light mode quadratures have transformed as

$$\hat{p}_L^{out} = \hat{p}_L - \kappa^2 \hat{x}_{A_4} - \kappa N_L, \tag{4.75}$$

and $N_L = \hat{x}_{i_5} + \hat{x}_{i_6}$. Note that the back-action terms, N_i, are composed of quadratures of the interaction light modes only. The interaction modes are momentum-squeezed and interact weakly with the ensembles so their back-action can be neglected (see also the related experiment [113] where this has been verified). We observe that we have a complete set of quadrature combinations that satisfies the composite cluster nullifier conditions (4.73). Finally, homodyne measuring i_5 and i_6 completes the protocol. We note that this protocol can be simply extended to creating general (m, n)-composite clusters of arbitrary shape. Further QND interactions can be used to add atomic ensembles and it is always possible to add a light mode to an atomic mode through the beam-splitter interaction. However adding extra nodes always results in extra back-action terms, N_i.

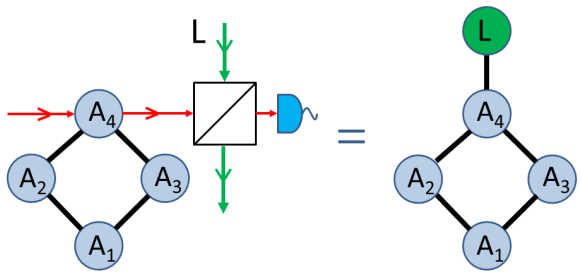

Figure 4.8: To add a light mode to the atomic cluster to form the $(4, 1)$-composite cluster pulses i_5 and i_6 interact with ensemble A_4 and the light mode L via a beam-splitter and are subsequently measured.

4.11 Limitations of CV cluster states

Here we will outline a fundamental problem with MBQC over CV cluster states. It can be shown that no matter what Gaussian local measurements are performed on systems distributed on a general graph, transport and processing of quantum information is not possible beyond a certain influence region, except for exponentially suppressed corrections. This result holds

even if non-Gaussian measurements are available. This result can be derived through the use of the *Gaussian projected entangled pairs* (GPEPS) formalism [112].

4.11.1 Gaussian PEPS

Projected entangled pair-states (PEPS) are a convenient class of quantum states that describe the ground states of local many-body Hamiltonians. They can be considered as a generalization of *matrix product states* (MPS) from one dimensional state to arbitrary graphs. PEPS forms a much richer class of states than MPS since they can be used to represent critical systems and systems with topological quantum order. Indeed it has been conjectured that all ground states of gapped local Hamiltonians in higher dimensions can be faithfully represented by PEPS [131]. PEPS are states defined over arbitrary graphs $G = (V, E)$ where quantum systems of local dimension d are placed at each vertex. The PEPS are then constructed by assigning to each edge $e \in E$ an entangled state $\sum_{i=1}^{D} |ii\rangle$, note at this point these represent maximal entanglement. Then each vertex $v \in V$ with degree k is associated with k virtual D-dimensional systems. The final step is to apply a map

$$A^{(v)} \ : \ \mathbb{C}^D \otimes \mathbb{C}^D \otimes ... \otimes \mathbb{C}^D \to \mathbb{C}^d, \tag{4.76}$$

which takes k D-dimensional systems to a single d-dimensional system. This single space now represents the physical system and $A^{(v)}$ is known as the PEPS projector. It is parameterized by tensors $A_i^{(v)}$ defined by

$$A^{(v)} = \sum_{i=1}^{d} \sum_{j_1,...,j_k=1}^{D} A_{i,j}^{(v)} |i\rangle\langle j_1, ..., j_k| \tag{4.77}$$

where $A_i^{(v)}$ is a tensor with k indices. Then we can write the PEPS as

$$|\psi\rangle = \sum_{i_1,...,i_n=1}^{d} \mathcal{C}[\{A_{i_v}^{(v)}\}_v]|i_1, ..., i_n\rangle, \tag{4.78}$$

where $\mathcal{C}$ is means the contraction of all tensors $A_i^{(v)}$ according to the edges of the graph.

These ideas can be generalized to CV systems, where each system is infinite dimensional [132]. If these systems are represented by Gaussian probability distributions we can specialize to Gaussian PEPS (GPEPS). Now we relax the condition of perfectly entangled pairs, instead the bonds we consider are two-mode squeezed states. For GPEPS on general graphs $G = (V, E)$, the vertices V represent physical systems and E the connections between them. In any such graph $d(.,.)$ is the natural graph-theoretical distance between two vertices.

When a particular vertex has N adjacent bonds, the CV equivalent of projection map $A^{(v)}$, is a Gaussian operation of the form

$$V : \mathcal{H}^{\otimes N} \to \mathcal{H}. \tag{4.79}$$

This operation can alway be made trace preserving [133, 134]. We refer to this operation as a Gaussian PEPS projection. This can alway be performed by mixing single-mode squeezed states on a suitably tuned beam-splitter.

We now look at some concepts that we will need to prove the limit on transport in CV graph states. First we consider a useful measure of the entanglement in graph states.

4.11.2 Localizable entanglement

The *localizable entanglement* between two sites A and B of the graph $G = (V, E)$ is defined by the maximal entanglement obtainable on average when performing projective measurements at all sites but A and B [135]. When we require both the initial state and the measurements to be Gaussian, the situation simplifies as the entanglement properties do not depend on the measurement outcomes. Thus, we do not need to average but only find the best measurement strategy. Then we measure the entanglement with the logarithmic negativity, which, we recall from Chapter 2 can be defined as

$$E(\rho) = \log ||\rho^{T_A}||_1, \tag{4.80}$$

where T_A denotes the partial transpose with respect to subsystem A and $||.||_1$ is the trace norm. Here we only allow for Gaussian local measurements, in which case Eq.(4.80) coincides with quantity known as *Gaussian localizable entanglement*, denoted E_G. It is possible to expand this definition for more general measurements by taking fixed subspaces S_A and S_B in the Hilbert spaces associated with site A and B that are entangled by means of some local but not necessarily Gaussian measurements. In this case we refer to the *subspace localizable entanglement*, E_S. Both concepts relate to the transport in measurement-based quantum computing.

4.11.3 One-dimensional chain

Our first statement on entanglement on GPEPS serves concerns just one-dimensional chains. We do not allow for multiple bonds in the construction of the chain. Then we can state the following [112],

Theorem 4.11.1. *(Exponential decay of Gaussian localizable entanglement in a 1D chain). Let G be a one-dimensional GPEPS and A and B two sites. Then*

$$E_G(A, B) \leq c_1 e^{-d(A,B)/\xi_1} \tag{4.81}$$

where $c_1, \xi_1 > 0$ are constants. The best performance is reachable by passive optics and homodyning only.

In [112] it was shown that the consequence of this theorem is the impossibility of building a one-dimensional quantum repeater relying on Gaussian states, if only local measurements and no distillation steps are used. This is the case even if the information encoded into the GPEPS is in the form of qubits. For our schemes, it also follows that we cannot build large scale one-dimensional cluster states without incurring large errors in a given computation. Or put another way, it is not possible to create a perfect quantum wire with just Gaussian operations.

4.11.4 General graphs

We can go further and ask how theorem 4.11.1 changes when we consider graphs of arbitrary dimension.

Theorem 4.11.2. *(Exponential decay of Gaussian localizable entanglement of GPEPS on general graphs). Consider a GPEPS on general graphs with finite dimension and let A and B be two vertices of this graph. Then there exist constants $c_2, \xi_2 > 0$ such that*

$$E_G(A, B) \leq c_2 e^{-d(A,B)/\xi_2}, \tag{4.82}$$

So it turns out that considering graphs in higher dimensions does nothing to improve the degree of entanglement loss. While this exponential loss of entanglement may seem the worst case scenario, it is still possible to create cluster states and perform computational processes since for any finite distance $d(A, B)$ and required entanglement $E(A, B)$ there exists a finite minimal squeezing λ_{min} which allows an arbitrary task to be performed. This result is important when considering quantum computation over CV cluster states using Gaussian operations to process that states. Essentially, this theorem implies that any quantum computational task must be restricted to small scale cluster implementations or we must have access to non-Gaussian resource states.

4.12 A new architecture

The decrease in localizable entanglement with increasing cluster size when only Gaussian operations are available places a limit on the size of useful cluster states, i.e. those that have sufficient entanglement available to perform processes below the computational error threshold. The MBQC model we described earlier in this chapter traditionally relies on creating large clusters on which the entire computation can be performed and read out. Here we seek to address this difficulty in the practical implementation of cluster state computation. We propose to split up large clusters into smaller building blocks or *qubricks* which are composed of an atomic cluster state, acting as a *quantum processor*, and a light mode that allows for communication to

other qubricks (Fig.4.9). A similar suggestion to increase the efficiency of generating qubit cluster states based on ancillia light modes was made in [137]. In our scheme, many atomic cluster states, labeled $(C_1, ..., C_N)$, are

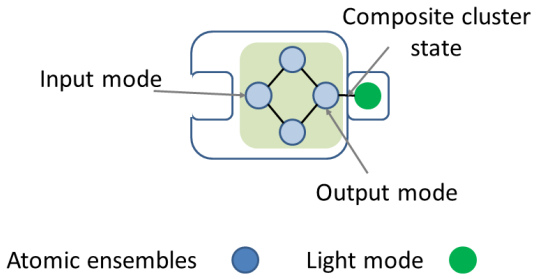

Figure 4.9: A basic *qubrick* composed of a four-mode atomic cluster state plus a light mode to create a composite cluster. Reprinted figure with permission from D. F. Milne and N. V. Korolkova,Phys. Rev. A **85**, 032310. Copyright (2012) by the American Physical Society.

created. Each of these act as a small quantum processor which performs some unitary operation $\hat{U}_i$ on an input state. Each processor C_i, *shares no entanglement* with any other in the array. We keep the number of nodes in each atomic cluster small, say four nodes each (Fig.4.5), which is minimum sufficient for any two-mode controlled quantum gate. By limiting the size of the cluster states, the decay of entanglement within each processor is kept to a minimum. To allow communication between the processors, we entangle an ancillary light mode L with the output node in the atomic cluster to form a qubrick which is a $(4, 1)$-composite cluster. The light mode of the qubrick can then be used to convey the output of the process performed on the atomic cluster contained in the brick to the next in the array (Fig.4.10). Given sufficient resources, the state can be processed in parallel using strings of qubricks. The total output from each of the strings can then be combined to give the final output. In more detail, a typical process would proceed as follows. A state $|\psi_{ini}\rangle$, is loaded onto the first cluster C_1. Adaptive measurements are then applied to the atomic ensembles to process the state with outcome $|\psi'\rangle = \hat{U}_1|\psi_{ini}\rangle$. A light mode L_1, is added to C_1 to form the qubrick and the state is transferred to L_1 by a further measurement (Fig.4.11). Since the cluster and its associated entanglement has been destroyed in the measurement process the light pulse is free to carry the information to the next qubrick, without inadvertently entangling the atomic clusters belonging to different bricks. Another measurement transfers the state onto the first node of the atomic cluster, C_2 and a gate operation is performed by a new sequence of measurements yielding $\hat{U}_2|\psi'\rangle$. A light mode

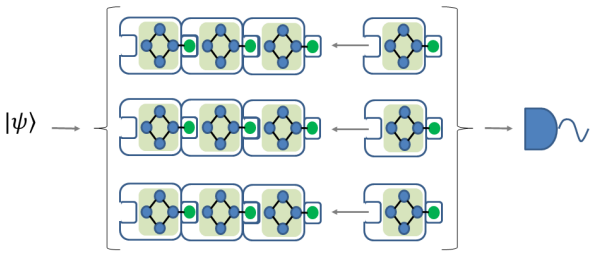

Figure 4.10: The qubricks interact by matching up their output light modes with the input of another qubrick. A state can be loaded onto the first brick at time t_1, the state is processed through adaptive measurements and the output encodes onto the light mode. The qubrick at t_1 having been measured no longer contributes to the state. The light pulse is connected with the next in the sequence of qubrick processes t_2 and the process is repeated. This operation can be run in parallel with other sequences of qubricks and the final state is given by their combined outputs. Reprinted figure with permission from D. F. Milne and N. V. Korolkova,Phys. Rev. A **85**, 032310. Copyright (2012) by the American Physical Society.

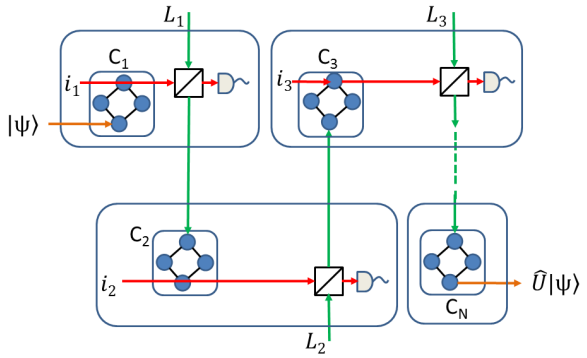

Figure 4.11: Each cluster C_i is kept separate and only communicate through light pulses L_i. The state to be computed is loaded onto C_1, which undergos a sequence of adaptive measurements. A composite cluster is formed to transfer the state to a light mode which is carried to the next cluster in the process. Each cluster acts on the state by some unitary $\hat{U}_i$ and the final state is given by $\hat{U}|\psi\rangle$. Reprinted figure with permission from D. F. Milne and N. V. Korolkova,Phys. Rev. A **85**, 032310. Copyright (2012) by the American Physical Society.

L_2, is added to C_2 to form a new qubrick and it carries the processed state is to the next cluster. Since each cluster applies some unitary transformation $\hat{U}_i$ to the state, this process can be repeated until the desired output if achieved and the state is given by $\hat{U}|\psi\rangle = \hat{U}_i \otimes \hat{U}_{i-1} \otimes ... \otimes \hat{U}_2 \otimes \hat{U}_1|\psi\rangle$.

It is important to note that we do not claim that this procedure outperforms the error rate of large cluster arrays in general. What the qubrick scheme does guarantee, is that the loss of entanglement and therefore the errors accumulated in each quantum gate are constant. Then the errors that propagate through the computation are just proportional to the number of qubricks used. This is in contrast to the large cluster state in which the entanglement decays exponentially with the size of the cluster and hence errors accumulate rather quickly as the cluster size increases. Note however, that the error rate of particular geometries of large scale cluster states actually outperform the qubrick scheme i.e., for a 16-node square cluster. In this case the entanglement scales as Ce^{-6}, where C is some constant. If we assume the error rate increases proportional to the degradation of entanglement then the errors scale as ae^6 where a is some constant that depends on the particular system in question. In the qubrick setting, to replicate this state exactly, we require four qubricks and the cumulative error then scales as ae^8, which is significantly worse. Here we do not propose that the qubricks mimic the large scale states exactly (since they can never beat the fundamental limit anyway). In this scheme, each qubrick and hence each quantum gate is initialized individually and only when it is required (Fig.(4.10)). These gates are then directly coupled to the light pulse carrying the output from previous processes. This scheme removes the need for nodes serving as quantum wires to convey information around the cluster and eliminates any redundant nodes. In doing so we suppress the exponential losses due to entanglement decay and hence reduce the error rate.

Furthermore, this method can be simplified to just one qubrick, if we loop the output from the brick back to the input in a similar manner to that proposed in [25]. In this scheme, the output from the first computation again gives $|\psi'\rangle = \hat{U}_1|\psi\rangle$. The atomic cluster is re-generated and the light mode is fed back into the input node where a different series of adaptive measurements is performed. This gives $\hat{U}_2|\psi'\rangle$ which is processed again until the desired unitary is enacted. This scheme eliminates the parallel element but it vastly decreases the number of resources required while maintaining a constant error rate. In this case the error depends on the number of times the state is reused. This type of scheme could form the basis of a proof of principle demonstration of CV cluster state computation with atomic ensembles since it is achievable with currently available technology.

Chapter 5

Topological quantum computation over continuous variables

We now leave behind the measurement-based model for QC and for the remainder of this thesis we focus on a relatively new paradigm in quantum information. That of *topological quantum computation* (TQC). Since its inception, this field has grown very rapidly, not just for its intrinsic value as a theoretical work but also due to its potential for practical implementations of quantum computation [140, 141, 142, 143, 144, 145, 146, 147, 148, 149, 150, 151]. The interested reader is referred to the literature for a more complete introduction to TQC, [152, 153]. In the following we will present a new model of quantum computation based on these ideas related to topology. Like previous proposals our scheme stores and manipulates information in *topological degrees of freedom* rather than in localized systems such as electron or nuclear spin [154, 155], or photon polarization [156]. In the ideal case, storing quantum information in these non-local degrees of freedom protects the information from local errors. Of course in practice this alone still does not give us perfect error protection. In reality a system Hamiltonian can be perturbed by external effects. This may lead to non-zero tunneling amplitudes between orthogonal ground states and depending on the encoding of the quantum information within the ground state these pertubations may lead to errors in the stored data and on any quantum processes performed on the system. However, within topological systems it has been shown that the errors induced by these events scale by factors of only $e^{-\alpha l}$, where l is the length scale of the system. This represents a significant improvement over traditional methods of QC as long as l is ensured to be fairly large. As with any quantum computational model we want to design a physical system capable of storing quantum information sufficiently accurately such that normal quantum error correction (QEC) can be successfully applied.

Systems that exhibit non-local properties are hoped to be the basis for such models.

Although in this thesis we focus in the creation of topological states from lattices composed of optical elements, such states have been known to occur in a condensed matter setting through collective electronic systems as in the Fractional Quantum Hall Effect (FQHE) [158, 159] and 2D cuprate superconductors above T_c [160, 161]. For a comprehensive review of the FQHE see [193, 163]. There has been much study into the connection between the FQHE and quantum computation. It has been shown that the ground state of the $\nu = 1/3$ electron liquid on the torus is 3-fold degenerate. This follows from the fact that excitations in this system are abelian *anyons* which have the property that moving one anyonic excitation around another multiplies the state vector by a phase factor $e^{i\theta}$ (for $\nu = 1/3$, $\theta = 2\pi/3$). We will be discussing anyons in some depth in later section. For now however it is sufficient to understand that the process of creating a particle-antiparticle pair, moving one of the particles around the torus and annihilating it specifies a unitary operation on the ground state. By moving the particle in two different directions one obtains two different unitary operators A_1 and A_2 with the commutation relation $A_1 A_2 A_1^{-1} A_2^{-1} = e^{i\theta}$, implying a ground state degeneracy. This argument is very robust and only requires the existence of an energy gap or, equivalently, finite correlation length l_0. The degeneracy is lifted only by spontaneously tunneling of virtual excitations around the torus. The resulting energy splitting scales as e^{-l/l_0}, where l is the size of the system. Interaction with the environment does not change this conclusion, although thermal noise can create actual excitation pairs rather than virtual ones.

Both the ground state degeneracy on the torus and the existence of anyons are manifestations of the topological properties of the $\nu = 1/3$ liquid itself. Anyons can be regarded as *topological defects* similar to Abrikosov vortices (a vortex of super-current in a type II super-conductor) but without any local order parameter. The presence of one particle enclosed by a loop can be detected by holonomy - moving another particle around the loop.

The most powerful and flexible way of storing quantum information in topological systems is based on non-abelian anyons. These will be the subject of chapter 6 but we will briefly introduce the concept here. They are believed to occur naturally in the $\nu = 5/2$ and $\nu = 12/5$ FQHE states [152]. Within the 5/2 state there exist charge 1/4 anyonic particles as well as some other excitations. The quantum state of the system with $2n$ particles with charge 1/4 on the plane is 2^{n-1} degenerate. The degeneracy is gradually lifted as two particles come close to each other. More precisely, the 2^{n-1} dimensional Hilbert space $\mathcal{H}_n$ splits into two 2^{n-2} dimensional subspaces. These subspaces correspond to two different types of charge 1/2 particles which can result from fusion of charge 1/4 particles. This splitting allows for the possibility to store qubits in the Hilbert spaces corresponding to these

fusions. i.e. the two different outcomes correspond to either a $|1\rangle$ or a $|0\rangle$. Thus observing the fusion outcome can be equivalent to measuring a qubit and hence a measurement on the Hilbert space $\mathcal{H}_n$. This model supports adaptive quantum computation where surfaces of high genus are included in the theory.

In the following we will construct a system that support continuous-variable analogues of anyons and develop a topological computational model. First we discuss the emergence and properties of anyons in some depth. We keep this discussion quite general since at this point we don't restrict ourselves to a particular physical scenario.

5.1 The emergence and behaviour of anyonic systems

Anyons can be considered as particles which obey more general statistical rules than those found in the usual Fermi-Dirac or Bose-Einstein statistics. Due to this, the term fractional statistics is often used in connection with anyons [164]. There exist two main approaches to describe anyonic behaviour. The first incorporates fractional statistics through fictitious Chern-Simons gauge fields [165, 166, 167] which transmute the statistics into the particular topological interactions. The second makes use of the quantum symmetries as described by *Hopf algebras* [140, 168, 169, 170, 171], which offer a unified description of the particle properties. Both approaches capture the same physics, but the latter approach is more useful when considering quantum computation as it provides more insight into the topological spaces that are used to encode quantum information. Here we will not directly require either theory, for our purposes it will be sufficient to derive anyonic properties from physical considerations. However, it should be possible to describe the system presented here in the Hopf algebra language thanks to work that has been done on generalizing the Hopf algebra construction from finite groups to Lie groups [172, 173].

To illustrate the defining property of anyons, consider the symmetry properties of an N-particle system of varying spatial dimension. Under the action of S_N, the permutation group of N particles, the Hamiltonian of the system remains invariant, but the eigenstates $|\psi_j\rangle$ are transformed according to an irreducible representation. Denote by $\psi_j(1,2,...,N) = \langle 1,2,...,N|\psi_j\rangle$ the N-particle wave function and let $U(\theta)$ be an operator implementing a particular permutation θ. The action of this operator is given by the transformation,

$$U(\theta)\psi_j(1,2,...,N) = \sum_k \psi_k(\theta(1),\theta(2),...,\theta(N))P_{kj}(\theta), \qquad (5.1)$$

where P_{kj} are the matrices representing the permutation θ. In most quantum

mechanical systems the Fermi-Dirac and Bose-Einstein statistics are sufficient to describe the symmetry properties of the wave function. However these two cases are merely the one-dimensional representations of the permutation group. In particular these are the trivial representation $P(\theta) = 1$ which corresponds to Bose statistics and the alternating representation $P(\theta) = (-1)^{|\theta|}$, with $|\theta|$ the number of interchanges in θ corresponding to fermions.

Anyons are also described by irreducible representations of the permutation group but they have different forms from those for bosons and fermions. These representations appear when one reduces the number of spatial dimensions. The symmetry group to which the permutation θ belongs, depends on the the structure of the fundamental group $\pi_1(M_N^D)$ where M_N^D is the D-dimensional configuration space for N-particles. From physical considerations, we note that M_N^D is not simply connected (otherwise indistinguishable particles would be allowed to coincide) and thus the fundamental group is non-trivial. The most interesting effect from our perspective is the dependence of the the first homotopy group on the spatial dimension. Of most importance here is the two dimensional case. For $D = 2$ the fundamental group is known to be isomorphic to the *N-string braid group*,

$$\pi_1(M_N^2) \cong B_N \tag{5.2}$$

whereas for $D \geq 3$ it is isomorphic to the permutation group of N-objects, $\pi_1(M_N^D) \cong S_N$. The one-dimensional irreducible representations of S_N are just the trivial and alternating representations. On an interesting note, clearly this group does have higher-dimensional irreducible representations, but the statistics that they would represent have not been observed in nature. Physically, we can put this difference down to the different ways of braiding in varying spatial dimensions. In $(3+1)D$ or higher, any closed loop around an object can be pulled over and contracted to the trivial loop, Fig. (5.1). Hence in higher dimensions we should never see any statistics other than those corresponding one-dimensional representations i.e., to bosons and fermions since those are the only cases that a complete loop results in the identity operation on the wave-function.

In the $(2 + 1)D$ case we are restricted to the plane and closed loops no longer have the freedom to be lifted over objects, Fig.(5.4). These loops can then be said to be topologically non-trivial since they cannot be reduced to points. Since the loops are non-trivial we are not restricted to only performing identity operations on the state. We can see this by considering the following. The spin statistics of the exchange of particles can be represented through their wavefunctions as

$$\psi(\vec{r}_1, \vec{r}_2) = e^{i\theta}\psi(\vec{r}_2, \vec{r}_1), \tag{5.3}$$

We consider our particle exchange as a rotation of one of the particles around the other. The center of mass of the system is just $\vec{R} = (\vec{r}_1 + \vec{r}_2)/2$. Then

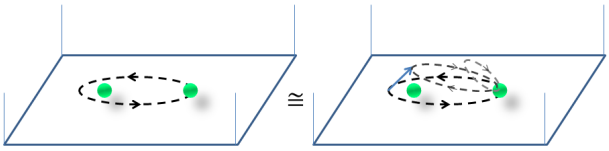

Figure 5.1: In (3+1)D we can always contract any loop that braids two particles to the trivial loop. Then only boson and fermion statistics can be observed in three spatial dimensions.

$\vec{r} = \vec{r}_1 - \vec{r}_2$ is the relative coordinate and for point-like particles we have $||\vec{r}|| \neq 0$. This allows us to visualize the particle exchange on the surface of a sphere in two or three dimensions, with $||\vec{r}|| = \text{const}$ the radius of the sphere. In $3D$ we can draw three closed trajectories. These are shown in Fig.5.2. The first case, Fig. 5.2(a), shows a trivial loop where the particles are

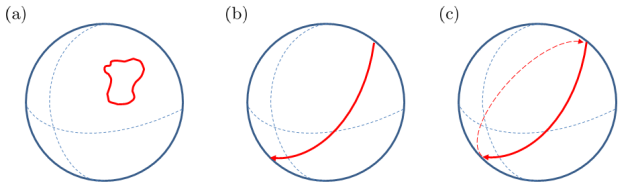

Figure 5.2: Closed trajectories in $3D$. (a) no exchange, $\theta = 0$. (b) Single exchange, cannot be deformed to a point. (c) Double exchange, trajectory can be shrunk to a point.

not exchanged and the trajectory may be shrunk to a point which implies that $\theta = 0$. In 5.2(b), there is an exchange, but the path may not be contracted. Finally in 5.2(c) we have the double exchange but this may also be contracted. Since cases (a) and (b) are equivalent we see that the following must hold

$$(e^{i\theta})^2 = e^0 = 1 \Longleftrightarrow e^{i\theta} = \pm 1 \tag{5.4}$$

This ties in nicely with our discussion above since we see now that this can only occur for $\theta = 0,\ \pi$ which correspond to bosons and fermions. The $2D$ situation is different, now we restricted to a circle. Now in the last case Fig.5.3(c) we cannot deform the double exchange to a point and so in general

$$1 \neq e^{i\theta} \neq (e^{i\theta})^2 \neq ... \neq (e^{i\theta})^n, \tag{5.5}$$

and we observe that the phase θ can take any value in $\mathbb{R}$. It is referred to as the statistics parameter and is connected to the particle spin by $s = \theta/2\pi$. This opens up the possibility for more exotic particles statistics since we may

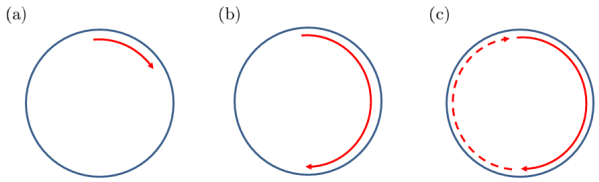

Figure 5.3: Closed trajectories in $2D$. (a) no exchange. (b) Single exchange. (c) Double change but now this path cannot be shrunk to a point so $e^{i\theta} \neq (e^{i\theta})^2$.

now have $P(\theta) = e^{i\theta}$ or even higher dimensional representations represented by unitary matrices acting on the state. Then we arrive at the conclusion

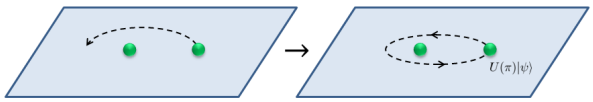

Figure 5.4: When restricted to two spatial dimensions, braids cannot reduced to trivial loops and so braiding particles can result in unitary evolutions of the wavefunction.

that anyonic behaviour only manifests in two spatial dimensions and the symmetry properties of the N-anyon wave-function are described by the braid group B_N.

The braid group is a non-abelian group of infinite order [157]. It is generated by $n-1$ elements $\tau_1, ..., \tau_{n-1}$, where τ_i establishes a counterclockwise interchange of the particles i and $i+1$. These generators are subject to the relations

$$\begin{aligned} \tau_i\tau_{i+1}\tau_i &= \tau_{i+1}\tau_i\tau_{i+1} \quad i = 1, ..., n \\ \tau_i\tau_j &= \tau_j\tau_i \qquad |i-j| \geq 2, \end{aligned} \tag{5.6}$$

which can be represented graphically as in Fig. (5.5) and (5.6). In fact,

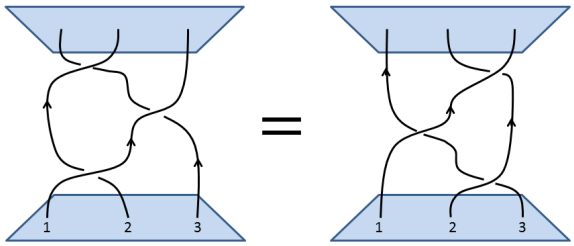

Figure 5.5: Pictorial representation of the first generator relation (5.6). Time is the vertical axis.

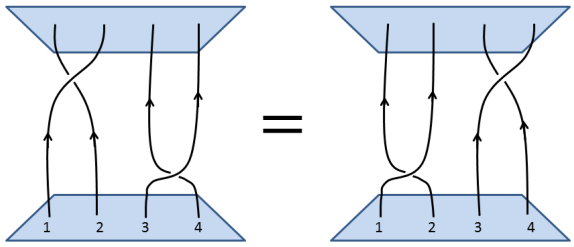

Figure 5.6: Pictorial representation of the second braid relation.

the permutation group S_N ruling the particle exchanges in three or more dimensions is given by the same set of generators with relations (5.6) and the additional relations $\tau_i^2 = e$ for all $i \in 1, ..., n-1$. These last relations are absent for $\pi_1(M_N^D) \cong B_N$, since in the plane a counterclockwise particle interchange τ_i ceases to be homotopic to the clockwise interchange τ_i^{-1}.

If the wave function transforms in some one-dimensional irreducible representation of B_N, one talks of *abelian anyons*. Wave-functions transforming in some higher dimensional irreducible representation are said to describe *non-abelian anyons*.

5.2 Requirements of anyon models

We have found that a model of anyons is a theory of particles on a two-dimensional surface. However the peculiar statistics of the anyons can be interpreted as a kind of interaction which is topological in nature. This is where we can make a connection with the *Aharonov-Bohm* effect taking place between magnetic flux and electric charge. Under this analogy, the representations carried by the quasiparticles can take the meaning of charge and flux and we have convenient illustration of anyons as charged topological excitations confined to the plane. This intuitive picture is useful

when considering anyonic behaviour and it holds regardless of the physical scenario in which the anyons arise. In some cases the flux-charge analogy is an accurate physical description, since in some superconductor systems the fluxes are magnetic vortices carrying quantized magnetic flux and the charges are condensates of the matter fields carrying some quantized electric charge as a collective property. In other cases, including those that will be discussed here, the quasiparticles may manifest themselves are collective excitations bearing no direct correspondence to the elementary magnetic of electric charge. The topological interactions still exist as if the quasiparticles were carrying some flux and charge, but these are to be regarded as fictitious properties having nothing to do with ordinary electromagnetism. Through the connection to the Ahanarov-Bohm effect we can assign to each particle a locally conserved *charge*. We also assume the theory has a mass gap, so there are no long range interactions between particles mediated by massless particles.

Based on this analogy we can construct general anyon models, these must have the following defining properties:

- A list of particle *types*. The types are labels that specify the possible values of the conserved charge that a particle can carry
- Rules for *fusing and splitting*, which specify the possible values of the charge that can be obtained when two particles of known charge are combined together and the possible ways in which the charge carried by a single particle can be split into parts.
- Rules for *Braiding*, which specify what happens when two particles are exchanged (or when one particle is rotated by 2π).

We now focus on specific topolgocial models. We begin with the abelian *toric code*. This is a topological surface code with a particularly simple and completely solvable Hamiltonian. Excitations on the surface turn out to correspond to abelian anyons. We briefly review the main features and dynamics of this model in the next section before going on to generalize the idea to the continuous-variable regime.

5.3 The Kitaev Model

The toric code is an exactly solvable spin 1/2 model on a square lattice (more generally, we can extend the model from a square lattice to any planar graph) [140, 174, 175]. It exhibits a ground state degeneracy of 4^g when embedded on a surface of genus g and a quasiparticle spectrum with both bosonic and fermionic sectors. We consider a square lattice, possibly embedded into a nontrivial surface such as a torus, with spins on the edges of the lattice.

This system has the Hamiltonian

$$H = -J_c \sum_v A_v - J_m \sum_f B_f \tag{5.7}$$

where A_v is defined for each vertex v as

$$A_v = \prod_{j \in star(v)} X_j \tag{5.8}$$

and the plaquette operator acts on the four spins surrounding a face

$$B_f = \prod_{j \in \partial(f)} Z_j, \tag{5.9}$$

$\partial(f)$ are the qubits forming the boundary of a plaquette. The operators X and Z denote the standard Pauli matrices σ_x and σ_z, respectively, The reason for using the X and Z notation will become clear in the next section when we make a connection to continuous-variable phase-space operators. The Pauli operators form the stabilizers A_v and B_f. In the square lattice, Fig. (5.7), each term of the Hamiltonian H represents four body interactions of local qubits. Clearly, the A_v all commute with one another, as do the B_f. Less obvious is the commutation

$$A_v B_f = B_f A_v \tag{5.10}$$

because any given vertex and face share an even number of edges (either none or two) and therefore the minus signs arising from the commutation of X and Z on those edges cancel. Since all of the terms commute, it is straightforward to find the ground state $|\psi\rangle$ of the Hamiltonian H. We will

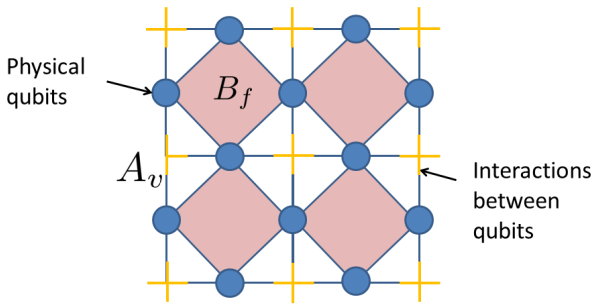

Figure 5.7: The Kitaev toric code on a square lattice. This has two stabilizer conditions A_v and B_f defining stars (yellow crosses) and plaqettes (red squares) respectively.

solve H working in the Z basis. Define classical variables $s_j = \pm 1$ to label the Z basis states. For each classical spin configuration $\{s\}$, we can define the plaquette flux

$$w_f(s) = \prod_{j \in \partial f} s_j \tag{5.11}$$

If $w_f = -1$, we say there is a *vortex* on face f.

5.3.1 Ground states

To find the ground states $|\psi\rangle$ of H, we minimize the energy. This in turn requires us to maximize the energy of the A_v and B_f terms. The plaquette terms provide the condition

$$B_f|\psi\rangle = |\psi\rangle \tag{5.12}$$

which only holds if and only if

$$|\psi\rangle = \sum_{w_f(s)=1 \ \forall f} c_s|s\rangle \tag{5.13}$$

That is, the ground state contains no vortices. The group of vertex operators act on the configurations s by flipping spins. Thus, the vertex conditions

$$A_v|\psi\rangle = |\psi\rangle \tag{5.14}$$

can only happen if the constants c_s are equal for each orbit of the action of the vertex operators, otherwise we would obtain violations of the ground state when acting on different vertices. This requirement uniquely determines the ground state.

On the torus, we can define conserved numbers given by the function

$$w_l(s) = \prod_{j \in l} s_j, \quad l = l_1, l_2 \tag{5.15}$$

where l_1 and l_2 are two independent non-trivial cycles on the square lattice wrapping the torus. Any given vertex will overlap with a loop l in either zero or two edges and therefore A_v preserves w_l. Since there are two independent loops on the torus, each of which can have $w_l = \pm 1$, there is a four-fold degenerate ground state:

$$|\psi\rangle = \sum_{w_p(s)=1 \ \forall f} c_{w_{l_1} w_{l_2}}|s\rangle. \tag{5.16}$$

5.3.2 Excitations of the toric code

The excitations of the toric code come in two varieties: the *electric charges* and *magnetic vortices*, similar to those of a $\mathbb{Z}_2$ gauge theory. To find electric charges, we define the operator

$$W_l^{(e)} = \prod_{j \in l} Z_j \tag{5.17}$$

where l is a path in the lattice going from s_1 to s_2. This operator clearly commutes with the plaquette operators B_f and with all vertex operators A_v except for at the end points s_1 and s_2, where only one edge overlaps between the vertex and the path and we have

$$W_l^{(e)} A_{v1} = -A_{v1} W_l^{(e)}. \tag{5.18}$$

Therefore the state

$$|\psi_{v1,v2}\rangle = W_l^{(e)} |\psi_0\rangle, \tag{5.19}$$

where $|\psi_0\rangle$ is the planar ground state, is an eigenstate of the Hamiltonian with excitations (charges) at v_1 and v_2 that each cost energy $2J_e$ to create relative to the ground state.

An analogous construction will find the magnetic vortices. For this we define the dual path operator

$$W_{l^*}^{(m)} = \prod_{j \in l^*} X_j \tag{5.20}$$

where the path l^* lies in the dual lattice and goes from f_1 to f_2. In this case, the vertices A_v all commute with $W_{l^*}^{(m)}$, as do all the plaquette operators B_f except the two at the end points of l^*, which anticommute. Thus the $W_{l^*}^{(m)}$ operator creates a pair of magnetic vortices on the plaquettes f_1 and f_2 at an energy of $2J_m$ each.

5.3.3 Abelian statistics and superselection sectors in toric code

Here we discuss what happens when we exchange two particles on the toric code. To ensure that particle statistics are well-defined, we assume there are no long-range interactions and the phase is gapped. Since path operators of the same type commute with one another, braiding particles of the same type will only act trivially on the ground state. Through these mutual statistics we infer that particles of the same type are bosons with respect to each other. However, we find nontrivial statistics when the two different particle types interact with each other. To calculate the mutual statistics, consider taking a charge e around a vortex m.

Let $|\psi_m\rangle$ be some state containing a magnetic vortex at f_1. Under the full braiding operation,

$$|\psi_{m,1}\rangle' \to \left(\prod_{j\in l} Z_j\right)|\psi_{m,1}\rangle = \left(\prod_{p\ inside\ l} B_f\right)|\psi_{m,1}\rangle \tag{5.21}$$

where the second equality is a Stoke's theorem like result relating the product around a loop to the product of the internal loops. Since

$$B_{f1}|\psi_{m,1}\rangle = -|\psi_{m,1}\rangle \tag{5.22}$$

for the plaquette f_1 containing the vortex, we have that

$$|\psi_{m,1}\rangle \to -|\psi_{m,1}\rangle \tag{5.23}$$

This is represented diagramatcially in Fig.(5.8). Going further, using the

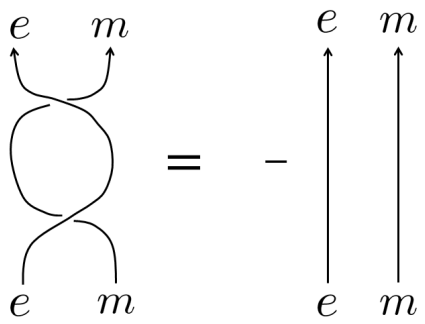

Figure 5.8: The braiding of e and m excitations is equivalent to aquiring a phase of -1.

bosonic self statistics equations, Fig. (5.9), we can derive the nontrivial corollary that composite $e-m$ particles are fermions, Fig.(5.10). We are now in a position to characterize all the particle types in the toric code. Each corresponds to a *superselection sector*, which is a representation of the local operator algebra. To avoid multiple counting of particle types we say that two particles (or composite objects) are *of the same type*, that is $a \propto b$ if a can be transformed into b by some operator acting in a finite region. For example, in the toric code, two e-type particles are equivalent to having no particles at all if acted upon with an appropriate, geometrically bounded electric path operator. Recalling our notation above, this is equivalent to to the relation

$$e \times e = 1 \tag{5.24}$$

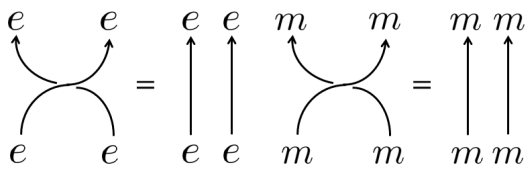

Figure 5.9: Particles of the same type are bosons with respect to each other as they have bosonic mutual statistics.

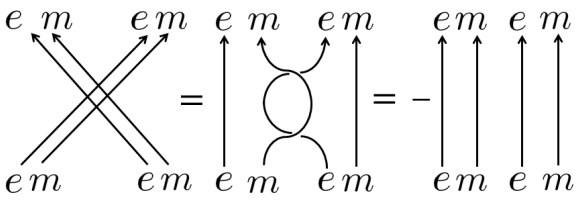

Figure 5.10: Composite particles composed of e- and m-types have fermionic statistics.

which represents the *fusion rule* of two e-particles which are equivalent to the vacuum sector 1. In the toric code, there are four superselection sectors

$$1,\ e,\ m \text{ and } \ \epsilon = e \times m \tag{5.25}$$

with the fusion rules

$$\begin{aligned} e \times e &= 1 \quad e \times m = \epsilon \\ m \times m &= 1 \quad e \times \epsilon = m \\ \epsilon \times \epsilon &= 1 \quad m \times \epsilon = e \end{aligned} \tag{5.26}$$

At this point we have a complete set of anyons that we can initialize and move around a lattice. We have found that they have interesting mutual statistics that cause phase changes of -1 on the wavefunction under braiding. However the toric code in the form presented here, while useful as a quantum memory, has limited use for quantum computation as the excitations produced are Abelian and hence cannot perform general unitary evolutions of the Hilbert space. This completes our introduction to the toric code. Much work has been done that goes far beyond what has been discussed here and we refer the reader to [175, 176, 177] and references therein for further information and recent developments.

Having understood this discrete model, we seek to generalize the Kitaev code to the continuous-variable regime. In the following sections we will discover that we can formulate a CV equivalent of anyons and furthermore, we can use them to perform CV quantum computation. First however we must construct the ground state for our anyonic excitations.

5.4 Continuous-Variable toric codes

There exist many proposals to realize the discrete-variable Kitaev toric code and hence abelian anyon statistics. In order to generate a CV analogue of the Kitaev state, we employ CV cluster states and seek to create the CV toric code dynamically via projective measurements. This is a particularly convenient method since the extension from discrete to CV cluster states is well understood. A similar procedure for qubits was proposed in [178]. In the following we will show how a CV toric code is produced from a CV cluster state, will then examine the excitations on the code and find that they constitute a CV equivalent to abelian anyons [179].

5.5 Generation of anyonic ground states from CV graph states

First we recall the basic principles of CV cluster states from our previous chapter. In the ideal case, CV cluster states are prepared from a collection

of N zero-momentum eigenstates, written $|0\rangle_p^{\otimes N}$, where the p-subscripted kets satisfy $\hat{p}|s\rangle_p = s|s\rangle_p$. These states are entangled via a collection of controlled-Z operations, denoted $C_Z = \exp(ig\hat{x}_i \otimes \hat{x}_j)$, where $g \in \mathbb{R}$ is the strength of the interactions (we will assume $g = 1$ throughout). Labeling the nodes of the graph in some arbitrary order, we can define a symmetric *adjacency matrix* $\mathbf{A} = \mathbf{A}^T$ whose $(j,k)th$ entry A_{jk} is equal to the weight of the edge linking node j to node k (with no edge corresponding to a weight 0). Note in the ideal case the diagonal entries are all zero since we do not allow for self loops in the graph [99]. The collection of controlled-Z operations used to make the CV cluster state are then a function of the graph adjacency matrix $\mathbf{A}$, denoted $C_Z[\mathbf{A}]$. The CV cluster state with the graph $\mathbf{A}$ is then

$$\begin{aligned} |\psi_A\rangle &= C_Z[\mathbf{A}]|0\rangle_p^{\otimes N} \\ &= \prod_{j,k=1}^{N} \exp\left(\frac{i}{2}A_{jk}\hat{x}_j\hat{x}_k\right)|0\rangle_p^{\otimes N} \\ &= \exp\left(\frac{i}{2}\hat{\mathbf{x}}^T\mathbf{A}\hat{\mathbf{x}}\right)|0\rangle_p^{\otimes N}, \end{aligned} \tag{5.27}$$

where $\hat{\mathbf{x}} = (\hat{x}_1, ..., \hat{x}_N)^T$ is a column vector of position operators. Ideal CV cluster states in the unphysical limit of infinite squeezing satisfy a set of *nullifier* relations, which can be written as

$$(\hat{\mathbf{p}} - \mathbf{A}\hat{\mathbf{x}})|\psi_A\rangle = 0, \tag{5.28}$$

where $\hat{\mathbf{p}} = (\hat{p}_1, ..., \hat{p}_N)^T$ is a column vector of momentum operators. This represents N independent equations, one for each component of the vector $(\hat{\mathbf{p}} - \mathbf{A}\hat{\mathbf{x}})$, which are the nullifiers for $|\psi_A\rangle$, because that state is a simultaneous zero-eigenstate of them. The nullifiers are written explicitly as

$$\hat{g}_a = (\hat{p}_a - \sum_{b \in N_a} \hat{x}_b) \to 0, \quad \forall a \in G, \tag{5.29}$$

where the modes $a \in G$ correspond to the vertices of the graph of$N$ modes and the modes $b \in N_a$ are the nearest neighbours of mode a. We saw previously that this corresponds to the stabilizer operator $G_a(\xi) = \exp(-i\xi\hat{g}_a) = X_a(\xi)\prod_{b\in N_a} Z_b(\xi)$.

To construct the CV Kitaev code from a CV cluster state, we follow the following protocol:

- Single-mode measurements in the position basis are performed on qumodes that are to be designated to define faces (plaquettes).
- Single-mode measurements in the momentum basis are performed on qumodes that will become vertices.

- All the remaining modes undergo a Fourier transform, F.

Let us demonstrate this with an example. We start with a nine-mode square cluster state as shown in Fig(5.11). To form the Kitaev lattice, we make X-basis measurements on the corner modes, labeled $\{a, b, c, d\}$ and a Z-basis measurement on the middle mode, call if e. The remaining modes are labeled $\{1, 2, 3, 4\}$ in clockwise order. It is the numbered modes that will remain after the procedure and will form the CV Kitaev lattice. This state

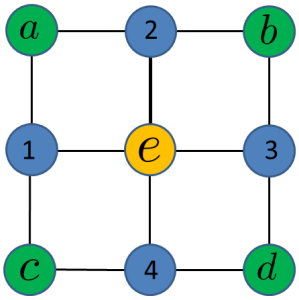

Figure 5.11: Nine-mode square CV cluster state. Blue nodes are unmeasured and will form the CV Kitaev lattice. Green nodes are measured in the X-basis and orange in the Z-basis.

has nullifier conditions

$$\begin{aligned} \hat{p}_a - \hat{x}_1 - \hat{x}_2 \to 0, \quad \hat{p}_b - \hat{x}_3 - \hat{x}_2 \to 0, \\ \hat{p}_c - \hat{x}_1 - \hat{x}_4 \to 0, \quad \hat{p}_d - \hat{x}_3 - \hat{x}_4 \to 0, \end{aligned} \tag{5.30}$$

for the mode to be measured in the position basis.

$$\hat{p}_e - \hat{x}_1 - \hat{x}_2 - \hat{x}_3 - \hat{x}_4 \to 0, \tag{5.31}$$

for the modes measured in the momentum basis and

$$\begin{aligned} \hat{p}_1 - \hat{x}_a - \hat{x}_e - \hat{x}_c \to 0, \quad \hat{p}_2 - \hat{x}_a - \hat{x}_b - \hat{x}_e \to 0, \\ \hat{p}_3 - \hat{x}_b - \hat{x}_e - \hat{x}_d \to 0, \quad \hat{p}_4 - \hat{x}_c - \hat{x}_d - \hat{x}_e \to 0, \end{aligned} \tag{5.32}$$

are the unmeasured modes. Performing the measurements on the modes converts the measured quantity to some classical number, so for $i = a, b, c, d, e$ we have $\hat{x}_i \to X_i$ and $\hat{p}_i \to P_i$ but leaves the unmeasured modes untouched.

This leaves us with

$$\begin{aligned}
&\hat{p}_1 - X_a - X_c - \hat{x}_e \\
&\hat{p}_2 - X_a - X_b - \hat{x}_e \\
&\hat{p}_3 - X_b - X_d - \hat{x}_e \\
&\hat{p}_4 - X_c - X_d - \hat{x}_e
\end{aligned} \tag{5.33}$$

and

$$P_e - \hat{x}_1 - \hat{x}_2 - \hat{x}_3 - \hat{x}_4. \tag{5.34}$$

What remains to do is find a new basis for the remaining modes. We can find this by taking combinations of the nullifiers and ensuring that they commute.

$$\begin{aligned}
\hat{p}_1 - \hat{p}_2 &= X_c - X_d \\
\hat{p}_2 - \hat{p}_3 &= X_a - X_d \\
\hat{p}_3 - \hat{p}_4 &= X_b - X_c \\
\hat{p}_4 - \hat{p}_1 &= X_a - X_a,
\end{aligned} \tag{5.35}$$

and (5.34) give commuting stabilizers (there are others such as $\hat{p}_1 - \hat{p}_3$ and $\hat{p}_2 - \hat{p}_4$ but these are redundant and infers that this construction is not unique). Since each of the nullifiers (5.35) are just equal to some classical number their variance tends to zero (assuming an ideal measurement) and hence they also stabilize the state. As a final step we take the Fourier transform on the remaining modes to give

$$\begin{aligned}
&\hat{x}_1 - \hat{x}_2 \to 0, \quad \hat{x}_2 - \hat{x}_3 \to 0 \\
&\hat{x}_3 - \hat{x}_4 \to 0, \quad \hat{x}_4 - \hat{x}_1 \to 0.
\end{aligned} \tag{5.36}$$

We associate each of these with a face of the lattice (although in our toy nine-mode example we have only two modes to define each face instead of four). Our vertex is defined by the node e, which under Fourier transform gives the nullifier

$$\hat{p}_1 + \hat{p}_2 + \hat{p}_3 + \hat{p}_4 \to 0. \tag{5.37}$$

Then we have the new graph state shown in Fig.(5.12). This state has only four remaining modes, but it defines a vertex v at its center and four faces f. This example is easily expanded to the general case. By iterating the above procedure for larger square CV clusters, we see that we just get more vertices and faces but the form of the nullifiers is unchanged. The new state created from an arbitrary sized square CV cluster is described by a set of correlations of the form

$$\hat{a}_s = (\hat{p}_{s,1} + \hat{p}_{s,2} + \hat{p}_{s,3} + \hat{p}_{s,4}) \to 0, \quad \hat{b}_f = (\hat{x}_{f,1} - \hat{x}_{f,2} + \hat{x}_{f,3} - \hat{x}_{f,4}) \to 0, \tag{5.38}$$

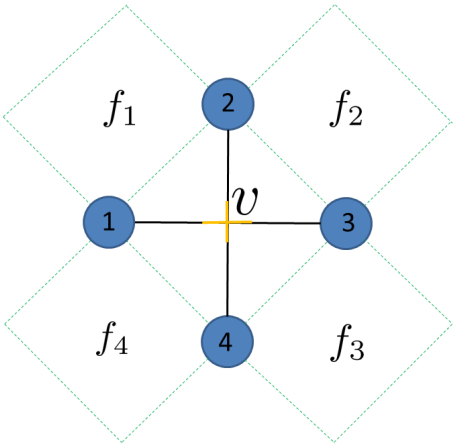

Figure 5.12: The four-mode CV Kitaev lattice generated from the nine-mode CV cluster state. Nodes 1 and 2 form face f_1, 2 and 3 form face f_2, 3 and 4 form face f_3 and 4 and 1 form face f_4. We have single vertex v (yellow).

where s and f label star and plaquettes, respectively, and the indices $1, .., 4$ of the position and momentum operators denote those modes located at a common star or at the boundary of a common plaquette. We can then associate new stabilizer operators that describe this state,

$$\begin{aligned} A_s(\xi) &= \exp(-i\xi\hat{a}_s) = \prod_{j\in star(s)} X_{s,j}(\xi), \\ B_f(\eta) &= \exp(-i\eta\hat{b}_f) = \prod_{j\in\partial(f)} Z_{f,j}((-1)^j\eta), \end{aligned} \tag{5.39}$$

with $\xi, \eta \in \mathbb{R}$. Comparing with Eq.(5.8,5.9), we see that these CV stabilizers are completely analogous to the stabilizers for the first Kitaev model on a two-dimensional spin 1/2 lattice. It is easy to show that these new stabilizer operators commute since they always meet at either two or zero points of the graph and so the phases cancel. Then we say the new ground state corresponds to an anyonic ground state with

$$\begin{aligned} A_s(\xi)|\psi\rangle &= |\psi\rangle \\ B_f(\xi)|\psi\rangle &= |\psi\rangle \end{aligned} \tag{5.40}$$

for all stars s and plaquettes f, in the limit of infinite squeezing.

This section has given us some remarkable results. It seems that we can create a surface code that is a CV analog of the Kitaev lattice and since this is a CV protocol this state can be built from Gaussian resources and linear optics, a far simpler task experimentally than arranging four-body

interactions between single spins. Mathematically the difference amounts to replacing the Pauli-X and Z operators with CV Weyl-displacement operators. In our next section we push this analogy further and examine the excitations that can be produced on the surface of the code. In the discrete case, we showed that excitations correspond to defects in the code with the property that when braided around each other produce phase changes of -1.

5.6 CV Anyon creation, fusion and braiding

We create excitations by applying $X_j(s)$ and $Z_j(t)$ displacement operators to some mode, j, of the ground state. Then the excited states differ from the ground states, $|\psi\rangle$, in their stabilizer operators. For the vertex stabilizer $A_s(\xi)$ we have

$$\begin{aligned} A_s(\xi)[Z_j(s)]|\psi\rangle &= e^{-i\xi\hat{a}_s} e^{is\hat{x}_j}|\psi\rangle \\ &= e^{\xi s[\hat{a}_s,\hat{x}_j]} Z_j(s) A_s(\xi)|\psi\rangle \\ &= e^{-i\xi s} Z_j(s)|\psi\rangle, \end{aligned} \tag{5.41}$$

$\forall \xi \in \mathbb{R}$. Then the stabilizer $A_s(\xi)$ no longer satisfies the ground-state condition $\hat{a}_s = 0$. Now it reads $\hat{a}_s = s$. Note that applying $X_j(t)$ to the vertex operator has no effect on the stabilizers since it commutes with $A_s(\xi)$. This displacement on mode j causes a stabilizer violation on the two neighbouring vertices.

Applying $X_j(t)$ to the ground-state defined by $B_f(\eta)$ gives

$$\begin{aligned} B_f(\eta)[X_j(t)|\psi\rangle] &= e^{i\eta\hat{b}_f} e^{-it\hat{p}_j}|\psi\rangle \\ &= e^{-\eta t[\hat{b}_f,\hat{p}_j]} X_j(t) B_f(\eta)|\psi\rangle \\ &= e^{\pm i\eta t} X_j(t)|\psi\rangle, \end{aligned} \tag{5.42}$$

$\forall \eta \in \mathbb{R}$. Now the ground-state condition $\hat{b}_f = 0$ for the stabilizer $B_f(\eta)$ has been violated. The excited state corresponds to a nullifier violation of $\hat{b}_f \pm t$. How do we interpret these continuous excitations? Comparing to discrete QEC we can say we have merely induced errors or holes in the CV surface code. So by applying a displacement to a mode j, an error is induced in either the neighbouring vertices or plaquettes which can be corrected by guiding the two holes around closed loops until they meet up and cancel each other out. Then this lattice can be thought of as another error correcting code for CV states.

A more interesting interpretation for the purposes of quantum computation is that the excitations are a continuous-variable analog of anyons, produced by applying Z and X operators on the ground state. Specifically,

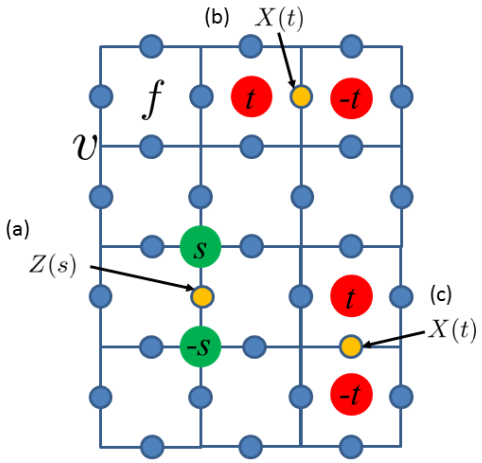

Figure 5.13: Anyon creation on CV Kitaev lattice: Blue lattice nodes are the physical modes. (a) Momentum-translation operator induces two e-type anyons on adjacent vertices v. (b) and (c) Position-translation operator creates two m-type anyons on adjacent plaquettes f. (Yellow nodes have been acted upon by a displacement operator

the position-translation operator applied to some mode of the lattice creates a pair of m-type anyons on adjacent plaquettes, given by

$$|m((-1)^d t)\rangle = X(t)|\psi\rangle \tag{5.43}$$

($d \in \{1, 2\}$), where $d = 1$ means the relevant mode lies on the vertical edges, and $d = 2$ refers to the horizontal edges). An e-type pair of anyons is created on adjacent vertices of the lattice by applying the momentum-translation operator

$$|e(s)\rangle = Z(s)|\psi\rangle. \tag{5.44}$$

We represent this in Fig. (5.14). Using this interpretation, we can go beyond merely correcting errors and use our CV Kitaev code to perform quantum computation. First however, we have to confirm that these excitations exhibit anyonic behaviour. We can check this by examining their fusion and braiding rules.

5.6.1 Fusion and braiding

To compute the fusion rules we consider the effect when two anyons are combined at a common star or face. Here our anyons are just momentum or position displacements so combining them just amounts to the sum of the

displacements. So for two star anyons created by displacements $Z(v)$ and $Z(u)$, the fusion gives

$$\begin{aligned} |e(v)\rangle \times |e(u)\rangle &= [Z(v)|\psi\rangle] \times [Z(u)|\psi\rangle] \\ &= [Z(v) \times Z(u)]|\psi\rangle \\ &= [e^{iv\hat{p}} e^{iu\hat{p}}]|\psi\rangle \\ &= [e^{i(u+v)\hat{p}}]|\psi\rangle \\ &= Z(u+v)|\psi\rangle \\ &= e(u+v) \end{aligned} \tag{5.45}$$

Similarly, fusing plaquette anyons created by position displacements $X(u)$ and $X(v)$ gives,

$$\begin{aligned} |m(v)\rangle \times |m(u)\rangle &= [X(v)|\psi\rangle] \times [X(u)|\psi\rangle] \\ &= [X(v) \times X(u)]|\psi\rangle \\ &= [e^{-iv\hat{x}} e^{-iu\hat{x}}]|\psi\rangle \\ &= [e^{-i(u+v)\hat{x}}]|\psi\rangle \\ &= X(u+v)|\psi\rangle \\ &= m(u+v) \end{aligned} \tag{5.46}$$

Note that zero displacements $|e(0)\rangle = X(0)|\psi\rangle = |\psi\rangle$ and $|m(0)\rangle = Z(0)|\psi\rangle = |\psi\rangle$ corresponds to the vacuum anyon. These have no effect on the ground state and we can see from (5.45) and (5.46) that fusing the vacumm anyon with anyon other type has no effect on the state. One might ask what the result of fusing an e- with an m-type would give. However, in this model it is not possible to directly fuse these two since they exist as different types of displacement in phase-space.

The CV anyon fusion rules can be summarized as

$$\begin{gathered} e(s) \times e(t) = e(s+t) \quad m(s) \times m(t) = m(s+t) \\ e(0) = m(0) = \mathbf{1}, \quad \mathbf{1} \times e(s) = e(s), \quad \mathbf{1} \times m(s) = m(s) \end{gathered} \tag{5.47}$$

Then we clearly have an abelian anyon model since the anyons can only ever fuse to give one result. However, we get a more complicated fusion behaviour compared to the discrete toric code. Recall in the discrete case, e- and m-types are always antiparticles of themselves and so $e \times e = 1$ and $m \times m = 1$. Here this is not true in general, now fusing anyon of the same type results in another of that type, characterized by a new continuous parameter. We note that it is always possible to retrieve the discrete anyon behaviour by choosing our displacements such that we fuse particles to antiparticles i.e., $e(s) \times e(-s) = \mathbf{1}$.

To complete our anyon model we have to establish braiding rules. By application of a sequence of X and Z operators we can construct loops in on

the surface code. Just as in the discrete case the anyons behave as bosons with respect to particles of the same type, that is braiding e around and e has no effect on the state. This can be shown by creating an e-type on mode i, $|\psi_{ini}\rangle = Z_i(s)|\psi\rangle$ and braiding another e by successive application of $Z(t)$ around a closed loop:

$$\begin{aligned} |\psi_{fin}\rangle &= Z_1(t)Z_2(t)Z_3(t)Z_4(t)|\psi_{ini}\rangle \\ &= Z_i(s)[Z_1(t)Z_2(t)Z_3(t)Z_4(t)|\psi\rangle] \\ &= |\psi_{ini}\rangle. \end{aligned} \tag{5.48}$$

Since all the Z operators commute. The mutual statistics between different types give a more interesting behaviour. For example, consider an initial state $|\psi_{ini}\rangle = Z_i(s)|\psi\rangle = |e(s)\rangle$. If an anyon of type m is at a neighbouring plaquette, it can be moved around e along a path generated by successive application of $X(t)$ on the four modes of the star. The final state is

$$\begin{aligned} |\psi_{fin}\rangle &= X_1(t)X_2(t)X_3(t)X_4(t)|\psi_{ini}\rangle \\ &= e^{-ist}Z_i(s)[X_1(t)X_2(t)X_3(t)X_4(t)|\psi\rangle] \\ &= e^{-ist}|\psi_{ini}\rangle. \end{aligned} \tag{5.49}$$

The phase factor is known as the topological phase factor, which reveals the

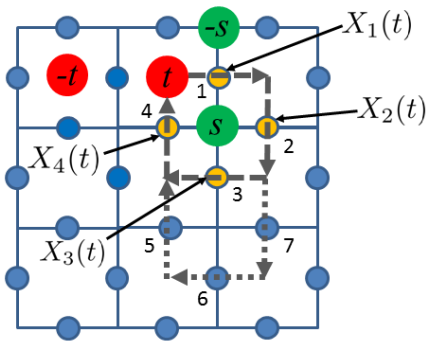

Figure 5.14: Braiding an m- around and e-type is performed by a sequence of X operators on the modes forming a closed loop around the e anyon.

presence of enclosed anyons. Again we compare to the discrete case where braiding only results in a phase of -1, here we have much more freedom in the phase we can acquire since we choose the initial displacements on the ground state. The phase factors constitute an abelian representation

of the braid group. The relation described by Eq.(5.49) can be obtained for different paths of the loop. For example, the loop 1-2-5-6-7-4 of m-type anyons Fig. (5.14), which corresponds to the application of

$$\begin{aligned} X_1(t)X_2(t)X_5(-t)X_6(-t)X_7(-t)X_4(t) =&[X_1(t)X_2(t)X_3(t)X_4(t)] \\ &\times [X_3(-t)X_5(-t)X_6(-t)X_7(-t)], \end{aligned} \tag{5.50}$$

involving two star operators, gives the same result for the topological phase in Eq.(5.49). This topological character reveals the potential robustness of operations with CV anyons and their use as a resource for fault-tolerant quantum computation.

5.7 Physical States - Finite Squeezing

So far, we have only considered the generation of anyonic statistics on an infinitely squeezed ground state. However, this state is highly unphysical. Here we extend our model to include finite squeezing of the initial state and calculate the effects on the braiding operations [180].

To this end, we must construct our CV Kitaev lattice again but this time we no longer assume that the modes are prepared in the unphysical momentum eigenstates, instead we allow the modes to be Gaussian states. In chapter 4 we described a method to extend the graph representations from ideal (infinitely squeezed) CV cluster states to their finitely squeezed Gaussian approximations. It was shown that the nullifier formalism for CV cluster states can be extended to general Gaussian pure states using the simple replacement of the CV cluster state graph $\mathbf{A}$ with the Gaussian graph $\mathbf{Z}$, so that $(\hat{\mathbf{p}} - \mathbf{Z}\hat{\mathbf{q}})|\phi_Z\rangle = 0$ with the new non-Hermitian nullifiers defined as

$$g_k = \hat{p}_k - ie^{-2r_k}\hat{x}_k - \sum_{l \in N_k} \hat{x}_l, \quad \forall k. \tag{5.51}$$

Then the adjacency matrix $\mathbf{Z}$ for a Gaussian pure state is a complex matrix with imaginary diagonal entries, ie^{-2r_k}, corresponding to self-loops on the modes, and the remaining entries either 0 or 1 depending on the particular CV cluster state.

Then our protocol proceeds as before, we start with an N-mode square cluster state defined by the nullifier (5.51), measure out every second mode in the X or Z basis in the same pattern described for the ideal cluster. Finally we apply a Fourier transform to each mode which generates the finitely squeezed Kitaev lattice Fig.(5.15). As and example, we derive the Gaussian Kitaev nullifiers from a nine-mode square cluster state. The unmeasured

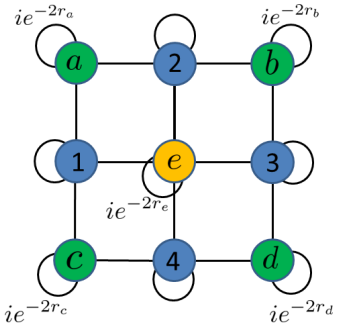

Figure 5.15: Measurement pattern for construction of CV Gaussian Kitaev state from CV Gaussian cluster state. Node e (yellow) is measured in the momentum basis, nodes a, b, c, d (green) are measured in the position basis. The self loops of the graph represent the finite squeezing with squeezing parameter r_k.

mode nullifiers are

$$\begin{aligned} &\hat{p}_1 - ie^{-2r_1}\hat{x}_1 - \hat{x}_a - \hat{x}_e - \hat{x}_c \to 0, \quad \hat{p}_2 - ie^{-2r_2}\hat{x}_2 - \hat{x}_a - \hat{x}_b - \hat{x}_e \to 0, \\ &\hat{p}_3 - ie^{-2r_3}\hat{x}_3 - \hat{x}_b - \hat{x}_e - \hat{x}_d \to 0, \quad \hat{p}_4 - ie^{-2r_4}\hat{x}_4 - \hat{x}_c - \hat{x}_d - \hat{x}_e \to 0, \end{aligned} \tag{5.52}$$

The cluster state nullifiers for the modes to be measured in the X basis are

$$\begin{aligned} &\hat{p}_a - ie^{-2r_a}\hat{x}_a - \hat{x}_1 - \hat{x}_2 \to 0, \quad \hat{p}_b - ie^{-2r_b}\hat{x}_b - \hat{x}_3 - \hat{x}_2 \to 0, \\ &\hat{p}_c - ie^{-2r_c}\hat{x}_c - \hat{x}_1 - \hat{x}_4 \to 0, \quad \hat{p}_d - ie^{-2r_d}\hat{x}_d - \hat{x}_3 - \hat{x}_4 \to 0, \end{aligned} \tag{5.53}$$

Finally the mode measured in the Z basis has nullifier

$$\hat{p}_e - ie^{-2r_e}\hat{x}_e - \hat{x}_1 - \hat{x}_2 - \hat{x}_3 - \hat{x}_4 \tag{5.54}$$

Performing X-measurements on modes a, b, c, d leaves us with

$$\begin{aligned} &\hat{p}_1 - ie^{-2r_1}\hat{x}_1 - X_a - X_c - \hat{x}_e, \\ &\hat{p}_2 - ie^{-2r_2}\hat{x}_2 - X_a - X_b - \hat{x}_e, \\ &\hat{p}_3 - ie^{-2r_3}\hat{x}_3 - X_b - X_d - \hat{x}_e, \\ &\hat{p}_4 - ie^{-2r_4}\hat{x}_4 - X_c - X_d - \hat{x}_e, \end{aligned} \tag{5.55}$$

and the Z measurement gives

$$P_e - ie^{-2r_e}\hat{x}_e - \hat{x}_1 - \hat{x}_2 - \hat{x}_3 - \hat{x}_4 \tag{5.56}$$

Then taking combinations of the remaining nullifiers, we find

$$\begin{aligned}
\hat{p}_1 - ie^{-2r_1}\hat{x}_1 - \hat{p}_2 + ie^{-2r_2}\hat{x}_2 &= X_c - X_b, \\
\hat{p}_2 - ie^{-2r_2}\hat{x}_2 - \hat{p}_3 + ie^{-2r_3}\hat{x}_3 &= X_a - X_d, \\
\hat{p}_3 - ie^{-2r_3}\hat{x}_3 - \hat{p}_4 - ie^{-2r_4}\hat{x}_2 &= X_b - X_c, \\
\hat{p}_4 - ie^{-2r_4}\hat{x}_4 - \hat{p}_1 - ie^{-2r_1}\hat{x}_2 &= X_a - X_d.
\end{aligned} \tag{5.57}$$

Then the nullifiers that define the four plaquettes read

$$\begin{aligned}
(\hat{p}_1 - ie^{-2r_1}\hat{x}_1) - (\hat{p}_2 - ie^{-2r_2}\hat{x}_2) &\to 0, \\
(\hat{p}_2 - ie^{-2r_2}\hat{x}_2) - (\hat{p}_3 - ie^{-2r_3}\hat{x}_3) &\to 0, \\
(\hat{p}_3 - ie^{-2r_3}\hat{x}_3) - (\hat{p}_4 - ie^{-2r_4}\hat{x}_4) &\to 0, \\
(\hat{p}_1 - ie^{-2r_1}\hat{x}_1) - (\hat{p}_4 - ie^{-2r_4}\hat{x}_4) &\to 0.
\end{aligned} \tag{5.58}$$

The star nullifier is given by

$$\hat{x}_1 + \hat{x}_2 + \hat{x}_3 + \hat{x}_4 \to 0. \tag{5.59}$$

Then we perform the Fourier transform on the remaining modes which leaves us with ,

$$\begin{aligned}
\hat{b}'_1 &= (\hat{x}_1 - ie^{-2r_1}\hat{p}_1) - (\hat{x}_2 - ie^{-2r_2}\hat{p}_2), \\
\hat{b}'_2 &= (\hat{x}_2 - ie^{-2r_2}\hat{p}_2) - (\hat{x}_3 - ie^{-2r_3}\hat{p}_3), \\
\hat{b}'_3 &= (\hat{x}_3 - ie^{-2r_3}\hat{p}_3) - (\hat{x}_4 - ie^{-2r_4}\hat{p}_4), \\
\hat{b}'_4 &= (\hat{x}_1 - ie^{-2r_1}\hat{p}_1) - (\hat{x}_4 - ie^{-2r_4}\hat{p}_4),
\end{aligned} \tag{5.60}$$

which define the four plaquettes and

$$\hat{a}'_s = [\hat{p}_1 + \hat{p}_2 + \hat{p}_3 + \hat{p}_4], \tag{5.61}$$

which defines the star Fig.(5.16), where (') indicates that this is the finitely squeezed nullifier. As with the infinite squeezed case, each nullifier $\hat{a}'_s$ defines a star and $\hat{b}'_f$ a plaquette. The general nullifiers are given by

$$\hat{a}'_s = (\hat{p}_{s,1} + \hat{p}_{s,2} + \hat{p}_{s,3} + \hat{p}_{s,4}) = 0 \tag{5.62}$$

$$\begin{aligned}
\hat{b}'_f = (&\hat{x}_{s,1} - \hat{x}_{s,2} + \hat{x}_{s,3} - \hat{x}_{s,4}) \\
&- ie^{-2r_1}\hat{p}_{f,1} + ie^{-2r_2}\hat{p}_{f,2} - ie^{-2r_3}\hat{p}_{f,3} + ie^{-2r_4}\hat{p}_{f,4} = 0,
\end{aligned} \tag{5.63}$$

where s and f label the stars and plaquettes, respectively, and ∂f denotes the boundary of a face. Comparing with the nullifiers in the infinitely squeezed limit,

$$\hat{a}'_s = \hat{a}_s = (\hat{p}_{s,1} + \hat{p}_{s,2} + \hat{p}_{s,3} + \hat{p}_{s,4}) = 0 \tag{5.64}$$

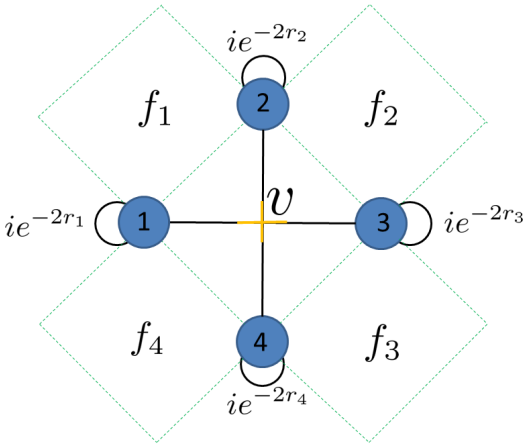

Figure 5.16: The Gaussian approximant of the CV Kitaev state with vertex v and plaquettes f. Self loop of the nodes represent finite squeezing with squeezing parameter r_k.

for the stars and

$$\hat{b}'_f = \hat{b}_f - ie^{-2r_1}\hat{p}_{f,1} + ie^{-2r_2}\hat{p}_{f,2} - ie^{-2r_3}\hat{p}_{f,3} + ie^{-2r_4}\hat{p}_{f,4} = 0, \tag{5.65}$$

we observe that finite squeezing introduces extra imaginary terms to the plaquette nullifiers. The stabilizers corresponding to these complex nullifiers are

$$A'_s(\xi) = e^{-i\xi\hat{a}'_s} = \prod_{j\in star(s)} X_{s,j}(\xi), \tag{5.66}$$

$$B'_f(\eta) = e^{-i\eta\hat{b}'_f} = \prod_{j\in\partial(f)} Z_{f,j}((-1)^j\eta)\exp[\eta(-1)^j e^{-2r_j}(\eta + \hat{p}_j)]. \tag{5.67}$$

These operators correspond to the Kitaev model with an extra complex terms, but note that these reduce exactly to the Kitaev stabilizers as the squeezing parameter $r \to \infty$. These new stabilizers still commute and so the new state $|\phi\rangle$ corresponds to the anyonic ground state with

$$A'_s(\xi)|\phi\rangle = |\phi\rangle, \quad B'_f(\eta)|\phi\rangle = |\phi\rangle. \tag{5.68}$$

In order to see the effects of finite squeezing, we apply the unphysical sta-

bilizers to the physical ground state,

$$\begin{aligned}
B_f(\eta)|\phi\rangle &= \exp[-i\eta\hat{b}_f]|\phi\rangle \\
&= \exp\left[\eta\sum_{j=1}^{4}(-1)^{j+1}e^{-2r_j}(\hat{p}_j+\eta)\right] \\
&\times \exp\left[-\eta\sum_{j=1}^{4}(-1)^{j+1}e^{-2r_j}(\hat{p}_j+\eta)\right]\exp[-i\eta\hat{b}_f]|\phi\rangle \\
&= \exp\left[-\eta\sum_{j=1}^{4}(-1)^{j+1}e^{-2r_j}(\hat{p}_j+\eta)\right]B'_f(\eta)|\phi\rangle \\
&= \exp\left[-\eta\sum_{j=1}^{4}(-1)^{j+1}e^{-2r_j}(\hat{p}_j+\eta)\right]|\phi\rangle, \qquad (5.69)
\end{aligned}$$

where we dropped the subscripts f of the momentum operators for simplicity. We observe that finite squeezing of the ground state violates the unphysical stabilizer conditions by an imaginary phase, $\sim i\eta^2$, and by imaginary position shifts, $\sim i\eta$. Having derived the form of our finitely squeezed CV lattice, we now turn to anyonic excitations and basic braiding operations.

5.8 Anyonic creation and braiding on finitely squeezed lattice

By applying single-mode operations to the ground state, we can examine the excitations above the physical ground state. The effects of finite squeezing on the creation of anyonic excitations are revealed when we calculate the violation of the finitely squeezed nullifiers due to the application of $X_i(t)$ and $Z_i(t)$ on some mode of the physical ground state defined by

$$A'_s(\xi)|\phi\rangle = e^{-i\xi\hat{a}'_s}|\phi\rangle = |\phi\rangle, \qquad (5.70)$$

$$B'_f(\eta)|\phi\rangle = e^{-i\eta\hat{b}'_f}|\phi\rangle = |\phi\rangle. \qquad (5.71)$$

Note that now, due to the non-Hermiticity of the physical nullifiers, their violations through anyonic excitations may in general be complex. An excitation of the vertex ground state due to $Z_j(t)$ corresponds to

$$A'_s(\xi)[Z_j(t)|\phi\rangle] = e^{-i\xi\hat{a}'_s}e^{it\hat{x}_j}|\phi\rangle, \qquad (5.72)$$

but $\hat{a}'_s = \hat{a}_s$, as the finite squeezing has no effect on the vertex nullifier. Hence,

$$\begin{aligned} A'_s(\xi)[Z_j(t)|\phi\rangle] &= e^{-i\xi\hat{a}_s} e^{it\hat{x}_j}|\phi\rangle \\ &= e^{\xi t[\hat{a}_s,\hat{x}_j]} Z_j(t) A_s(\xi)|\phi\rangle \\ &= e^{-i\xi t} Z_j(t) A'_s(\xi)|\phi\rangle \\ &= e^{-i\xi t}[Z_j(t)|\phi\rangle]. \end{aligned} \tag{5.73}$$

Just as in the infinitely squeezed case, this yields a stabilizer violation of t. The $Z_j(t)$ applied to the plaquette stabilizers gives

$$\begin{aligned} B'_f(\eta)[Z_j(t)|\phi\rangle] &= e^{-i\eta\hat{b}'_f} e^{it\hat{x}_j}|\phi\rangle \\ &= e^{\eta t[\hat{b}'_f,\hat{x}_j]} Z_j(t) B'_f(\eta)|\phi\rangle \\ &= e^{\eta t[-ie^{-2r_j}\hat{p}_{f,j},\hat{x}_j]}[Z_j(t)|\phi\rangle] \\ &= e^{-\eta t e^{-2r_j}}[Z_j(t)|\phi\rangle], \end{aligned} \tag{5.74}$$

This differs from the infinitely squeezed case (where we had no violation at all), with an imaginary nullifier violation of ite^{-2r_j}. This time physical anyons may appear as complex violations of the ground-state stabilizers. Applying $X_j(t)$ to the ground state yields,

$$\begin{aligned} A'_s(\xi)[X_j(t)|\phi\rangle] &= e^{-i\xi\hat{a}'_s} e^{-it\hat{p}_j}|\phi\rangle \\ &= e^{-i\xi\hat{a}_s} e^{-it\hat{p}_j}|\phi\rangle \\ &= X_j(t) A'_s(\xi)|\phi\rangle \\ &= [X_j(t)|\phi\rangle], \end{aligned} \tag{5.75}$$

so no stabilizer violation occurs. Finally, the plaquette stabilizer gives

$$\begin{aligned} B'_f(\eta)[X_j(t)|\phi\rangle] &= e^{-i\eta\hat{b}'_f} e^{-it\hat{p}_j}|\phi\rangle \\ &= e^{-\eta t[\hat{b}'_f,\hat{p}_j]} X_j(t) B'_f(\eta)|\phi\rangle \\ &= e^{-\eta t[\hat{b}_f,\hat{p}_j]} X_j(t) B'_f(\eta)|\phi\rangle \\ &= e^{\pm i\eta t}[X_j(t)|\phi\rangle], \end{aligned} \tag{5.76}$$

which corresponds to a violation of $\pm t$.

In summary, finite squeezing gives us a violation of the plaquette ground state stabilizer due to the action of $Z(t)$, whereas it did not exhibit violations in the infinitely squeezed case. The vertex stabilizers are unaffected and yield violations of the same form as in the infinitely squeezed case. This seems to imply that any topological operations carried out on e anyons are topologically are invariant to the degree of squeezing. The anyons are now

represented in general by complex violations. These may then said to be new types of excitations produced through finite squeezing which we call *complex anyons*.

The effects on the braiding procedure and hence gate operations are determined by generating vertex and plaquette anyons and guiding them around each other in closed loops.

$$\begin{aligned}|\phi_{fin}\rangle &= [Z_1(-t)Z_2(t)Z_3(-t)Z_4(t)]|\phi_{ini}\rangle \\ &= [Z_1(-t)Z_2(t)Z_3(-t)Z_4(t)]X_k(s)|\phi\rangle. \end{aligned} \tag{5.77}$$

Commuting through to enact the braid yields

$$|\phi_{fin}\rangle = \exp[ist]X_k(s)[Z_1(-t)Z_2(t)Z_3(-t)Z_4(t)]|\phi\rangle$$

$$= \exp[ist]X_k(s)\exp\left[-t\sum_{j=1}^{4}(-1)^{j+1}e^{-2r_j}(\hat{p}_j+t)\right]B'_f(t)|\phi\rangle. \tag{5.78}$$

Using our definition of the ground state, $B'_f(t)|\phi\rangle = |\phi\rangle$, we obtain

$$\begin{aligned}|\phi_{fin}\rangle &= \exp[ist]X_k(s)\exp\left[-t\sum_{j}(-1)^{j+1}e^{-2r_j}(\hat{p}_j+t)\right]|\phi\rangle \\ &= \exp[ist]\exp\left[-t\sum_{j}(-1)^{j+1}e^{-2r_j}(\hat{p}_j+t)\right]|\phi_{ini}\rangle. \end{aligned} \tag{5.79}$$

We can express the term proportional to t as an imaginary displacement,

$$|\phi_{fin}\rangle = \exp[ist]\exp\left[-t^2\sum_{j}(-1)^{j+1}e^{-2r_j}\right]\prod_j X_j\left(-it(-1)^{j+1}e^{-2r_j}\right)|\phi_{ini}\rangle. \tag{5.80}$$

As in the infinitely squeezed case, we observe a phase change of e^{ist}, but this time, for finite squeezing, we have an extra imaginary displacement and a term proportional to t^2 (corresponding to an extra imaginary phase, similar to what we had before for the ground-state plaquette stabilizers with finite squeezing). We may call the combination of these terms the *topological factor for the braiding of finitely squeezed anyons*, and we note that this factor would not be obtained if the initial states were unexcited. We can absorb the complex displacement into the definition of the ground state such that the nullifier $\hat{b}_f$ is no longer zero, but has an imaginary violation $\hat{b}_f = it\sum_j(-1)^{j+1}e^{-2r_j}$. Then $\hat{b}_f = s + it\sum_j(-1)^{j+1}e^{-2r_j} = s'$ is the nullifier corresponding to a finitely squeezed m-anyon. The topological phase produced when braided with an e-type anyon is then

$$\exp[is't] = \exp[i(s + it\sum_j(-1)^{j+1}e^{-2r_j})t]. \tag{5.81}$$

This is one of the central results of this chapter, extending the simple (infinite squeezing) factor e^{ist} of [179] to the realistic case of finite squeezing. Similar to the infinitely squeezed case, the state can acquire any phase, but now the phase is modified by extra factors.

Having completed our anyon model, we now turn to the question of the computational power of the CV toric code. In the following we propose a computational model in which CV quantum information is encoded into the anyonic states. We begin by establishing a computational basis and deriving quantum gate operations that can be performed on these anyons.

5.9 Quantum computation with CV abelian anyons

In this section we will derive protocols to enact a universal set quantum gates using CV abelian anyons. Our first step is to define a computational basis. The natural basis is in terms of pairs of anyons that are created by a single displacement on some mode of the CV lattice. This gives us two bases depending on the initial displacement. We label the bases $|r\rangle_{v/f}$ on vertices, v and plaquettes, f, with $r \in \mathbb{R}$, which are defined as

$$\begin{aligned} |r\rangle_v &= |e(r)\rangle_{v_1}|e(-r)\rangle_{v_2}, \\ |r\rangle_f &= |m(r)\rangle_{f_1}|m(-r)\rangle_{f_2}. \end{aligned} \tag{5.82}$$

These define the logical basis that our gate operations will act on. We begin our discussion of quantum computational operations with those gates that form the Clifford group.

5.10 Clifford Gates

The Clifford group operations are achieved using both topological and non-topological means. We recall the set $\{Z(s), F, P(\eta), C_Z; s, \eta \in \mathbb{R}\}$ generates the Clifford group, where $P(\eta) = \exp[i(\eta/2)\hat{x}^2]$ is a CV squeezing gate, $F = \exp[i\pi/4(\hat{x}^2 + \hat{p}^2)]$ is the Fourier Transform operator, and $C_Z = \exp(ig\hat{x}_i \otimes \hat{x}_j)$ is the controlled-Z gate, as defined before. Transformations within the Clifford group correspond to Gaussian transformations mapping Gaussian states onto Gaussian states. We see below that the topological operations available to CV abelian anyons are not sufficient to generate the entire group and we will require non-topological operations to complete the set.

5.10.1 Topological Operations

Our first topological operations are quadrature displacements, $Z(s) = e^{is\hat{x}}$. Phase-space displacements are achieved through the creation and fusion of anyons. It is easy to see that creation of an anyon results in a displacement away from the ground state. For non-trivial displacements we fuse anyons

of the same type, created by displacements on modes i and j. The anyon on site j can then be moved to site i to implement fusion,

$$\begin{aligned} |e(s)\rangle \times |e(t)\rangle &= Z_i(s)|\psi\rangle \times Z_j(t)|\psi\rangle \\ &= [Z(s) \times Z(t)]_i|\psi\rangle \\ &= e^{i(s+t)\hat{x}_i}|\psi\rangle. \end{aligned} \tag{5.83}$$

To act our quadrature displacement on the computational basis we must ensure that both anyons in the produced pair are fused with its counterpart. Hence the effect of our displacement on the computational basis is

$$|r+s\rangle_v = |e(r+s)\rangle_{v_1}|e(-(r+s))\rangle_{v_2}. \tag{5.84}$$

The change in the computational basis for the m-type anyons follows similarly. We can extend this to the two mode SUM gate, Fig. (5.17), which is a controlled displacement $C_X = e^{-i\hat{x}_i \otimes \hat{p}_j}$, i.e., $|x\rangle_1|y\rangle_2 \to |x\rangle_1|x+y\rangle_2$. We affect the SUM gate by fusing one of the anyons from the first mode with an anyon from the second mode. This results in a displacement of the second mode dependent on the state of the first:

$$\begin{aligned} |s\rangle_1|t\rangle_2 &= (|e(s)\rangle|e(-s)\rangle)_1(|e(-t)\rangle|e(t)\rangle)_2 \\ &\to |e(-s)\rangle_1|e(s+t)\rangle_2 \\ &= |-s\rangle_1|s+t\rangle_2, \end{aligned} \tag{5.85}$$

where we treat the second anyon of mode two as a spectator anyon that will be annihilated at the end of the computation and the control is left in the original state (up to a sign change). We can also perform a controlled-Z gate,

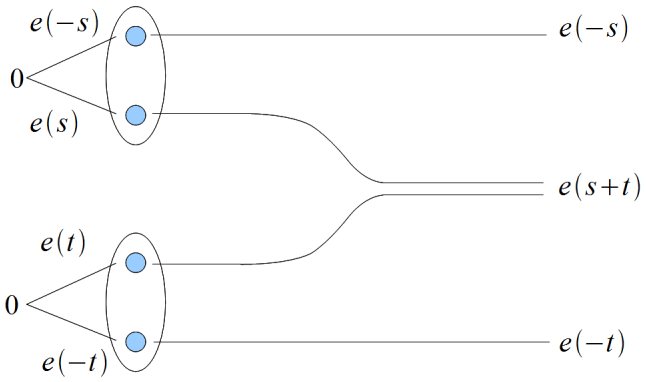

Figure 5.17: The two mode SUM gate. Reprinted figure with permission from D. F. Milne, N. V. Korolkova and P. van Loock,Phys. Rev. A **85**, 052325. Copyright (2012) by the American Physical Society.

Fig. (5.18), which acts on the computational basis as $|x\rangle_1|y\rangle_2 \to |x\rangle_1 e^{i\phi}|y\rangle_2$.

This time we affect this transformation by braiding the anyons. For example to perform a controlled displacement in the conjugate basis on an m-type anyon we braid an e-type anyon around it. From equation (5.49), we see that the state picks up a phase dependent on the anyonic states. Hence,

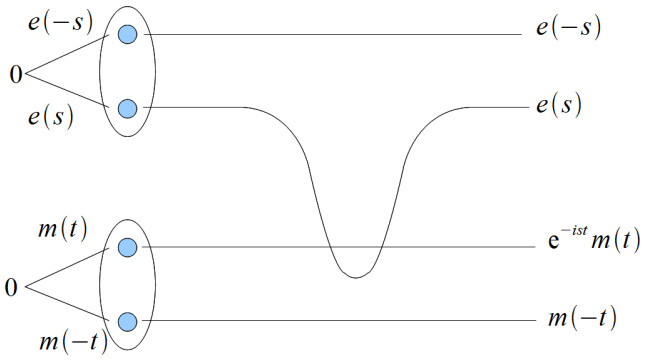

Figure 5.18: The two-mode phase gate. Braiding e- around an m-type induces a phase rotation of e^{-ist} on the state. Reprinted figure with permission from D. F. Milne, N. V. Korolkova and P. van Loock,Phys. Rev. A **85**, 052325. Copyright (2012) by the American Physical Society.

we have found that the controlled shift operation C_X, $e^{i\hat{x}_i\hat{p}_j}$, corresponds to partial fusions of e-type anyon pairs, while the controlled shift operation C_Z, $e^{i\hat{x}_i\hat{x}_j}$, corresponds to partial braiding between e- and m-type anyon pairs. Similarly, we note that the operations $e^{i\hat{p}_i\hat{p}_j}$ and $e^{i\hat{p}_i\hat{x}_j}$ are achieved by partial braiding between m and e-type anyon pairs and partial fusion of m-anyon pairs, respectively.

5.10.2 Non-Topological Operations

Above we saw how we can implement single mode displacements, displacements in the conjugate basis and two-mode controlled displacement gates. Now we go beyond simple first-moment Gaussian operations and consider the manipulation of second moments. In particular, we seek to complete the set of Clifford gates by the inclusion of a squeezer and a Fourier transform. The squeezing operation compresses the position quadrature by a factor η while stretching the conjugate quadrature by $1/\eta$. We cannot directly squeeze our anyons since the only action we can take on the anyons is fusion and braiding. Instead, we squeeze on some mode i of the ground state,

$$|\tilde{\psi}\rangle = P_i(\eta)|\psi\rangle. \tag{5.86}$$

Then creating an anyon on this squeezed ground state mode and commuting through gives us

$$\begin{aligned} Z_i(s)|\tilde{\psi}\rangle &= Z_i(s)P_i(\eta)|\psi\rangle \\ &= P_i(\eta)e^{i2\eta s\hat{x}_i}Z_i(s)|\psi\rangle. \end{aligned} \tag{5.87}$$

We find that squeezing the ground state is equivalent to squeezing the anyon with an additional phase space displacement. This squeezing operation combined with a measurement in the X basis can be used to implement a Fourier transform F. The action of F is to switch between the position and momentum bases, i.e., $F|x\rangle_x = |x\rangle_p$. This corresponds to a generalization of the Hadamard gate for qubits. To perform F on our anyons, we begin by preparing a zero-momentum squeezed ground state $|0\rangle_p$. We proved above that up to a displacement, any squeezer on the ground state acts on the anyonic excitations in the same way. Hence we can produce zero-momentum anyons. For example, consider an m-type anyon in the computational basis $|\psi'\rangle = X(s)\int dtf(t)|t\rangle_x$. We fuse this anyon with the momentum squeezed anyon:

$$\begin{aligned} \mathrm{SUM}[|\psi'\rangle \times |0\rangle_p] &= \mathrm{SUM}[X(s)|\psi\rangle \times |0\rangle_p] \\ &= \mathrm{SUM}\left[\int dtf(t)X(s)|t\rangle_x|0\rangle_p\right] \\ &= \int dtf(t)|t+s\rangle_x|t+s\rangle_p. \end{aligned} \tag{5.88}$$

Then, performing a measurement of $\hat{p}$ with outcome m on the mode corresponding to the first anyon collapses this to

$$\int dtf(t)e^{i(t+s)m}|s+t\rangle_p = X(m)F|\psi'\rangle. \tag{5.89}$$

We see that the effect of this procedure is to apply a Fourier transform modulo a known quadrature displacement. This completes our set of Clifford gates, and so with appropriate non-topological operations we can apply any Gaussian transformation. As stated above, Gaussian transformations are not sufficient for universal QC and we address the question of universality in the next section.

5.11 Non-Clifford gates and universality

For our abelian anyon computational scheme, we require either a non-Gaussian gate or a non-Gaussian resource. In a similar fashion to our squeezing operation, we apply a cubic phase, $V(\gamma) = e^{i\gamma\hat{x}^3}$, $\gamma \in \mathbb{R}$, to some mode i of the ground state. Then we commute $V(\gamma)$ through the X and Z operators to find the effect on the anyons:

$$|\psi_c\rangle = V_i(\gamma)|\psi\rangle. \tag{5.90}$$

Now applying X and Z operators to create e- and m-type anyons and commuting the cubic phase gate through we find

$$\begin{aligned} X_i(s)Z_i(t)|\psi_c\rangle &= X_i(s)Z_i(t)V_i(\gamma)|\psi\rangle \\ &= V_i(\gamma)e^{-i(s\hat{p}_i - t\hat{x}_i + 3\gamma s\hat{x}_i^2)}X_i(s)Z_i(t)|\psi\rangle. \end{aligned} \tag{5.91}$$

Hence we find that applying a cubic phase to the ground state is equivalent to applying the cubic phase to the anyons with extra displacements and squeezing operations. This produces non-Gaussian anyons that can then be used to obtain a universal gate set.

5.12 Classification of operations

To conclude our discussion, we attempt to provide a classification of our gate operations. We found that robust topological operations correspond to controlled or uncontrolled WH gates. Non-robust, non-topological Clifford operations correspond to symplectic operations. Non-robust, non-topological, non-Clifford operations correspond to non-WH, non-symplectic operations. This is summed in this table:

Topological	**non-Topological**
uncontrolled WH (X, Z)	uncontrolled non-WH (P, F)
controlled WH (C_Z)	controlled non-WH (Two-mode P)
-	non-Clifford ($V(\gamma)$)

In group theoretical terms, all operations that are not elements of the normalizer of the WH group (Clifford group) cannot be topologically realized using abelian anyons. Of those operations that are elements of the normalizer of WH, only the elements of the normal subgroup of the Clifford group can be topologically realized using abelian anyons; those Clifford elements that are not elements of the normal subgroup cannot be realized topologically using abelian anyons [1].

5.13 Effect of finite squeezing on quantum gates

We have assumed in this computational scheme that we are using the infintely squeezed CV Kitaev lattice. We may also ask what effect there is on the gate operations if we use the finite squeezed (physical) lattice.

It appears that finite squeezing has no effects on topological operations since the displacements and dampings are taken into account through the definition of the ground state and they depend on the known squeezing

[1] Note that in standard CV encoding, the C_x and C_z gates are symplectic operations involving squeezers and beam splitters. In the abelian-anyon encoding, however, they would only result in controlled shifts.

r_j available at each qumode. As a result, topological operations on CV abelian anyons would be protected from errors due to finite squeezing of the initial ground state. If this was indeed true, this result would be a significant extension of that of Ref. [179]. There it was argued that in the case of finite squeezing, excited (anyonic) states can be experimentally distinguished from the ground state and, similarly, the effects of braiding loops can still be detected, provided the corresponding phase-space displacements are sufficiently large. In our treatment, such a requirement is unnecessary. Using the complex-nullifier formalism, we find that any finite-squeezing effects on the 1st-moment-shifts can be absorbed into the definition of the excited states as well as into the topological phases. Note also that these re-defined WH frames would always depend on the explicit values of the corresponding anyonic excitations and anyon-braidings [i.e., the t-dependencies in Eqs. (5.72-5.81)]. However, an important question here is whether this apparent fault tolerance against finite squeezing has any measurable effect. In particular, compared to Ref. [202] (see Eq.(4) and Fig.(2)), can we make the interferometric verification of the topological phase more robust against finite squeezing. That scheme relies on converting the topological phases to phase-space displacement. These displacements are then measured through homodyne measurement however in doing this we lose the benefit we gain from the topological protection. To recover the protection would require us to measure in the complex nullifier basis - clearly impossible - so finite squeezing remains a potential source of error even in these topological CV systems.

If a measurement scheme were devised that made use of this apparent fault tolerance, then all those gates shown to be implementable in a topological fashion would be robust against finite squeezing errors. Nonetheless, non-topological operations such as the Fourier transform do pick up extra errors due to finite squeezing since they rely on the ability to create zero-momentum eigenstates. In fact, all these non-topological gates include 2nd-or higher-moment manipulations which will be affected by the finite squeezing of the initial graph states. These operations would then require CV error correction protocols, to ensure the gates operate below the error threshold. Similarly, of course, the entanglement of the ground and excited states, becoming manifest through non-classical 2nd-moment correlations, does depend on the finite squeezing of the initial states.

So, mathematically at least, we have derived a nice result, that of finite squeezing protection. We are still hindered by the fact that only WH gates can be performed fault tolerantly. In our next chapter we suggest a new strategy that enables us to use the intrinsic protection available to us but over a universal set of quantum gates. For this we have to enter the realm of *non-Abelian CV anyons*.

Chapter 6

Topological quantum computation with non-abelian continuous-variable anyons

The work of our previous chapter has shown that it is possible to construct fractional mutual statistics between continuous-variable excitations on the surface of specially designed ground states. However, the simple CV excitations that we produced correspond to abelian anyons which have limited computational power. This is in perfect analogy with discrete models, where the simplest incarnation of the toric code is unable to support universal quantum operations through topological means alone. Though some suggestions have been made to augment abelian models with non-topological operations [181], they are not ideal since they open the system up to local errors. The solution then is to use non-abelian states. It has been shown that certain classes of non-abelian anyons can perform universal quantum computation through just braiding alone [182, 183]. Such concepts lead us to investigate an extension of our scheme of the CV anyon model to a non-abelian CV model and consider its use for universal quantum computation. In the following we postulate new types of excitation, derive their fusion and braiding rules and present a computational model that stores qubits within the CV resources. Before we delve into the details of the CV model, we first briefly review the properties of general non-abelian anyon models [157, 164, 182].

6.1 Non-abelian anyons

As we discussed in the previous chapter, an anyon model must satisfy a minimum set of requirements. First, we must have clearly defined list of particle types, with at least one of the particles corresponding to the vacuum (or no particle). The various particle types correspond to irreducible representations, Π_a, of the underlying group, known as the quantum double, $D(H)$, of the residual symmetry group H. The particle types must be closed under composition, that is, if we combine two or more particles we must get another representation of $D(H)$. Then one could think of the tensor product of different representations $\Pi_a \otimes \Pi_b$ as describing the transformation properties of a two-particle system. The possible outcomes of the fusion of two particles are determined by the decomposition of $\Pi_a \otimes \Pi_b$ into irreducible representations, provided by the Clebsch-Gordon series,

$$\Pi_a \otimes \Pi_b = \bigoplus_c N_{ab}^c \Pi_c. \tag{6.1}$$

We have already observed examples of these compositions or *fusions* in our abelian models. There, in analogy with other abelian models, we found that combining our excitations always resulted in a single outcome but this need not be the case in general. Since the fusion of two anyons could generate multiple particle types we must establish fusion rules to determine which particle types c may be produced for a given composition of particles a and b. We refer to the outcomes c as the fusion channels. The general fusion rules (6.1), are more simply written

$$a \times b = \sum_c N_{ab}^c c \tag{6.2}$$

where each N_{ab}^c is a non-negative integer and the sum is over the complete set of labels denoting the different particle types. Note that a, b and c are labels, not vector spaces; the product on the left hand side is not a tensor product and the sum on the right hand side is not a direct sum. Rather, the fusion rules can be regarded as an abstract relation on the label set that maps the ordered triple $(a, b; c)$ to N_{ab}^c. This relation is both commutative and associative

$$\begin{aligned} a \times b = b \times a &\Leftrightarrow N_{ab}^c = N_{ba}^c, \\ (a \times b) \times d = a \times (b \times d) &\Leftrightarrow \sum_x N_{ab}^x N_{xd}^c = \sum_x N_{ax}^c N_{bd}^x. \end{aligned} \tag{6.3}$$

By inverting Eq.(6.2), we specify the possible ways for the charge c to split into two parts with charges a and b. If $N_{ab}^c = 0$, then the charge c cannot be obtained when we combine a and b. If $N_{ab}^c = 1$, then c is obtained in a unique way and if $N_{ab}^c > 1$, then c can be obtained in N_{ab}^c distinguishable ways.

The distinguishable ways that anyons can arise from fusion forms an orthonormal basis of a Hilbert space, V_{ab}^{c}. We call V_{ab}^{c} a *fusion space* and the states it contains *fusion states*. The basis elements for V_{ab}^{c} may be denoted

$$\{|ab;c,\mu\rangle_{\mu=1,2,\ldots,N_{ab}^{c}}\}. \tag{6.4}$$

There is a dual vector space V_{c}^{ab} describing the states that arise when charge c splits into charges a and b given by

$$\{\langle ab;c,\mu|_{\mu=1,2,\ldots,N_{ab}^{c}}\}. \tag{6.5}$$

The spaces V_{ab}^{c} are mutually orthogonal, so the fusion basis elements satisfy

$$\langle ab;c'\mu'|ab;c\mu\rangle = \delta_{c}^{c'}\,\delta_{\mu}^{\mu'}, \tag{6.6}$$

The structure of the fusion spaces is given by the direct sum over all the subspaces indexed by the possible fusion outcomes c.

$$V_{ab} = \bigoplus_{c} V_{ab}^{c}, \quad dim(V_{ab}) = \sum_{c} N_{ab}^{c}. \tag{6.7}$$

The completeness of the fusion basis can be expressed as

$$\sum_{c,\mu} |ab;c\mu\rangle\langle ab;c'\mu'| = I_{ab}, \tag{6.8}$$

where I_{ab} is the projector onto the space V_{ab}. Then each order of fusion corresponds to a different basis within this space. The fusion space of anyons is a collective non-local property, it cannot be influenced by local operations on any single anyon. It is this property that hints towards fusion spaces as a robust medium to store quantum information.

In the language of fusion spaces, an anyon model is called *non-abelian* if

$$dim(V_{ab}) = \sum_{c} N_{ab}^{c} \geq 2 \tag{6.9}$$

for at least some pair of labels ab, otherwise the model is *abelian*. In an abelian model, such as we discussed in Chapter 5, any two particles fuse in a unique way, in contrast to the non-abelian case where there can be multiple possible fusion paths. Then non-abelian anyons have a Hilbert space of two or more dimensions spanned by the distinguishable states.

Our next requirement states that a given anyon model must include rules for operations acting on the fusion space. These operations are known as the F- and R-moves. F and R are unitary operators and in general have a matrix representation. The F-moves serve to switch between the fusion bases of any three anyons a, b and c. This is represented in Fig. (6.1(a)). More explicitly, when three particles a, b and c are fused to give d, there are

two ways to decompose the topological Hilbert space in terms of the fusion spaces of particle pairs,

$$V_{abc}^{d} \cong \bigoplus_{c} V_{ab}^{e} \otimes V_{ec}^{d} \cong \bigoplus_{e'} V_{ae'}^{d} \otimes V_{bc}^{e'} \tag{6.10}$$

This decomposition allows us to write the two orthonormal bases for V_{abc}^{d},

$$\begin{aligned} |(ab)c; d, e\mu\nu\rangle &\equiv |ab; e\mu\rangle \otimes |ec; d\nu\rangle \\ |a(bc); d, e'\mu'\nu'\rangle &\equiv |ae'; d\nu'\rangle \otimes |bc; e'\mu'\rangle \end{aligned} \tag{6.11}$$

The F-matrices give the relation between these equivalent bases,

$$|(ab)c; d, e\mu\nu\rangle = \sum_{e'} |a(bc); d, e'\mu'\nu'\rangle (F_{abc}^{d})_{e\mu\nu}^{e'\mu'\nu'} \tag{6.12}$$

The R-matrices correspond to braiding of the anyons. They act as a maps

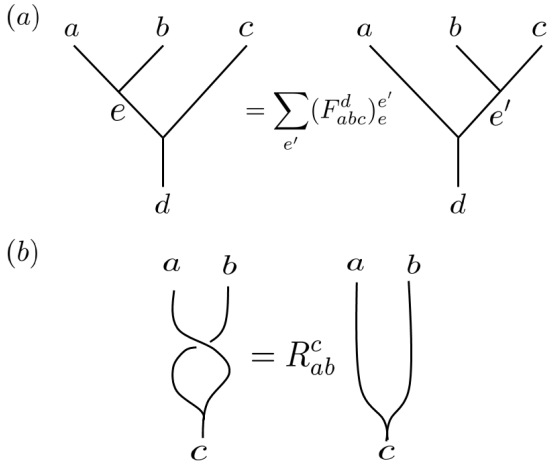

Figure 6.1: (a) The F-matrix switches between equivalent fusion bases, with intermediate fusion products e and e'. (b) The R-matrix swaps the position of particles.

on the fusion space of two anyons a and b at some well defined locations to the space where the particles have undergone an exchange. The map can be written as

$$R : V_{ba}^{c} \to V_{ab}^{c}. \tag{6.13}$$

If we choose the bases $\{|ba; c, \mu\rangle\}$ and $\{|ab; c, \mu'\rangle\}$ for these two spaces, R can be expressed as the unitary matrix

$$R : |ba; c, \mu\rangle \to \sum_{\mu'} |ab; c, \mu'\rangle (R_{ab}^{c})_{\mu}^{\mu'}. \tag{6.14}$$

Note that R may have a nontrivial action on the fusion states which we represent in Fig. (6.1(b)).

The *monodromy* operator

$$R^2 : V_{ab}^c \to V_{ab}^c \tag{6.15}$$

is an isomorphism from V_{ab}^c to itself, representing the effect of winding a counterclockwise around b. The eigenvalues of the monodromy operators are determined by the topological spins of the particles,

$$(R_{ab}^c)^2 = e^{i(\theta_c - \theta_a - \theta_b)}. \tag{6.16}$$

The F and R matrices are constrained by certain consistency conditions. These conditions arise due to the isomorphisms connecting the alternative fusion spaces. They are known as the *pentagon* and *hexagon* equations [184]. The pentagon equation imposes consistency on changes between fusion bases. We derive it by considering the fusion of four particles, this can be represented by the fusion space $V_{abcd}^e = \bigoplus_{x\in f(ab), y\in f(xc)} V_{ab}^x \otimes V_{xc}^y \otimes V_{yd}^e$. This is not unique of course but this choice is known as the standard basis and is represented in the left most fusion diagram in Fig.(6.2). There are multiple ways to fuse these particles, each of these is a fusion basis and they are related to each other through the F-matrices. Applying an F-matrix to a particular basis to change to the next is referred to as an F-move. There are two F-move sequences as depicted in Fig.(6.2). The moves along the top of the digram are given by

$$\bigoplus_{\substack{x\in f(ab),\\ y\in f(xc)}} V_{ab}^x \otimes V_{xc}^y \otimes V_{yd}^e \overset{F^e_{xcd}}{\to} \bigoplus_{\substack{x\in f(ab),\\ y\in f(cd)}} V_{ab}^x \otimes V_{xy'}^e \otimes V_{cd}^{y'} \overset{F^e_{aby'}}{\to} \bigoplus_{\substack{x'\in f(by'),\\ y'\in f(cd)}} V_{ax'}^e \otimes V_{by'}^{x'} \otimes V_{cd}^{y'}. \tag{6.17}$$

where $f(ij)$ denotes the outcomes from the fusion of particles i and j. The moves along the bottom are

$$\bigoplus_{\substack{x\in f(ab),\\ y\in f(xc)}} V_{ab}^x \otimes V_{xc}^y \otimes V_{yd}^e \overset{F^y_{abc}}{\to} \bigoplus_{\substack{x'\in f(bc),\\ y\in f(ax')}} V_{ax'}^y \otimes V_{bc}^{x'} \otimes V_{yd}^e$$

$$\overset{F^e_{ax'd}}{\to} \bigoplus_{\substack{x'\in f(bc),\\ y'\in f(x'd)}} V_{ay'}^e \otimes V_{bc}^{x'} \otimes V_{x'd}^{y'} \overset{F^{y'}_{bcd}}{\to} \bigoplus_{\substack{x''\in f(cd),\\ y'\in f(bx'')}} V_{ay'}^e \otimes V_{bx''}^{y'} \otimes V_{cd}^{x''}. \tag{6.18}$$

Since the decompositions yield the same result, the F-moves along the top have to be equal to those along the bottom and hence must satisfy

$$\sum_{\substack{y'\in f(cd),\\ x'\in f(by')}} (F_{aby}^e)_x^{x'} (F_{xcd}^e)_y^{y'} = \sum_{\substack{x'\in f(bc),\\ y'\in f(x'd), x''\in f(cd)}} (F_{bcd}^y)_{x'}^{x''} (F_{ax'd}^e)_y^{y'} (F_{abc}^y)_x^{x'}. \tag{6.19}$$

This is the pentagon equation, we have suppressed the fusion state indices $\mu, \nu, ...$ for brevity. The hexagon equation is similar, but this time we con-

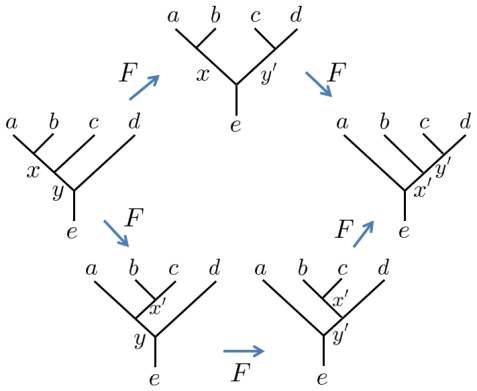

Figure 6.2: The fusion bases related by the F moves obey a consistency condition known as the pentagon equation, that requires the moves along the top to be equal to those along the bottom.

sider the fusion of just three particles and include the possibility that the particles may be interchanged through braiding. This is known as an R-move. Across the top of the diagram, Fig. (6.3), the two bases are related by the moves FRF while across the bottom by the moves RFR. Performing a similar fusion basis decomposition as above and comparing the F- and R-moves yields the hexagon equation

$$\sum_{x' \in f(ac)} R^{x'}_{ac} (F^d_{bac})^{x'}_{x} R^{x}_{ab} = \sum_{\substack{x' \in f(bc), \\ x'' \in f(ca)}} (F^d_{bca})^{x''}_{x'} R^{d}_{ax'} (F^d_{abc})^{x'}_{x} . \tag{6.20}$$

It is known, due to the *MacLane coherence theorem* [185], that there are no further consistency conditions and thus solutions to (6.19) and (6.20) define viable anyon models.

We now apply these ideas by briefly reviewing a well studied non-abelian anyon model that will turn out to be significant for the CV non-abelian model that we propose later in this Chapter.

6.2 The Ising anyon model

One of the best understood schemes that employs non-abelian braid statistics is that of the lowest energy excitations of the fractional quantum Hall effect (FQHE) at filling factor $\nu = 5/2$ [186, 187]. Extensive analytical and

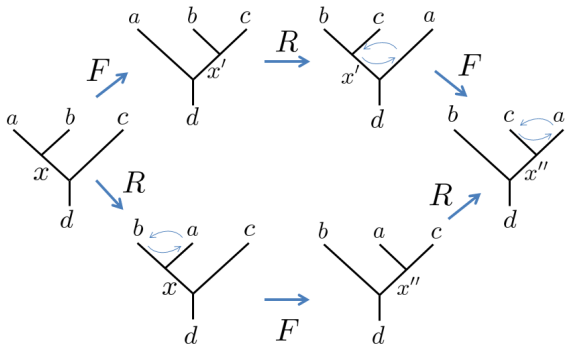

Figure 6.3: Pictorial representation of the hexagon equation. The move FRF across the top must equal the RFR move along the bottom.

numerical studies have been carried out on this state, [188, 189, 190, 191], which has led to the conclusion that the excitations, also known as Ising anyons are in the universality class of the Moore-Read Pfaffin state [192]. The main advantage of the the FQH state at $\nu = 5/2$ in a quantum computational setting is its relative stability compared to other non-abelian FQH states. This stability is a result of the Ising model having the largest bulk energy gap of any of the non-abelian models, ensuring that random excitations are less likely to interfere with quantum operations on the non-abelian anyons. On the other hand it has been shown that the quasiparticle braid matrices of the Moore-Read Pfaffin states are not sufficient for universal quantum computation because the braid group representation over the Ising model correlation functions is finite [193, 194, 195]. However, using these particles, it is possible to generate the set of Clifford gates which play a central role in quantum error correction [196].

Recently it has been shown that excitations of this type can also be artificially generated in lattice models [140, 174, 197, 198]. Systems of particular relevance to us here are spin lattices with Hamiltonians that exhibit abelian or non-abelian behaviour for different coupling regimes. An example of such a system is the *Honeycomb lattice model*, a hexagonal spin lattice model that features frustration of its ground state [199, 200, 201].

The Ising model has three distinct particle types, which we call $\mathbb{1}$, σ and ψ. The fusion rules are

$$\begin{aligned} \sigma \times \sigma &= \mathbb{1} + \psi, \quad \sigma \times \psi = \sigma, \\ \psi \times \psi &= \mathbb{1}, \quad \mathbb{1} \times x = x, \end{aligned} \tag{6.21}$$

for $x = \mathbb{1}, \psi, \sigma$. The defining characteristic of this model is the non-unique fusion of the σ anyons which implies that the fusion spaces have dimension greater than one. We can demonstrate this by creating four of the σ particles from the vacuum and fusing them. To obey conservation the four particles must eventually fuse back to the vacuum, $\mathbb{1}$. However, due to the non-unique fusion rule for σ anyons there are two ways to achieve this i.e., If we first split the four particles into pairs that fuse to the vacuum the four particle fusion results in the vacuum. Alternatively both could fuse to a ψ, then fusing both ψs we arrive at the vacuum again. Note that these are the only possibilities that conservation allows since otherwise we would be left with an extra ψ. This defines a two dimensional space associated with the fusion and hence the fusion matrix for σ fusion will be two-dimensional and this fusion defines the only non-trivial F matrix given by

$$F^{\sigma}_{\sigma\sigma\sigma} = \frac{1}{\sqrt{2}} \begin{pmatrix} 1 & 1 \\ 1 & -1 \end{pmatrix}. \tag{6.22}$$

We also require braiding rules, given by the R-matrices. The one-dimensional R matrices are

$$R^{\psi\psi}_{\mathbb{1}} = -1, \quad (R^{\sigma\psi}_{\sigma})^2 = -1 \tag{6.23}$$

Then the ψ particles have antisymmetric behaviour under braiding, due to this they are often referred to as the fermions of the Ising model. Since we have a two-dimensional fusion space we require a non-trivial braid matrix. The braid matrices acting on the two dimensional space can be written,

$$R_1 = \begin{pmatrix} 1 & 0 \\ 0 & i \end{pmatrix}, \quad R_2 = \frac{e^{i\pi/4}}{\sqrt{2}} \begin{pmatrix} 1 & -i \\ -i & 1 \end{pmatrix}, \tag{6.24}$$

in the basis $\{\mathbb{1}, \psi\}$.

Due to topological degeneracy in the Ising model, it is possible to realize n-qubits by $2n + 2$ Ising anyons. The states of the Ising anyons are represented by conformal field theory (CFT) correlation functions which belong to one of two inequivalent spinor representations of the covering group $Spin(2n + 2)$ of the rotation group $SO(2n + 2)$. Unfortunately, the set of matrices (6.24), that can be obtained from braiding Ising anyons only generates members of the Clifford group of quantum gates. While important, the Clifford group by itself is insufficient for universal quantum computation. Further, it has been shown that not all Clifford gates, such as embeddings of the two-qubit SWAP, can be realized by braiding three or more Ising qubits [194].

6.3 A continuous-variable non-Abelian anyon model

Now we present the main result of this chapter. We show how we may extend the CV toric code [202] to include non-abelian anyons. To specify

this model we follow our usual prescription of identifying the particle types, with the fusion and braiding rules. We recall our results from the chapter 5, the ground state that we defined to generate abelian excitations. There is was shown that applying simple displacements onto this CV analog of the Kitaev state produced continuous-variable abelian anyons. Here we seek to generate non-abelian statistics from this ground state. There have been several previous proposals to produce non-abelian statistics from abelian models in discrete theories [203, 204, 205]. Such ideas have led us to consider whether this is possible in the CV regime.

6.3.1 Particle types

The ground state that we defined in Chapter 5 gives rise to anyonic excitations when acted upon by CV displacement operators. The resulting excitations form the particle spectrum for the CV toric code. We label the particle types $\{\mathbf{1}, e(s), m(s), \epsilon(s,t)\}$ where $\epsilon(s,t) = e(s) \times m(t)$ is the result of fusing e- and m-types and $\mathbf{1}$ is the vacuum particle which corresponds to the absence of an excitation. Then fusing particles is equivalent to summing the value of the displacements, i.e., $e(s) \times e(t) = e(s+t)$, $m(s) \times m(t) = m(s+t)$. These fusions are unique and so the fusion spaces are one-dimensional and all the fusion matrices are trivial. The monodromies of the CV toric particles are more interesting. We showed that braiding e- and m-type anyons results in phase rotations dependent on the displacements that produced the particles. Since the fusion spaces are one-dimensional so are the braid matrices, these are written

$$\left(R^{e(s)e(t)}_{e(s+t)}\right)^2 = 1, \quad \left(R^{m(s)m(t)}_{m(s+t)}\right)^2 = 1 \text{ and } \left(R^{e(s)m(t)}_{\epsilon(s,t)}\right)^2 = e^{-ist}. \tag{6.25}$$

While the state space of the CV anyons is infinite (which we made use of in our CV computation model), they only have a one-dimensional fusion space. Then these fusion spaces are unsuitable from a quantum information point of view as we cannot store multiple states within them. In order to produce a useful anyon model for storing and manipulating quantum information we must find a way to increase the fusion space dimension and so turn our abelian model to a non-abelian one.

To achieve this we postulate the existence of excitations $\{\mathbb{1}, \psi(s,t), \sigma(s,t)\}$ and associate the toric anyon with these in the following way:

$$\mathbb{1} = \{\mathbf{1}\}, \quad \psi(s,t) = \{\epsilon(s,t)\}, \quad \sigma = \{e(s), m(t)\}. \tag{6.26}$$

The vacuum and ϵ sectors correspond one to one with what we shall call the vacuum and ψ sectors of our new anyon model. The σ-type is a superposition m- and e-anyons.

To devise the fusion rules for these new anyons we decompose back into CV toric anyons. Clearly fusing any of the anyon types with the vacuum

has no effect. However, fusing ψ-anyons, $\psi_1(s,t)$ and $\psi_2(u,v)$ we find

$$\begin{aligned} |\psi_1(s,t)\psi_2(u,v)\rangle &= |e(s)m(t) \times e(u)m(v)\rangle \\ &= |e(s+u)m(t+v)\rangle \\ &= |\psi(s+u,t+v)\rangle. \end{aligned} \tag{6.27}$$

Another ψ anyon emerges, parameterized by displacements that are just the sum of the contributing CV toric anyons. Since this fusion only ever results in a unique outcome, the ψ anyons are considered to be abelian.

The fusion of two σ types yields an interesting and potentially useful behaviour. We create pairs of σs at sites 1 and 2 on the lattice. These are defined by $\sigma_1 = \{e(s), m(t)\}$ and $\sigma_2 = \{e(u), m(v)\}$. Fusing yields multiple outcomes:

$$\begin{aligned} |\sigma_1\sigma_2\rangle &= a|e(s)e(u)\rangle + b|m(t)m(v)\rangle, \\ |\sigma_1\sigma_2\rangle &= a|e(s)m(t)\rangle + b|e(u)m(v)\rangle, \\ |\sigma_1\sigma_2\rangle &= a|e(s)m(v)\rangle + b|e(u)m(t)\rangle. \end{aligned} \tag{6.28}$$

Each outcome has a multiplicity of two. We have three possible fusion spaces from the fusion of the σ particles which can be labeled

$$V_{\sigma\sigma}^{(e+m)} \cong V_{\sigma\sigma}^{\psi_1} \cong V_{\sigma\sigma}^{\psi_2}, \tag{6.29}$$

respectively and the continuous parameters are suppressed for brevity. We neglect the second and third fusion possibilities and just consider the first case. Then we can state that the fusion of σs gives

$$|\sigma_1\sigma_2; j\rangle = \frac{1}{\sqrt{2}}\Big[|e_1(s)e_2(u)\rangle + j|m_1(t)m_2(v)\rangle\Big]. \tag{6.30}$$

This state is depicted in Fig.(6.4). and represents what we will refer to as a

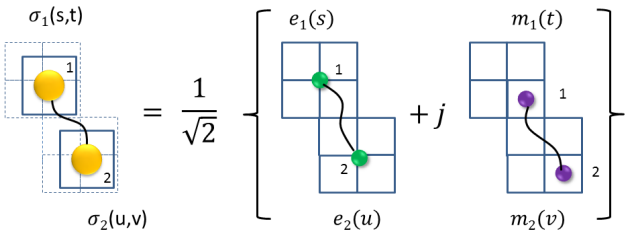

Figure 6.4: The σ anyon string, composed of a superposition of e and m-type toric anyons.

σ-string. It has a non-local term j that be altered by braiding but cannot be determined by a local measurement of the endpoints. We can produce

many such strings on our lattice, defined over pairs of lattice sites. It seems initially that there are no restrictions on the value of the displacements we can apply to the underlying lattice to produce these strings. However, in following we find this is not the case. For our CV scheme to be considered a proper anyon model we show that the CV parameters s, u, t and v must satisfy certain constraints.

6.3.2 Consistency of the model

To investigate the behaviour and consistency of this model we consider the fusion of three σ strings generated at different locations on the lattice Fig.(6.5). By decomposing the strings into toric particle we can write our three strings as,

$$|\sigma_1\sigma_2; j\rangle = \frac{1}{\sqrt{2}}\Big[|e_1(s)e_2(u)\rangle + |m_1(t)m_2(v)\rangle\Big], \tag{6.31}$$

$$|\sigma_3\sigma_4; j\rangle = \frac{1}{\sqrt{2}}\Big[|e_3(p)e_4(r)\rangle + |m_3(q)m_4(w)\rangle\Big], \tag{6.32}$$

$$|\sigma_5\sigma_6; j\rangle = \frac{1}{\sqrt{2}}\Big[|e_5(g)e_6(h)\rangle + |m_5(k)m_6(n)\rangle\Big], \tag{6.33}$$

Each of these are parameterized by different initial displacements. We consider fusing in the two bases shown in Fig.(6.5). In the left basis (a) we have the fusion $(|\sigma_1\sigma_2; j\rangle|\sigma_3\sigma_4; j\rangle)|\sigma_5\sigma_6; j\rangle$ corresponding to the decomposition $\bigoplus_y V^y_{\sigma_{12}\sigma_{34}\sigma_{56}} \cong \bigoplus_{x,y} V^x_{\sigma_{12}\sigma_{34}} \otimes V^y_{x\sigma_{56}}$ where $x \in \{(e+m), \psi\}$ and $y \in \{\sigma, \psi\}$. Fusing the left two strings yields

$$\begin{aligned}|\sigma_1\sigma_2; j\rangle \times |\sigma_3\sigma_4; j\rangle = \frac{1}{2}\Big[&|e_1(s)e_2(u)e_3(p)e_4(r)\rangle \\ &+|m_1(t)m_2(v)m_3(q)m_4(w)\rangle \\ &+j|e_1(s)e_2(u)m_3(q)m_4(w)\rangle \\ &+j|m_1(t)m_2(v)e_3(p)e_4(r)\rangle\Big].\end{aligned} \tag{6.34}$$

The first and second terms in this fusion are just e- and m-types which can be regarded collectively as a single outcome. The third and fourth terms are abelian anyons which we call $\psi_1 = |e_1(s)e_2(u)m_3(q)m_4(w)\rangle$ and $\psi_2 = |m_1(t)m_2(v)e_3(p)e_4(r)\rangle$. We regard these anyons as distinguishable since under braiding they yield different phases. This fusion is summarized as

$$\sigma_{12} \times \sigma_{34} = (e + m) + \psi_1 + \psi_2, \tag{6.35}$$

where σ_{ik} abbreviates $|\sigma_i\sigma_k; j\rangle$. This fusion has multiple outcomes and so σ-strings are non-abelian anyons. We now fuse our remaining σ-string, $|\sigma_5\sigma_6; j\rangle$, to the outcomes of Eq.(6.34) to give $\sigma_{12} \times \sigma_{34} \times \sigma_{56}$.

- $(e+m)$ outcome:

$$\Big(|\sigma_1\sigma_2;j\rangle|\sigma_3\sigma_4;j\rangle\Big)|\sigma_5\sigma_6;j\rangle = \frac{1}{2}\Big[|e_1(s)e_2(u)e_3(p)e_4(r)e_5(g)e_6(h)\rangle + j|m_1(t)m_2(v)m_3(q)m_4(w)m_5(k)m_6(n)\rangle + |m_1(t)m_2(v)m_3(q)m_4(w)e_5(g)e_6(h)\rangle + j|e_1(s)e_2(u)e_3(p)e_4(r)m_5(k)m_6(n)\rangle\Big]. \tag{6.36}$$

  Note that the first two terms are form another σ-string while the third and fourth are another two abelian anyon which we label ψ_3 and ψ_4.

- ψ_1 outcome:

$$\Big(|\sigma_1\sigma_2;j\rangle \times |\sigma_3\sigma_4;j\rangle\Big)|\sigma_5\sigma_6;j\rangle = \frac{1}{\sqrt{2}}\Big[|m_1(t)m_2(v)e_3(p)e_4(r)m_5(k)m_6(n)\rangle + j|m_1(t)m_2(v)e_3(p)e_4(r)e_5(g)e_6(h)\rangle\Big]. \tag{6.37}$$

  Which are another pair of ψ particles that we name ψ_5 and ψ_6.

- ψ_2 outcome:

$$\Big(|\sigma_1\sigma_2;j\rangle \times |\sigma_3\sigma_4;j\rangle\Big)|\sigma_5\sigma_6;j\rangle = \frac{1}{\sqrt{2}}\Big[|e_1(s)e_2(u)m_3(q)m_4(w)m_5(k)m_6(n)\rangle + j|e_1(s)e_2(u)m_3(q)m_4(w)e_5(g)e_6(h)\rangle\Big]. \tag{6.38}$$

  We label these outcomes ψ_7 and ψ_8.

Then the fusion of three σ-strings in the left fusion basis can be summarized as

$$\sigma_{12} \times \sigma_{34} \times \sigma_{56} = \sigma + \psi_3 + \psi_4 + \psi_5 + \psi_6 + \psi_7 + \psi_8, \tag{6.39}$$

Now we consider fusion in the right hand basis Fig.(6.5(b)) with decomposition $\bigoplus_{y'} V^{y'}_{\sigma_{12}\sigma_{34}\sigma_{56}} \cong \bigoplus_{x',y'} V^{y'}_{\sigma_{12}x'} \otimes V^{x'}_{\sigma_{34}\sigma_{56}}$ where $x' \in \{(e+m), \psi\}$ and $y' \in \{\sigma, \psi'\}$. We begin by fusing σ_{34} with σ_{56},

$$|\sigma_3\sigma_4;j\rangle|\sigma_5\sigma_6;j\rangle = \frac{1}{2}\Big[|e_3(p)e_4(r)e_5(g)e_6(h)\rangle + |m_3(q)m_4(w)m_5(k)m_6(n)\rangle + j|e_3(p)e_4(r)m_5(k)m_6(n)\rangle + j|m_3(q)m_4(w)e_5(g)e_6(h)\rangle\Big]. \tag{6.40}$$

As before we have three outcomes, $(e+m)'$ and two abelian anyons, ψ_1' and ψ_2'. Then the results of fusing σ_{12} to the result of Eq.(6.40) are given by:

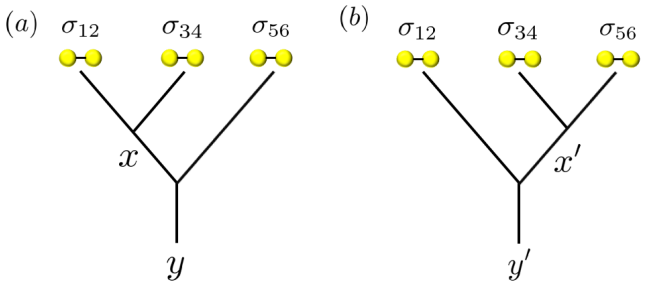

Figure 6.5: (a) The left fusion basis: The left and center σ-strings fuse to $x \in \{(e+m), \psi_1, \psi_2\}$. These fuse to the right σ-string to give $y \in \{\sigma, \psi_3, \psi_4, \psi_5, \psi_6, \psi_7, \psi_8\}$ (b) The right fusion basis: The right and center σ-strings fuse to $x \in \{(e+m)', \psi_1', \psi_2'\}$. These fuse to the left σ-string to give $y' \in \{\sigma, \psi_3', \psi_4', \psi_5', \psi_6', \psi_7', \psi_8'\}$. In general $\psi_i \neq \psi_i'$ and hence $y \neq y'$ so we conclude that the model is not in general associative.

- $(e+m)'$ outcome:

$$\begin{aligned}|\sigma_1\sigma_2; j\rangle\Big(|\sigma_3\sigma_4; j\rangle|\sigma_5\sigma_6; j\rangle\Big) = \frac{1}{2}\Big[&|e_1(s)e_2(u)e_3(p)e_4(r)e_5(g)e_6(h)\rangle \\ &+ j|m_1(t)m_2(v)m_3(q)m_4(w)m_5(k)m_6(n)\rangle \\ &+ |e_1(s)e_2(u)m_3(q)m_4(w)m_5(k)m_6(n)\rangle \\ &+ j|m_1(t)m_2(v)e_3(p)e_4(r)e_5(g)e_6(h)\rangle\Big].\end{aligned} \tag{6.41}$$

  Similar to the case above we find the $(e+m)$-channel gives a σ and two abelian anyons ψ_3' and ψ_4'.

- ψ_1' outcome:

$$\begin{aligned}|\sigma_1\sigma_2; j\rangle\Big(|\sigma_3\sigma_4; j\rangle|\sigma_5\sigma_6; j\rangle\Big) = \frac{1}{\sqrt{2}}\Big[&|m_3(q)m_4(w)e_5(g)e_6(h)m_1(t)m_2(v)\rangle \\ &+ j|m_3(q)m_4(w)e_5(g)e_6(h)e_1(s)e_2(u)\rangle\Big].\end{aligned} \tag{6.42}$$

  Giving particles that we call ψ_5' and ψ_6'.

- ψ_2' outcome:

$$|\sigma_1\sigma_2;j\rangle\Big(|\sigma_3\sigma_4;j\rangle|\sigma_5\sigma_6;j\rangle\Big) = \frac{1}{\sqrt{2}}\Big[|e_3(p)e_4(r)m_5(k)m_6(n)m_1(t)m_2(v)\rangle + j|e_1(s)e_2(u)e_3(p)e_4(r)m_5(k)m_6(n)\rangle\Big]. \tag{6.43}$$

  Giving particles that we call ψ_7' and ψ_8'.

However upon examining these fusion outcomes we see that the non-abelian anyons ψ_i and ψ_i', $i \in \{3,...8\}$, are not equal and hence this model is not associative under braiding as demanded by Eq.(6.3). Then the excitations in the form Eq.(6.30), do not form a proper anyon model. We can restore associativity by restricting our allowed anyonic states. In particular if we ensure that the initial displacements $s = g = p$ and $t = q = k$ then the abelian anyons produced in the right and left bases become equivalent. Stated another way, these conditions require us to only consider the fusion of identical σ-strings which we write as

$$|\sigma_i\sigma_k;j\rangle = \frac{1}{\sqrt{2}}\Big[|e_i(s)e_k(u)\rangle + j|m_i(t)m_k(v)\rangle\Big]. \tag{6.44}$$

Then we may only apply identical initial displacements to create our σ-strings from the CV toric lattice for the particles to constitute a valid anyon model. In the following we continue our analysis by examining the fusion rules under the identical particle restriction.

6.3.3 Fusion of identical particles

Here we will establish the fusion rules for the CV non-abelian anyons assuming that the σ-strings are identical and of the form in Eq.(6.44). Then we expand the fusions to the many particle case and construct the pentagon equation for the model.

We begin with the simple two string fusion $\sigma_{12} \times \sigma_{34}$:

$$|\sigma_1\sigma_2;j\rangle|\sigma_3\sigma_4;j\rangle = \frac{1}{2}\Big[|e_1(s)e_2(u)e_3(s)e_4(u)\rangle + |m_1(t)m_2(v)m_3(t)m_4(v)\rangle + j|e_1(s)e_2(u)m_3(t)m_4(v)\rangle + j|m_1(t)m_2(v)e_3(s)e_4(u)\rangle\Big]. \tag{6.45}$$

We collect the first and second terms together. This gives us a new particle that is distinguishable from the σ-string since it does not contain the non-local parameter j. We call this outcome $(e+m)$, defined by $|(e+m)\rangle = (|e_1(s)e_2(u)e_3(s)e_4(u)\rangle + |m_1(t)m_2(v)m_3(t)m_4(v)\rangle)/\sqrt{2}$, the remaining terms are abelian anyons. Note that these anyons have identical behaviour under braiding and hence we define $\psi_0 = (|e_1(s)e_2(u)m_3(t)m_4(v)\rangle +$

$|m_1(t)m_2(v)e_3(s)e_4(u)\rangle)/\sqrt{2}$. The fusion of the $(e+m)$-particle at sites (1,2) and (3,4) with a σ-string at (5,6) yields

$$\begin{aligned}|(e+m)\rangle|\sigma_5\sigma_6;j\rangle =&\frac{1}{2}\Big[|e_1(s)e_2(u)e_3(s)e_4(u)e_5(s)e_6(u)\rangle\\ &+j|m_1(t)m_2(v)m_3(t)m_4(v)m_5(t)m_6(v)\rangle\\ &+|m_1(t)m_2(v)m_3(t)m_4(v)e_5(s)e_6(u)\rangle\\ &+j|e_1(s)e_2(u)e_3(s)e_4(u)m_5(t)m_6(v)\rangle\Big].\end{aligned} \tag{6.46}$$

The first and second terms form another σ-string, we label the remaining terms ψ_1. Then our two string fusion rules are of the form

$$\sigma\times\sigma=(e+m)+\psi_0,\quad \sigma\times(e+m)=\sigma+\psi_1,\quad \psi_1\times\sigma=\psi_2+\psi_3, \tag{6.47}$$

where $1, 2.3...$ label abelian anyons that are distinguishable from each other through braiding. These fusion rules clearly indicate that the under this identical particle condition the σ-strings are non-abelian anyons. From the fusion rules, (6.47), we can construct the multi-particle fusions,

$$\sigma\times\sigma\times\sigma=\sigma+\psi_1+\psi_2, \tag{6.48}$$

$$\sigma\times\sigma\times\sigma\times\sigma=(e+m)+\psi_3+2\psi_4+2\psi_5, \tag{6.49}$$

It is clear that if we continue fusing σ-strings, we will generate further ψ_i anyons. Each of these anyons implements abelian phase changes under braiding but the value of the phase is arbitrary and will vary with the addition of more σ-strings. We now simplify our fusion rules by grouping all the ψ_i into a single term, simply labeled ψ since in our CV schemes we distinguish particle based on the type of braiding behaviour they exhibit rather than the specific phase changes they produce. Then our fusion rules for the identical CV non-abelian anyons are

$$\begin{aligned}&\sigma\times\sigma=(e+m)+\psi,\quad \sigma\times(e+m)=\sigma+\psi,\\ &\sigma\times\psi=\psi,\quad \psi\times\psi=\psi,\end{aligned} \tag{6.50}$$

with multi-particle fusion rules given as

$$\sigma\times\sigma\times\sigma=\sigma+2\psi, \tag{6.51}$$

$$\sigma\times\sigma\times\sigma\times\sigma=(e+m)+5\psi. \tag{6.52}$$

From these we identify the non-trivial fusion space, $V^{\psi}_{\sigma\sigma\sigma}$, with dimension $N^{\psi}_{\sigma\sigma\sigma}=2$. It is this non-trivial space that makes such models potential candidates for storing quantum information. In particular, within this two-dimensional fusion space we could, in principle store a qubit and in general for $N^c_{ab}=d$ it is possible to store d-dimensional qudits. Unitary operations

can then be carried out on the states contained in the fusion spaces through basis changes and braiding. To find how braiding acts on the fusion basis we must construct the F- and R- moves of our anyon model as solutions of the pentagon (6.19) and hexagon (6.20) equations.

By considering the decomposition of the fusion space $V^{\psi}_{\sigma\sigma\sigma}$ into

$$V^{\psi}_{\sigma\sigma\sigma} \cong \bigoplus_{\substack{x\in\{(e+m),\psi\},\\ y\in\{\sigma,\psi\}}} V^{x}_{\sigma\sigma} \otimes V^{y}_{x\sigma} \otimes V^{\psi}_{y\sigma}, \tag{6.53}$$

and considering the two ways (6.17) and (6.18) to implement the transformation

$$\bigoplus_{\substack{x\in\{(e+m),\psi\},\\ y\in\{\sigma,\psi\}}} V^{x}_{\sigma\sigma} \otimes V^{y}_{x\sigma} \otimes V^{\psi}_{y\sigma} \rightarrow \bigoplus_{\substack{y'\in\{(e+m),\psi\},\\ x'\in\{\sigma,\psi\}}} V^{\psi}_{\sigma x'} \otimes V^{x'}_{\sigma y'} \otimes V^{y'}_{\sigma\sigma} \tag{6.54}$$

we can derive the pentagon equation

$$\sum_{y',y} (F^{\psi}_{\sigma\sigma y})^{x'}_{x} (F^{\psi}_{x\sigma\sigma})^{y'}_{y} = \sum_{x',y',x''} (F^{y'}_{\sigma\sigma\sigma})^{x''}_{x} (F^{\psi}_{\sigma x'\sigma})^{y'}_{y} (F^{y}_{\sigma\sigma\sigma})^{x'}_{x}. \tag{6.55}$$

However, this equation has multiple non-trivial fusion matrices and it is not obvious how it can be solved, especially in light of the complex braiding behaviour which will yield different phases depending on the number of σ-string fusions. The complexity of the fusion bases and the associated F- and R-moves do not yield an intuitive method to establish a good computational model as it is not clear how to efficiently store and manipulate quantum information within these states. However there is a further simplification we can make to reduce the complexity of the fusion and braiding behaviour and find useful fusion bases to act as computational spaces.

6.4 Continuous-variable Ising anyon model

In this section we finalize our anyon model by placing further constraints on the states of the excitations. With these constraints in place we rederive our fusion rules and calculate the braid matrices. We find that the fusion rules and in particular the non-trivial F-moves are similar to those of the Ising anyon model which motivates us to call our σ-strings *CV Ising anyons*. We find however that the braiding for these restricted σ-strings, yield braid matrices that correspond to general phase rotations. This property leads us to consider a quantum computational model using the σ-strings as the computational resource.

By examining the fusion rules of our general model Eq.(6.50), we see that a sensible restriction is to ensure that the allowed states for our σ strings are those composed of particle and antiparticles, located at the ends

of the strings. This is a natural assumption motivated by the fact that the CV toric anyons are naturally produced in particle/antiparticle pairs on the lattice. Our string is then defined by endpoints that are combinations of $\sigma_a = \{e(s), m(t)\}$ and $\sigma_b = \{e(-s), m(-t)\}$ and so our CV Ising σ string is written:

$$|\sigma_i \sigma_k; j\rangle = \frac{1}{\sqrt{2}}\Big[|e_i(s)e_k(-s)\rangle + j|m_i(t)m_k(-t)\rangle\Big]. \tag{6.56}$$

We proceed as before, we begin with the two string fusion and derive a set of fusion rules. We then find the multi-particle fusion outcomes and find the solutions to the pentagon equation before considering the braiding rules which completes our model.

The first fusion we consider is between a pair of σ-strings located at sites (1,2) and (3,4):

$$\begin{aligned}|\sigma_1\sigma_2; j\rangle|\sigma_3\sigma_4; j\rangle =& \frac{1}{2}\Big[|e(0)e(0)\rangle + |m(0)m(0)\rangle + j|m_1(t)m_2(-t)e_3(s)e_4(-s)\rangle \\ &+ j|e_1(s)e_2(-s)m_3(t)m_4(-t)\rangle\Big].\end{aligned} \tag{6.57}$$

Here it is assumed that the endpoint of the first string at site 1 fuses with the endpoint of the other string at site 4, of course this leaves the endpoint at site 2 to fuse with 3, Fig.6.6. This ensures that particles always fuse to antiparticles so the first and second terms correspond to the vacuum channel, defined as $\mathbb{1} = |\mathbb{1}_{1,4}\mathbb{1}_{2,3}\rangle = (|e(0)e(0)\rangle + |m(0)m(0)\rangle)/\sqrt{2}$ and we have an abelian anyon $\psi = |\psi_{1,4}\psi_{2,3}\rangle = (|m_1(t)m_2(-t)e_3(s)e_4(-s)\rangle + |e_1(s)e_2(-s)m_3(t)m_4(-t)\rangle)/\sqrt{2}$. We find the result of the fusion $\sigma \times \psi$ for

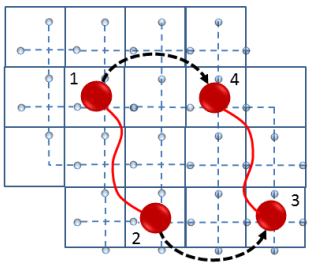

Figure 6.6: When fusing σ-strings, we assume that the particle ends of the string, at sites 1 and 3 always fuse the antiparticle ends, at 2 and 4. This ensures that the fusion always has some probability of resulting in the vacuum.

a σ-string at lattice sites 5 and 6. This gives,

$$|\sigma_5\sigma_6; j\rangle|\psi_{1,4}\psi_{2,3}\rangle = \frac{1}{2}\Big[|m_1(t)m_2(-t)\rangle + j|e_3(s)e_4(-s)\rangle + |e_1(s)e_2(-s)\rangle + j|m_3(t)m_4(-t)\rangle\Big]. \tag{6.58}$$

Which is a pair of σ-strings. Finally, we can always ensure that the fusion $\psi \times \psi$ always yields the vacuum since all the abelian anyons are identical and contain the appropriate antiparticles to cancel out. Then our fusion rules are summarized as

$$\begin{aligned} &\sigma \times \sigma = \mathbb{1} + \psi, \quad \sigma \times \psi = \sigma \\ &\psi \times \psi = \mathbb{1}, \quad \mathbb{1} \times x = x, \end{aligned} \tag{6.59}$$

where $x \in \{\mathbb{1}, \psi, \sigma\}$. We find the many particle fusions are

$$\sigma \times \sigma \times \sigma = 2.\sigma \tag{6.60}$$

$$\sigma \times \sigma \times \sigma \times \sigma = 2.\mathbb{1} + 2.\psi \tag{6.61}$$

Then one can read off the smallest non-trivial fusion spaces

$$V^{\sigma}_{\sigma\sigma\sigma} \Leftrightarrow N^{\sigma}_{\sigma\sigma\sigma} = 2, \tag{6.62}$$

$$V^{\mathbb{1}}_{\sigma\sigma\sigma\sigma} \Leftrightarrow N^{\mathbb{1}}_{\sigma\sigma\sigma\sigma} = 2, \tag{6.63}$$

$$V^{\psi}_{\sigma\sigma\sigma\sigma} \Leftrightarrow N^{\psi}_{\sigma\sigma\sigma\sigma} = 2, \tag{6.64}$$

We anticipate that the fusion basis, (6.63), that belongs the vacuum channel is the most convenient choice for our computational space as the space is two-dimensional. This lends itself naturally to the storage of quantum information as qubits. This basis can be decomposed into the left standard basis as

$$V^{\mathbb{1}}_{\sigma\sigma\sigma\sigma} \cong V^{\sigma}_{\sigma\sigma\sigma} \cong \bigoplus_{x\in\{\mathbb{1},\psi\}} V^{x}_{\sigma\sigma} \otimes V^{\sigma}_{x\sigma} \otimes V^{\mathbb{1}}_{\sigma\sigma} \tag{6.65}$$

This decomposition is related to the right standard basis through a sequence of F-moves, Fig.(6.7). Along the top of the diagram this transformation is given by

$$\begin{aligned} &\bigoplus_{x\in\{\mathbb{1},\psi\}} V^{x}_{\sigma\sigma} \otimes V^{\sigma}_{x\sigma} \otimes V^{\mathbb{1}}_{\sigma\sigma} \\ \overset{F^{\mathbb{1}}_{x\sigma\sigma}}{\rightarrow} &\bigoplus_{x,y'\in\{\mathbb{1},\psi\}} V^{x}_{\sigma\sigma} \otimes V^{\mathbb{1}}_{xy'} \otimes V^{y'}_{\sigma\sigma} \\ \overset{F^{\mathbb{1}}_{\sigma y'\sigma}}{\rightarrow} &\bigoplus_{y'\in\{\mathbb{1},\psi\}} V^{\mathbb{1}}_{\sigma\sigma} \otimes V^{\sigma}_{\sigma y'} \otimes V^{y'}_{\sigma\sigma}. \end{aligned} \tag{6.66}$$

The moves along the bottom are

$$\begin{aligned}
&\bigoplus_{x\in\{\mathbb{1},\psi\}} V^{\mathbb{1}}_{\sigma\sigma}\otimes V^{\sigma}_{x\sigma}\otimes V^{\mathbb{1}}_{\sigma\sigma}\\
\xrightarrow{F^{y}_{\sigma\sigma\sigma}}\ &\bigoplus_{x'\in\{\mathbb{1},\psi\}} V^{\sigma}_{x'\sigma}\otimes V^{x'}_{\sigma\sigma}\otimes V^{\mathbb{1}}_{\sigma\sigma}\\
\xrightarrow{F^{\mathbb{1}}_{\sigma x'\sigma}}\ &\bigoplus_{x'\in\{\mathbb{1},\psi\}} V^{\mathbb{1}}_{\sigma\sigma}\otimes V^{x'}_{\sigma\sigma}\otimes V^{\sigma}_{x'\sigma}\\
\xrightarrow{F^{\sigma}_{\sigma\sigma\sigma}}\ &\bigoplus_{x''\in\{\mathbb{1},\psi\}} V^{\mathbb{1}}_{\sigma\sigma}\otimes V^{\sigma}_{\sigma x''}\otimes V^{x''}_{\sigma\sigma}\,.
\end{aligned} \tag{6.67}$$

Then the pentagon equation reads

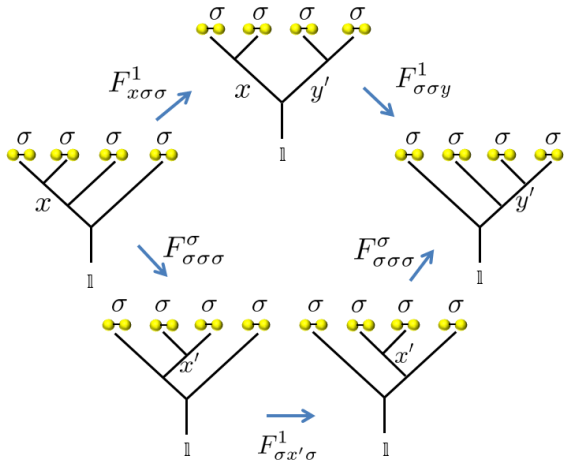

Figure 6.7: Diagrammatic representation of the pentagon equation for the CV non-abelian anyons assuming particle/antiparticle pairs.

$$\sum_{y'\in\{\mathbb{1},\psi\}} (F^{\mathbb{1}}_{\sigma\sigma y'})^{\sigma}_{x}(F^{\mathbb{1}}_{x\sigma\sigma})^{y'}_{\sigma} = \sum_{x,x'\in\{\mathbb{1},\psi\}} (F^{\sigma}_{\sigma\sigma\sigma})^{y'}_{x}(F^{\mathbb{1}}_{\sigma x'\sigma})^{\sigma}_{\sigma}(F^{\sigma}_{\sigma\sigma\sigma})^{x'}_{x}\,. \tag{6.68}$$

This equation states that there are seven possible F-moves. However, only $F^{\sigma}_{\sigma\sigma\sigma}$ acts on a non-trivial fusion space. The others only act on one-dimensional spaces and are hence just equal to some constant. Further, we recall that the F-moves must be unitary so the trivial moves are in general complex constants with unit norm. This implies that these moves produce global phase shifts and can be arbitrarily set to unity,

$$F^{\mathbb{1}}_{\sigma\sigma y'} = F^{\mathbb{1}}_{x\sigma\sigma} = F^{\mathbb{1}}_{\sigma x'\sigma} = 1 \tag{6.69}$$

The F-move of interest is $F^{\sigma}_{\sigma\sigma\sigma}$ as it acts on a two-dimensional space. It is represented as a 2×2 unitary matrix,

$$F^{\sigma}_{\sigma\sigma\sigma} = \begin{pmatrix} F_{\mathbb{1}\mathbb{1}} & F_{\mathbb{1}\psi} \\ F_{\psi\mathbb{1}} & F_{\psi\psi} \end{pmatrix} \tag{6.70}$$

To satisfy unitarity the matrix components must satisfy the constraints

$$\begin{gathered} |F_{\mathbb{1}\mathbb{1}}|^2 + |F_{\mathbb{1}\psi}|^2 = 1, \quad |F_{\psi\mathbb{1}}|^2 + |F_{\psi\psi}|^2 = 1, \\ F_{\mathbb{1}\mathbb{1}}(F_{\psi\mathbb{1}})^* + F_{\mathbb{1}\psi}(F_{\psi\psi})^* = 0. \end{gathered} \tag{6.71}$$

Simplifying the pentagon equation (6.68) using (6.69) and (6.71) we find the components are the solution to the polynomial equations

$$F_{\mathbb{1}\mathbb{1}}(F_{\mathbb{1}\mathbb{1}} + F_{\mathbb{1}\psi}) + F_{\mathbb{1}\psi}(F_{\psi\mathbb{1}} + F_{\psi\psi}) = 1, \tag{6.72}$$

and

$$F_{\psi\mathbb{1}}(F_{\mathbb{1}\mathbb{1}} + F_{\mathbb{1}\psi}) + F_{\psi\psi}(F_{\psi\mathbb{1}} + F_{\psi\psi}) = 1. \tag{6.73}$$

These equations admit solutions of the form

$$\pm \begin{pmatrix} 1 & 0 \\ 0 & 1 \end{pmatrix}, \quad \pm \begin{pmatrix} 1 & 0 \\ 0 & -1 \end{pmatrix}, \quad \pm \begin{pmatrix} 0 & e^{i\theta} \\ e^{-i\theta} & 0 \end{pmatrix}, \quad \pm \frac{1}{\sqrt{2}} \begin{pmatrix} 1 & e^{i\theta} \\ e^{-i\theta} & -1 \end{pmatrix}, \tag{6.74}$$

where $\theta \in [0, 2\pi]$ is an arbitrary parameter. The first three merely redefine the basis up to some global phase and are hence somewhat trivial. The last matrix is of more interest. Setting the phase $\theta = 0$ we find that the non-trivial F-move in the vacuum fusion basis is

$$F^{\sigma}_{\sigma\sigma\sigma} = \frac{1}{\sqrt{2}} \begin{pmatrix} 1 & 1 \\ 1 & -1 \end{pmatrix}, \tag{6.75}$$

which is identical to the non-trivial matrix fusion matrix from the Ising anyon model Eq.(6.22). This feature is what leads us to identify our CV non-abelian anyon model as a continuous-variable analog of the Ising model. Having made this connection we now turn to the question of braiding. We can use the Ising model as a guide which in general has a non-trivial braid matrix of the form

$$R = \begin{pmatrix} R^{\mathbb{1}}_{\sigma\sigma} & 0 \\ 0 & R^{\psi}_{\sigma\sigma} \end{pmatrix} \tag{6.76}$$

where $R^{y}_{\sigma\sigma}$, for $y \in \{\mathbb{1}, \psi\}$, is the phase due to braiding σ-strings and fusing to y. We can find these R-move elements by examining the decomposition of the σ-string fusion into CV toric anyons and examining the phases that

occur when we braid the endpoints.

$$\begin{aligned}|\sigma_1\sigma_2;j\rangle|\sigma_3\sigma_4;j\rangle &= \frac{1}{2}\Big[|\mathbb{1}_{1,4}\mathbb{1}_{2,3}\rangle + je^{ist}|e_1(s)e_2(-s)m_3(t)m_4(-t)\rangle \\ &\quad + je^{ist}|m_1(t)m_2(-t)e_3(s)e_4(-s)\rangle\Big] \\ &= \frac{1}{2}\Big[|\mathbb{1}_{1,4}\mathbb{1}_{2,3}\rangle + e^{ist}\Big(|e_1(s)e_2(-s)m_3(t)m_4(-t)\rangle \\ &\quad + |m_1(t)m_2(-t)e_3(s)e_4(-s)\rangle\Big)\Big]. \end{aligned} \tag{6.77}$$

The braiding in the vacuum channel give no phase change while the ψ channel gives e^{ist}. Then the braid matrix elements are $R^{\mathbb{1}}_{\sigma\sigma} = 1$ and $(R^{\psi}_{\sigma\sigma})^2 = e^{ist}$. Then the R-moves for the CV Ising model are

$$R = \begin{pmatrix} 1 & 0 \\ 0 & e^{ist/2} \end{pmatrix} \tag{6.78}$$

Once again, comparing to the Ising model, this braid rule is far more general since we can arbitrarily set the value of the phase obtained under braiding by adjusting the initial displacements s and t.

The fact that the relevant fusion spaces are two-dimensional and the convenient form of the fusion and braid matrices suggests that the CV Ising model will be a useful candidate for quantum computation. In the next section we define a computational basis and discuss the various quantum gate operations that we can enact through braiding.

6.5 Quantum computation with CV Ising anyons

From our analysis we have determined that the vacuum fusion space $V^{\mathbb{1}}_{\sigma\sigma\sigma\sigma}$ is an ideal candidate for our computational space. Then the computational space for a single qubit may be written

$$C^2 \equiv V^{\mathbb{1}}_{\sigma\sigma\sigma\sigma} \cong \bigoplus_{x\in\{\mathbb{1},\psi\}} V^{x}_{\sigma\sigma} \otimes V^{\sigma}_{x\sigma} \otimes V^{\mathbb{1}}_{\sigma\sigma} \tag{6.79}$$

It follows that the computational basis is identified with

$$|i\rangle \equiv |\sigma\sigma\sigma\sigma;\mathbb{1},i\rangle \cong |\sigma\sigma;x_i\rangle|x_i,\sigma,\sigma\rangle, \quad i=0,1. \tag{6.80}$$

where $x_i \in \{\mathbb{1},\psi\}$. Consequently the n-qubit computational space is defined as

$$C \equiv (V^{\mathbb{1}}_{\sigma\sigma\sigma\sigma})^{\otimes n} \tag{6.81}$$

which corresponds to the fusion space carried by M σ-strings for some M. This basis C is given by the tensor product of the computational basis states.

From our decomposition Eq.(6.79), an n-qubit basis $|i_1\rangle|i_2\rangle...|i_n\rangle \in C$ can be expressed in the left standard basis of the fusion space as

$$\begin{aligned}|i_1\rangle|i_2\rangle...|i_n\rangle &= |\sigma\sigma\sigma\sigma;\mathbb{1},i_1\rangle|\sigma\sigma\sigma\sigma;\mathbb{1},i_2\rangle...|\sigma\sigma\sigma\sigma;\mathbb{1},i_n\rangle,\\ &= |\sigma\sigma;x_{i1}\rangle|x_{i1}\sigma;\sigma\rangle|\sigma\sigma;x_{i2}\rangle|x_{i2}\sigma;\sigma\rangle...|\sigma\sigma;x_{in}\rangle|x_{in}\sigma;\sigma\rangle.\end{aligned} \tag{6.82}$$

Quantum gate operations are carried out within this space through the F- and R-moves derived above. Our model contains only one non-trivial F move Eq.(6.75). We recall from Chapter 3 that this matrix has an interpretation in terms of quantum computation, this is the Hadamard transform. This is a particularly important gate operation that is one of the basic requirements for universal quantum computation over qubits.

We also found that the CV Ising model has the non-trivial R-moves Eq.(6.78). The R matrices form a representation of the Braid group on two strands (B_2). In order to find a full representation of B_N, we require a second generator which is given in the fusion spaces by an R_2 move. This is constructed by the matrix product

$$R_2 \equiv F^{-1}RF = -\frac{1}{\sqrt{2}}\begin{pmatrix}-1 & -1\\ -1 & 1\end{pmatrix}\begin{pmatrix}1 & 0\\ 0 & e^{ist}\end{pmatrix}\begin{pmatrix}1 & 1\\ 1 & -1\end{pmatrix}, \tag{6.83}$$

which gives our second braid group generator

$$R_2 = \frac{1}{2}\begin{pmatrix}1+e^{ist/2} & 1-e^{ist/2}\\ 1-e^{ist/2} & 1+e^{ist/2}\end{pmatrix}. \tag{6.84}$$

From this braiding and fusion behaviour we find a set of quantum gates that can be performed over the computational space. We begin by examining gates on single qubits before expanding on these ideas to derive a two-qubit operation.

6.5.1 Single-bit gates

The single-qubit gates that we would like to perform are the Pauli Z or phase gate, the Pauli X and Hadamard H. The Pauli operations perform rotations on the Bloch sphere while the Hadamard gate performs a change of basis.

- (Pauli Z): We perform a phase rotation in the Z basis through applying R-moves (6.78) on our computational basis, Fig.6.8(a). Note that the rotations that we can apply depend only on the value of the anyonic displacements, s and t, so we can perform arbitrary Z rotations on single qubits. This result goes beyond the discrete Ising model where the phase rotations are restricted to certain non-computationally universal values.

- (Hadamard H): The Hadamard's effect on the computational basis is given by Eq.(3.8). We see that this is exactly the same as the F-move that we found above Eq.(6.75). Then the Hadamard gate is performed by merely changing the fusion basis.

- (Pauli X): To enact the Pauli X we note that

$$(R_2)^2 = \frac{1}{2}\begin{pmatrix} 1+e^{ist} & 1-e^{ist} \\ 1-e^{ist} & 1+e^{ist} \end{pmatrix} \tag{6.85}$$

  Now let $st = \pi$. We see then that Eq.(6.85) reduces to

$$(R_2)^2 = \begin{pmatrix} 0 & 1 \\ 1 & 0 \end{pmatrix} = X \tag{6.86}$$

  Under this condition we get the desired bit flip however, we could pick any X rotation since we control the phase through the initial displacements. This gives us $X = (R_2)^2$.

Our model allow for general rotations on the Bloch sphere on both the X and Z axes. This goes beyond the discrete Ising model where only certain rotations are allowed. Since we can perform arbitrary rotations on the qubits, our scheme allows for the implementation of non-Clifford gates such as the T gate (see chapter 3). To complete our model, we require that the qubits are able to interact. For this we construct a two-qubit gate.

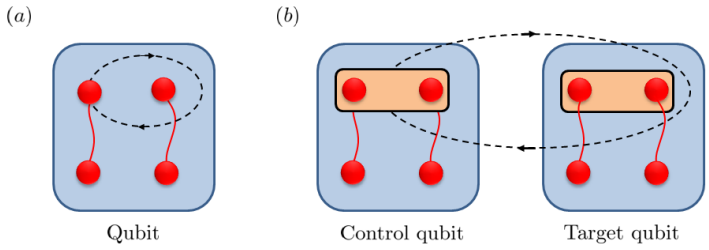

Figure 6.8: (a) A single qubit Z rotation is achieved by braiding the endpoints of string within a qubit. (b) The two-qubit controlled Z is performed by braiding the endpoints of the control qubit around those of the target.

6.5.2 Two-qubit gate

As we have shown that we can induce general single-bit rotations on our qubits through braiding so it is natural to choose the controlled-phase gate,

C_Z as a suitable two-qubit gate. We construct two qubits, each composed of two σ strings, we define the control qubit C on sites 1,2,3 and 4 as

$$C = |\sigma_1, \sigma_2; j\rangle|\sigma_3, \sigma_4; j\rangle = \frac{1}{2}|\mathbb{1}_{1,4}\mathbb{1}_{2,3}\rangle + j|\psi(s,-t)_{1,4}\psi(-s,t)_{2,3}\rangle. \quad (6.87)$$

The target T is defined similarly on sites 5,6,7 and 8 as

$$T = |\sigma_5, \sigma_6; j\rangle|\sigma_7, \sigma_8; j\rangle = \frac{1}{2}|\mathbb{1}_{5,8}\mathbb{1}_{6,7}\rangle + j|\psi(s,-t)_{5,8}\psi(-s,t)_{6,7}\rangle. \quad (6.88)$$

Then we examine the effect of braiding the anyons at $\{1,4\}$ around those at $\{5,8\}$.

- ($|00\rangle$): In this case, both C and T are in the vacuum channel and so braiding has no effect.
- ($|01\rangle$): C is in the vacuum channel so braiding has no effect on the target.
- ($|10\rangle$): Similarly, braiding the ψ of the target about the vacuum has no effect.
- ($|11\rangle$): Now both are in the ψ channel and under braiding we acquire a phase of e^{ist}. However we note there is a back-action on the control anyons. This can be corrected by braiding $\psi_{1,3}$ with $\psi_{2,4}$ after the controlled operation is completed. This removes the unwanted phase and leaves an effect only on the target.

Thus we can perform a controlled-Z gate through braiding, this is depicted in Fig.6.8(b). Note that we put the restriction that the qubit have identical CV parameters s and t. This allows us to correct the extra phase acquired on the control during braiding.

6.6 Discussion

It seems that the CV non-abelian model is extremely powerful as a computational resource. Our qubits are stored in a non-local state that cannot be altered through local operations at the endpoints of the anyon string. Through braiding alone we are able to perform arbitrary single- and two-qubit rotations. Further, we can also perform Hadamard transformations by changing the fusion basis. This leaves us with some important questions.

The first natural question concerns the origin of the computational complexity, after all the operations we apply are basically just displacements which only generate first order shifts and by themselves are usually insufficient to implement universal computation. Then the answer must lie in the anyonic states themselves. These states are superpositions in phase space

and are thus highly non-Gaussian. This may provide a clue to the computational power as we can draw a parallel to the GKP proposal, [87], where it was shown that qubits could be stored within CV resources but they required non-Gaussian operations to implement a universal gate set. It is yet unclear if the non-Gaussianity is the root of mystery but we hope to provide an answer in future works.

The second question relates to the fault tolerance of the topological operations. Since this scheme is based on the same lattice as the abelian anyon of Chapter 5 we run into the familiar problems of finite squeezing. This will cause fluctuations in the magnitudes of the displacements and hence in the values of the anyon continuous parameter. These fluctuations ensure that we cannot produce perfect particle-antiparticle pairs and hence when fusing σ pairs we can never guarantee that one of our fusion channels corresponds to the vacuum. Then any braiding operations with this noisy 'vacuum' channel will produce small unwanted phase shifts on the stored qubit.

This appears to be the price we pay for our protected qubits. We require very large squeezing to implement accurate gates or we have to include error correcting protocols before each braid which significantly increases the complexity for a physical realization.

Chapter 7

Conclusions

This thesis was concerned with the construction of alternative quantum computational models from continuous-variable resources. We focused on two main quantum computational paradigms: the measurement-based model and topological quantum computation. We showed that it is possible to create states that support universal quantum computation for both of these models from Gaussian resources. As Gaussian states are readily available in an experimental setting it is hoped that these CV protocols may be used as the fundamental building blocks for a scalable quantum computer.

7.1 Main results

The first set of results presented in this thesis dealt with the generation of Gaussian cluster states for use in the CV measurement-based model. In particular, we derived protocols to construct CV cluster states from ensembles of neutral atoms via entangling quantum non-demolition (QND) operations mediated by sequences of light pulses. We gave examples of how to construct small cluster states and showed that our protocol can be used to create cluster states of arbitrary shape and size. Such states can serve not only as useful computational resources but also as short term quantum memories. We showed that the upper limit on the number of nodes that can be included in these states is limited by Gaussian noise that the states accumulate during the preparation process.

In our next section we extended our construction to include light modes as part of the cluster states. This lead to a new type of state that we have called *composite cluster states*. We gave an explicit construction for small composite clusters that makes use of QND measurements in conjunction with linear optics. We investigated the properties of these states using the symplectic formalism and found values for the atom/light coupling constants that yield suitably entangled states. However, we found that these states are still plagued with the intrinsic problems of noise and finite squeezing.

To combat this we suggested a new architecture for the measurement-based model that seeks to reduce the number of resources and increase the efficiency of computational processes. This scheme relies on the construction of small composite cluster states called *qubricks*. Each qubrick takes the place of a single quantum gate and arrays of them can be assembled in a circuit model like fashion to simulate any particular computational process. This scheme represents an improvement over the traditional MBQC method that relies on creating large scale clusters and deleting nodes. Our protocol removes the need for redundant nodes and hence keeps the rate of entanglement decay and rate of error accumulation constant.

In Chapter 5 we moved beyond the measurement-bases model to investigate the topological model of quantum computation. We showed how a continuous-variable analog of Kitaev's toric code may be prepared from a square CV cluster state. We then described the excitations on the lattice which turned out to a CV version of abelian anyons due to their non-trivial mutual statistics. However, this scheme is based on perfect resources states and is thus highly unphysical.

We then extended our analysis to include finite squeezing effects on the ground state. Then the qumodes of the underlying state are Gaussian modes with non-zero quantum fluctuations. We derived the excitation spectrum and found that the excitations on this physical ground state correspond to Gaussian anyon states. We showed that these physical anyons are mathematically represented by complex stabilizer violations. We analysed the braiding behaviour of the Gaussian anyons in some detail and found that the phases gained under braiding retain their path independence which is vital for any possibility of using such states in a fault tolerant quantum computational setting.

The CV anyon model, while similar in some respects, differs from the discrete models in two important ways. First, the phases produced from braiding are of the form e^{-ist}. Hence the phases are just proportional to the magnitude of the initial displacements on the ground state and can be chosen arbitrarily. The other major difference to note is the lack of a finite energy gap. This means that a displacement of any magnitude will result in an anyonic excitation and then any small fluctuation of the lattice Gaussian states about their mean will produce small magnitude anyons. This leads us to examine the fault tolerance of the topological operations against finite squeezing. We showed that the braiding operations and hence the topological quantum gates do appear to have an associated fault-tolerance since in the finite squeezing regime the phases merely pick up extra terms proportional to the squeezing parameter. These extra terms disappear as the squeezing tends to infinity. However, we were unable to find a measurement scheme that takes full advantage of this fault-tolerance. Despite the lack of protection from finite squeezing errors, the CV Gaussian anyons retain the property that their braiding behaviour is independent of the path they take

when moving on the lattice.

We then went on to show that the abelian anyons are a useful resource for continuous-variable quantum computation. We have described the quantum gates that can be achieved by topological operations alone and found this did not form a sufficiently powerful gate set. By including offline squeezing, measurements, and cubic phase gates, we have shown that the computational power can be increased significantly. These additional resources provide a universal gate set for the CV anyons. It has therefore been possible for us to give a classification of the topological operations available to CV abelian anyons. We have shown that braiding and fusion only account for controlled and uncontrolled WH gates, non-topological operations are essential to complete the Clifford group, and a further non-Gaussian element is required to achieve universality.

Then we conclude that even with an improved measurement scheme that takes advantage of the mathematical fault tolerance, we cannot create a fully protected gate set, since some gates require non-topological operations. Nonetheless, we have been able to identify those operations which are theoretically protected.

Unsatisfied with the computational limits of the CV abelian anyon model our next chapter investigated the possibility of creating CV non-abelian anyon. We showed that the CV toric code can simulate non-abelian statistics if we allow for the creation of anyonic superpositions. We derived the fusion and braiding rules for this new model but it was not instantly obvious how they would be useful in a quantum computational setting. To reduce the complexity of the fusion and braid rules we placed a restriction on the allowed superposition states. We then derived the new fusion and braiding rules and found that under this restriction the properties of our CV anyons are similar to those of well known Ising anyons.

We then moved on to test the computational potential of the CV non-abelian anyons. It was shown that qubits can be stored in the fusion spaces of our anyons and that these qubits are well protected from decoherence as they cannot be affected by any local operations on the underlying lattice. We then investigated quantum gate operations that can be achieved by braiding the anyons. We found that this CV model is substantially more powerful than the standard Ising model as braiding alone allows for arbitrary qubit rotations. We established a set of single- and two-qubit gates. However, the increased flexibility of the braiding operations comes as at price. Namely, as with the abelian model, the effect of finite squeezing remains a difficult hurdle to overcome.

7.2 Future work and concluding remarks

In the introduction we alluded to the many possible roads ahead for the study and implementation of quantum computation. In this thesis we have added to the ever growing list of options but work is still required to take them from theoretical possibility to experimental reality. Here we present some suggestions for future work that would aid our understanding of the physical systems and computational models that we have discussed.

With current technology the creation of CV cluster states from atomic ensembles, while difficult, is a real possibility and could already be used for standard MBQC. Further, extending such schemes to the creation of small composite cluster states would open the door for the alternative architectures suggested here. As a first step the experimental factors for a proof of principle demonstration should be calculated. Then the remaining major theoretical works are to design protocols that implement specific quantum processes. Such protocols will reduce the experimental overheads and with the availability of increasingly sophisticated technology could form the basis of a scalable network of quantum processors.

In terms of theoretical work, our topological models are still far from well understood. In subsequent works it would be interesting to examine the CV anyon models on more fundamental grounds. While we can show that anyonic excitations occur in these lattice models there must be some underlying Hopf algebra structure that may yield more insight into the origin of our unusual statistics. Such algebras may rely on continuous groups, rather than the small finite groups of the traditional anyon models. This presents us with an interesting theoretical complication as continuous group are notoriously harder to work with.

On a more practical note, we are currently testing the fault tolerance of the CV non-abelian model against the effects of finite squeezing and amplitude damping. These calculation will hopefully give some ideas as to the viability of the scheme as a realistic competitor in the arena of quantum computation.

Bibliography

[1] R. P. Feynmann, Int. J. Theor. Phys, 21, 467 (1982).

[2] D. Deutsch, *Proceedings of the Royal Society of London*, A, 400, 97-117 (1985).

[3] M. A. Nielsen. *Quantum Information Science*. PhD thesis submitted to University of New Mexico, (1998).

[4] H. Ollivier and W. H. Zurek, Phys. Rev. Lett. **88**, 017901 (2001).

[5] W. H. Zurek, Phys. Rev. A **67**, 012320 (2003).

[6] P. Perinotti, Phys. Rev. Lett. **108**, 120502 (2012).

[7] S. L. Braunstein and P. van Loock, Rev. Mod. Phys. **77**, 513 (2005).

[8] S. L. Braunstein and H. J. Kimble, Phys. Rev. Lett. **80**, 869 (1998)

[9] S. L. Braunstein, Phys. Rev. Lett. **80**, 4084 (1998).

[10] W. P. Bowen, N. Treps, B. C. Buchler, R. Schnabel, T. C. Ralph, H.-A. Bachor, T. Symul1, and P. Koy Lam, Phys. Rev. A **67**, 032302 (2003).

[11] T. C. Ralph, Phys. Rev. A **61**, 010303 (1999).

[12] F. Grosshans and P. Grangier, Phys. Rev. Lett. **88**, 057902 (2002).

[13] S. Lloyd and S. L. Braunstein, Phys. Rev. Lett. **82**, 1784 (1999).

[14] P. Kok, W. J. Munro, K. Nemoto, T. C. Ralph, J. P. Dowling, and G. J. Milburn, Rev. Mod. Phys. **79**, 797 (2007).

[15] M. Mohseni, J. S. Lundeen, K. J. Resch, and A. M. Steinberg, Phys. Rev. Lett. **91**, 187903 (2003)

[16] A. N. de Oliveira et al., J. Opt. B **7**, 288 (2005).

[17] C. Ju, J. Zhu, X. Peng, B. Chong, X. Zhou, and J. Du, Phys. Rev. A *81*, 012322 (2010).

[18] L. M. K. Vandersypen and I. L. Chuang, Rev. Mod. Phys. **76**, 1037 (2005).

[19] M. S. Tame et al., Phys. Rev. Lett. **98**, 140501 (2007).

[20] Y. Nakamura et al., Nature (London) 398, 786 (1999).

[21] T. Hayashi, T. Fujisawa, H. D. Cheong, Y. H. Jeong, and Y. Hirayama, Phys. Rev. Lett. **91**, 226804 (2003).

[22] M. A. Nielsen and I. L. Chuang, *Quantum Computation and Quantum Information*. Cambridge University Press, Cambridge (2000).

[23] J. Preskill, arXiv:quant-ph/9712048v1 (1997).

[24] P. W. Shor, Phys. Rev. A **52**, R2493R2496 (1995).

[25] T. C. Ralph, Phys. Rev. A **84**, 022339 (2011).

[26] R. Raussendorf, D. E. Browne, and H. J. Briegel, Phys. Rev. A **68**, 022312 (2003).

[27] M. Gu, C. Weedbrook, N. C. Menicucci, T. C. Ralph, and P. van Loock, Phys. Rev. A **79**, 062318 (2009).

[28] N. C. Menicucci, P. van Loock, M. Gu, C. Weedbrook, T. C. Ralph, and M. A. Nielsen, Phys. Rev. Lett. **97**, 110501 (2006).

[29] P. van Loock, C. Weedbrook, and M. Gu, Phys. Rev. A **76**, 060301 (2007).

[30] N. C. Menicucci, S. T. Flammia, and O. Pfister, Phys. Rev. Lett. **101**, 130501 (2008).

[31] S. T. Flammia, N. C. Menicucci, and O. Pfister, J. Phys. B **42**, 114009 (2009).

[32] N. C. Menicucci, X. Ma, and T. C. Ralph, Phys. Rev. Lett. **104**, 250503 (2010).

[33] N. C. Menicucci, Phys. Rev. A **83**, 062314 (2011).

[34] D. F. Milne and N. V. Korolkova, Phys. Rev. A **85**, 032310 (2012).

[35] J. Stasinska, C. Rod, S. Paganelli, G. Birk, and A. Sanpera, Phys. Rev. A **80**, 062304 (2009).

[36] J. Stasinska, S. Paganelli, C. Rod, and A. Sanpera, arXiv:10070403v3 [quant-ph] (2011).

[37] K. Hammerer, A. S. Srensen, and E. S. Polzik, Rev. Mod. Phys. **82**, 1041 (2010).

[38] E. Dennis, A. Kitaev, A. Landahl, and J. Preskill, J. Math. Phys. **43**, 4452 (2002).

[39] J. R. Wootton, V. Lahtinen, B. Doucot, J. K. Pachos, Ann. Phys. **326**, 2307 (2011).

[40] H. Bombin, M. A. Martin-Delgado, Phys. Rev. **B78**, 115421 (2008).

[41] S. L. Braunstein, and P. van Loock, *Quantum information with continuous variables*, Rev. Mod. Phys, **77**, 513, (2005).

[42] P. van Loock, Fortschr Phys, **12**, 1177, (2002).

[43] W. M. Zhang, Rev. Mod. Phys, **62**, 867, (1990).

[44] G. Adesso and F. Illuminati, J. Phys. A: Math Theor, **40**, 7821, (2007).

[45] A. Ferraro, S. Olivares, and M. G. A. Paris, arXiv:quant-ph, 0503.237, (2005).

[46] M . Hillery, R. F. O'Connell, M. O. Scully and E. P. Wigner, Phys. Rep **106**, 121 (1984).

[47] H. W. Lee, Phy, Rep, **259**, 147, (1995).

[48] R. Loudon, *The quantum theory of light*, Oxford University Press, (1973).

[49] D. Walls and G. Milburn, *Quantum Optics*, Spinger, (1995).

[50] L. Mandel and E. Wolf, *Optical Coherence and Quantum Optics*, Cambridge University Press, (1995).

[51] M. O'Scully and M. Zubairy, *Quantum Optics*, Cambridge University Press, (1997).

[52] U. Leonhardt, *Measuring the Quantum State of Light*, Cambridge University Press, (1997).

[53] C. Gerry and P. Knight, *Introductory Quantum Optics*, Cambridge University Press, (2005).

[54] G. Auletta, *Foundations and Interpretations of Quantum Mechanics*, World Scientific, (2001).

[55] A. Einstein, B. Podolsky, and N. Rosen. Phys. Rev. **47**, 777 (1935)

[56] M. M. Wolf, J. Eisert and M. B. Plenio, Phys. Rev. Lett **90**, 047904 (2003).

[57] J. Williamson, Am. J. Math, **58**, 141 (1936).

[58] A. Serafini, PhD thesis, www.tampa.phys.ucl.uk/quinfo/people/alessiothesis, (2004).

[59] A. Serafini, Phys. Rev. Lett, **96**, 110402 (2006).

[60] J. S, Bell, Physics (N.Y.) **1**, 195, (1964).

[61] G. J, Milburn, and S. L. Braunstein, Phys. Rev. A **60**, (1999).

[62] R. F. Werner, Phys. Rev. A **40**, 4277, (1989)

[63] A. Peres, Phys. Rev. Lett. **77**, 1413, (1996)

[64] M. Horodecki, P. Horodecki, and R. Horodecki, Phys. Lett. A **223** (1996)

[65] R. Simon, Phys. Rev. Lett. **84**, 2726, (2000).

[66] R. Simon, N. Mukunda, and B. Dutta, Phys. Rev. A **49**, 1567 (1994).

[67] R. Simon, E. C. G. Sudarshan and N. Mukunda, Phys. Rev. A **36**, 3868 (1987).

[68] G. Vidal and R. F. Werner, Phys. Rev. A **65**, 032314, (2002)

[69] L. Adleman, Science **266**, 1021-1024 (1994).

[70] D. DiVincenzo, Science **270**, 255-261 (1995).

[71] S. Lloyd, Sci. Am. **273**, 140 (1995).

[72] D. Deutsch, A. Barenco, and A. Ekert, Proc. R. Soc. London A **449**, 669 (1995).

[73] J. I. Cirac, P. Zoller, Phys. Rev. Lett, **74**, 4091 (1995).

[74] T. Pellizzari, S. A. Gardener, J. I. Cirac, Phys. Rev. Lett, **75**, 3788 (1995).

[75] Q. A. Turchette, C. J. Hood, W. Lange, H. Mabuchi, H. J. Kimble, Phys. Rev. Lett, **75**, 4714 (1995).

[76] P. Domokos, J. M. Raimond, M. Brune, S. Haroche, Phys. Rev. Lett, **52**, 3554 (1995).

[77] C. M. Tesch, R. de Vivie-Riedle, Phys. Rev. Lett, **89**, 157901 (2002).

[78] B. E. Kane, Nature **393**, 133 (1998).

[79] L. M. Vandersypen, M. Steffen, G. Breyta, C. S. Yannoni, M. H. Sherwood, I. L. Chuang, Nature **414**, 883 (2001).

[80] A. Barenco, C. H. Bennet, R. Cleve, D. P. DiVincenzo, N. Margolus, P. Shor, T. Sleator, J. A. Smolin, and H. Weinfurter, Phys. Rev. A, **52**, 3457-3467 (1995).

[81] A. Steane, Rep. Prog. Phys. **61**, 117-173 (1998).

[82] J. Jones, Phys. Rev. **A**, **67**, 012317 (2003).

[83] S. Ghose, B. C. Sanders, J. Mod. Opt, **54**, 6 (2007).

[84] M. Stobinska, G. J. Milburn, K. Wodkiewicz, arXiv: 0810.2618v1 [quant-ph] (2008).

[85] Ramakrishna, V., M. V. Salapaka, M. Dahleh, H. Rabitz, and A. Peirce, Phys. Rev. A **51**, 960 (1995).

[86] D. Gottesman, in Group 22: *Proceedings of the XXII International Colloquium on Group Theoretical Methods in Physics*, edited by S. P. Corney, R. Delbourgo, and P. D. Jarvis (Cambridge, MA, International Press), p. 32. (1999).

[87] D. Gottesman, A. Kitaev and J. Preskill, arXiv:quant-ph/0008040v3 (2001).

[88] S. L. Braunstein and P. van Loock *Quantum information with continuous variables* (2004).

[89] R. Raussendorf and H. J. Briegel, Phys. Rev. Lett **86**, 5188 (2001).

[90] R. Raussendorf, D. E. Browne and H. J. Briegel. *J. Mod. Opt*, 49(8):1299-1306, (2002)

[91] M. A. Nielsen, Phys. Rev. Lett **93**, 040503 (2004)

[92] P. Walther, K. J. Resch, T. Rudolph, E. Schenck, H. Weinfurter, V. Vedral, M. Aspelmeyer,and A. Zeilinger, Nature, **434**, (2005)

[93] D. L. Zhou, B. Zeng, Z. Xu, and C. P. Sun, Phys. Rev. A **68**, 062303 (2003).

[94] N. C. Meniucci *et al*, Phys. Rev. Lett **97**, 110501 (2006).

[95] *Introduction to graph theory*, (Prentice Hall, 2002).

[96] D. Gottesman, *The Heiesenberg representation of quantum computers*, arXiv:quant-ph/9807006 (1998).

[97] R. L. Barnes, arXiv:quant-ph/0405064 (2004).

[98] J. Zhang and S. L. Braustein, Phys. Rev. A **73**, 032318 (2006).

[99] N. C. Menicucci, S. T. Flammia, and P. van Loock, Phys. Rev. A **83**, 042335 (2011)

[100] J. Zhang, Phys. Rev. A **78**, 052307 (2008).

[101] M. Gu *et al*, Phys. Rev. A, **79**, 062318 (2009).

[102] D. Gottesman, A. Kitaev, and J. Preskill, Phys. Rev. A **64**, 012310 (2001).

[103] M. A. Nielsen, Phys. Rev. Lett **93**, 040503 (2004).

[104] D. E. Browne, and T. Rudolph, Phys. Rev. Lett **95**, 010501, (2005).

[105] L.-M. Duan and R. Raussendorf, Phys. Rev. Lett **95**, 080503 (2005).

[106] S. L. Braunstein, Phys. Rev. A **71**, 055801 (2005).

[107] B. Yurke, J. Opt. Soc. Am. B **2**, 732 (1985).

[108] Radim Filip, Petr Marek, and Ulrik L. Andersen, Phys. Rev. A **71**, 042308 (2005).

[109] J. Yoshikawa *et al*, Phys. Rev. Lett **101**, 250501 (2008).

[110] D. F. Milne, and N. V. Korolkova, *Generation of atomic cluster states by QND measurements*,
$www.st-andrews.ac.uk/\ cewqo10/abstracts.htm$

[111] D. F. Milne, and N. V. Korolkova, *Generation of hybrid cluster states using non-demolition measurements*,
$www.icssur09.upol.cz/fileadmin/slo08/user$
$/dokumenty/bookabs090506.pdf$

[112] M. Ohliger, K. Kieling, and J. Eisert, Phys. Rev. A **82**, 042336 (2010).

[113] B. Julsgaard, A. Kozhekin and E. Polzik, Nature **413** (2001).

[114] B. Julsgaard, *Entanglement and Quantum Interactions with Macroscopic Gas Samples.* PhD thesis, University of Aarhus, Denmark (2003).

[115] J. F. Sherson, *Quantum Memory and Teleportation Using Macroscopic Gas Samples*. PhD thesis, University of Aarhus, Denmark (2006).

[116] D. Kupriyanov et al., Phys. Rev. A **71**, 032348 (2005).

[117] K. Hammerer, E. S. Polzik, and J. I. Cirac, Phys. Rev. A **72**, 052313 (2005).

[118] E. Knill, R. Laflamme and G. J. Milburn, Nature (London) **409**, 46 (2001)

[119] R. A. Horn and C. R. Johnson, *Matrix Analysis*, Cambridge University Press, (1985).

[120] G. Giedke, and J. I. Cirac. Phys. Rev. A **66**, 032316 (2002).

[121] G. Adesso, and F. Illuminati, arXiv: [quant-ph] 0510052v2 (2007).

[122] G. Adesso, and F. Illuminati, J. Phys. A: Math Theor, **40** 7821 (2007).

[123] A. Peres, Phys. Rev. Lett **77**, 1413 (1996).

[124] R. Horodecki, P. Horodecki, and M. Horodecki, Phys. Rev. Lett **210**, 377 (1996).

[125] J. Williamson, Am. J. Math **58**, 141 (1936).

[126] R. Simon, Phys. Rev. Lett **84**, 2726 (2000).

[127] R. F. Werner and M. M, Wolf, Phys. Rev. Lett **86**, 3658 (2001).

[128] G. Vidal, and R. F. Werner, Phys. Rev. A **65**, 032314 (2002).

[129] M. B. Plenio, Phys. Rev. Lett **95**, 090503 (2005).

[130] L-.H. Duan, G. Giedke, J. I. Cirac, and P. Zoller, Phys. Rev. Lett **84**, 2722 (2000).

[131] M. Schwarz, K. Temme, and F. Verstraete, arXiv:1104.1410v2 [quant-ph] (2012).

[132] N. Schuch, J. I. Cirac, and M. M. Wolf, Commun. Math. Phys. **267**, 65 (2006).

[133] G. Giedke and J. I. Cirac, Phys. Rev. A **66**, 032316 (2002).

[134] J. Eisert, S. Scheel, and M. B. Plenio, Phys. Rev. Lett. **89**, 137903 (2002).

[135] M. Popp, F. Verstraete, M. A. Martin-Delgado, and J. I. Cirac, Phys. Rev. A **71**, 042306 (2005).

[136] P. van Loock, and A. Furusawa, Phys. Rev. A **67**, 052315 (2003).

[137] C. Horsman, K.L. Brown, W. J. Munro, and V.M. Kendon, Phys. Rev. A **83**, 042327 (2011)

[138] W. Happer and B. S. Mathur, Phys. Rev. Lett. 18, 577 (1967).

[139] T. Holstein and H. Primakov, Phys. Review **58**, 1098 (1940)

[140] A. Y. Kitaev, Ann. Phys. **303**, 2 (2003).

[141] M. H. Freedman, A. Kitaev, and Z. Wang, Comm. Math.Phys. **227**, 587 (2002).

[142] M. H. Freedman, M. J. Larsen, and Z. Wang, Comm. Math. Phys.**227**, 605 (2002).

[143] M. H. Freedman, M. J. Larsen, and Z. Wang, Comm. Math. Phys. **228**, 177 (2002).

[144] A. Marzuoli and M. Rasetti, Phys. Lett. A **306**, 79 (2002).

[145] A. Marzuoli and M. Rasetti, Ann. of Phys. **318**, 345 (2005).

[146] N. E. Bonesteel, L. Hormozi, G. Zikos, and S. H. Simon, Phys. Rev. Lett. **95**, 140503 (2005).

[147] S. H. Simon et al., Phys. Rev. Lett. **96**, 070503 (2006).

[148] L. Hormozi, G. Zikos, N. E. Bonesteel, and S. H. Simon, Phys. Rev. B **75**, 165310 (2007).

[149] L. Hormozi, N. E. Bonesteel, and S. H. Simon, Phys. Rev. Lett. **103**, 160501 (2009).

[150] H. Xu and X. Wan, Phys. Rev. A **78**, 042325 (2008).

[151] H. Xu and X. Wan, Phys. Rev. A **80**, 012306 (2009).

[152] C. Nayak et al, Rev. Mod. Phys. **80**, 1083 (2008).

[153] G. K. Brennen and J. K. Pachos, Proc. R. Soc. A 464, 1 (2008).

[154] M. V. Gurudev Dutt, L. Childress, L. Jiang, E. Trogan, J. Maze, F. Jelezko, A. S. Zibrov, P. R. Hemmer, and M. D. Lukin, Science, **316**, 5829 (2007).

[155] J. M. Taylor, C. M. Marcus, and M. D. Lukin, Phys. Rev. Lett **90**, 206803 (2003).

[156] M. Gundogan, P. M. Ledingham, A. Almasi, M. Cristiani and H. de Riedmatten, arXiv:1201.4149v2 [quant-ph] (2012).

[157] J. Preskill, Lecture Notes on Topological Quantum Computation, available online at www.theory.caltech.edu/ preskill/ph219/topological.pdf.

[158] B.I. Halperin, Phys. Rev. Lett. **52**, 1583 (1984).

[159] H. L. Stormer *et al.*, Phys. Rev. Lett **50**, 1953 (1983).

[160] T. Senthil and M.P.A. Fisher, Fractionalization, topological order, and cuprate superconductivity, cond-mat/0008082.

[161] C. Nayak, and K. Shtengel, Phys. Rev. B, **64**, 064422 (2001).

[162] S. Das Sarma, and A. Pinczuk, *Perspectives in quantum Hall effects: novel quantum liquids in low-dimensional semiconductor structures*, Wiley, New York (1997).

[163] R. Prange, and S. M. Girvin, *The Quantum Hall effect*, Springer-Verlag, New York, (1990).

[164] F. Wilczek, Phys. Rev. Lett. **48**, 1144 (1982).

[165] J. M. F. Labastida, arXiv:hep-th/9905057v1 (1999).

[166] E. Fradkin, *Field theories of condensed matter systems*, thesis submitted to University of Illinois (1991).

[167] F. Wilczek, *Fractional statistics and anyon superconductivity.* World Scientific, Singapore, (1990).

[168] C. Kassel, *Quantum groups*, Springer-Verlag, New York (1995).

[169] P. J. Burton, M. D. Gould, Rep. Math. Phys, **57**, 1, (2006).

[170] V. Lahtinen, *Topological quantum computation - an analysis of an anyon model based on quantum double symmetries*, thesis submitted to Universitas Helsingiensis (2006).

[171] M. de Wild Propitius, and F. A. Bais, arXiv:hep-th/9511201 (1995).

[172] T. H. Koornwinder, F. A. Bais, N. M. Muller, Comm. Math. Phys. **198**, 157-186 (1998).

[173] F. A. Bais, N. M. Muller, Nucl. Phys, **B530** (1998).

[174] A. Kitaev, C. Laumann, arXiv:0904.2771v1[cond-mat.mes-hall] (2009).

[175] A. Kitaev, Ann. Phys, **321** (2006).

[176] S. Dusuel, K. Phillip Schmidt, J. Vidal, Phys. Rev. Lett, **100**, 177204 (2008).

[177] S. Mandal, N. Surendran, Phy. Rev. B, **79**, 024426 (2009).

[178] Y. -J. Han, R. Raussendorf and L.-M. Duan, Phys. Rev. Lett, **98**, 150404 (2007).

[179] J. Zhang, C. Xie, K. Peng, P. van Loock, Phy. Rev. A, **78**, 052121 (2008).

[180] D. F. Milne, N. V. Korolkova, and P. van Loock, arXiv:1112.5385v1 [quant-ph] (2011).

[181] J. R. Wootton, V. Lahtinen, and J. K. Pachos, LNCS 5906, 56-65 (2009).

[182] C. Nayak, S. Simon, A. Stern, M. Freedman, and S. Das Sarma, Rev. Mod. Phys. **80**, 1083 (2008).

[183] L. Hormozi, G. Zikos, N.E. Bonesteel, S.H. Simon, Phys. Rev. B **75**, 165310 (2007).

[184] P. Etingof, D. Nikshych and V. Ostrik, math. QA/0203060.

[185] Mac Lane, Saunders, *Categories for the Working Mathematician* (2nd ed.). New York: Springer-Verlag,(1998).

[186] J. Eisenstein, K. Cooper, L. Pfeiffer, and K. West, Phys. Rev. Lett **88**, 076801 (2002).

[187] J. Xia, W. Pan, C. Vincente, E. Adams, N. Sullivan, H. Stormer, D. Tsui, L. Pfeiffer, K. Baldwin and K. West, Phys. Rev. Lett **93**, 176809, (2004).

[188] R. Morf, Phys. Rev. Lett, **80**, 1505 (1998).

[189] E. Rezayi and F. Haldane, Phys. Rev. Lett, **84**, 4685 (2000).

[190] N. Read and D. Green, Phys. Rev. B **61**, 10267 (2000).

[191] D. Ivanov, Phys. Rev. Lett, **86**, 268 (2001).

[192] G. Moore and N. Read, Nucl. Phys. **B360**, 362 (1991).

[193] S. D. Sarma, M. Freedman and C. Nayak, Phys. Rev. Lett. **94**, 166802 (2005).

[194] A. Ahlbrecht, L. S. Georgiev, and R. F. Werner, Phys. Rev. A **79**, 032311 (2009).

[195] N. Read, J. Math. Phys. **44**, 558 (2003).

[196] L. S. Georgiev, Phys. Rev. B **74**, 235112 (2006)

[197] M. Levin and X.-G. Wen, Phys. Rev. B, **71**, 045110 (2005).

[198] S. S. Bullock and G. K. Brennan, J. Phys. A **40**, 3481-3505 (2007).

[199] S. Yang, S. J. Gu, C. P. Sun, H. Q. Lin, Phys. Rev. A **78**, 012304 (2008).

[200] H. D. Chen and Z. Nussinov, J. Phys. A **41**, 075001 (2008).

[201] Z. Nussinov and G. Ortiz, Phys. Rev. B **79**, 214440 (2009).

[202] Jing Zhang, Changde Xie, Kunchi Peng, and Peter vanLoock, Phys. Rev. A **78**, 052121 (2008)

[203] J. R. Wootton, V. Lahtinen, Z. Wang, and J. K. Pachos, Phys. Rev. B **78**, 161102 (2008).

[204] J. R. Wootton, V. Lahtinen, B. Doucot and J. K. Pachos, arXiv:0908.0708v2 [quant-ph], (2009).

[205] H. Bombin, Phys. Rev. Lett. **105**, 030403 (2010).